TECHNISCHE UNIVERSITÄT DRESDEN

Faculty of Electrical and Computer Engineering Institute of Semiconductors and Microsystems

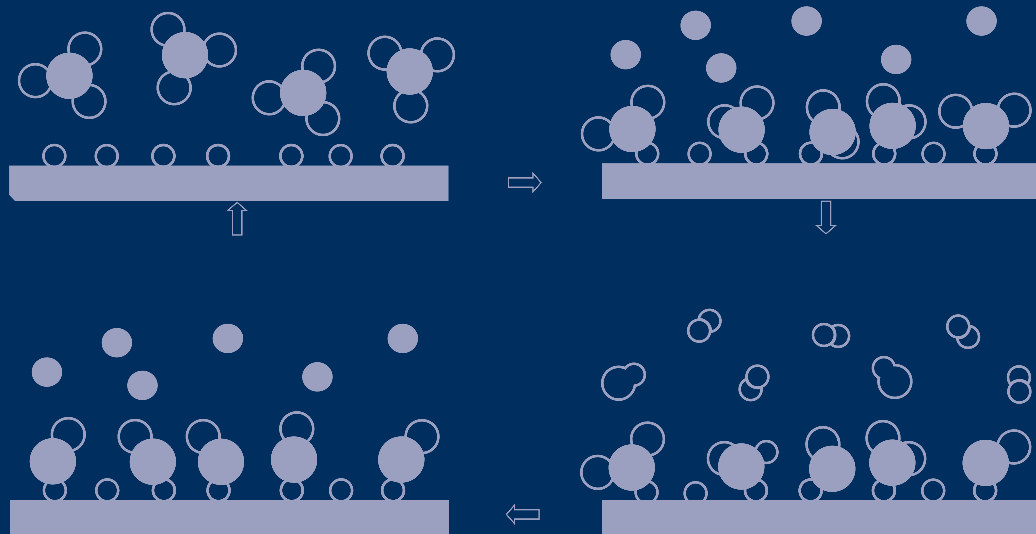

Master Thesis

EVALUATION OF NOVEL METALORGANIC PRECURSORS FOR ATOMIC LAYER DEPOSITION OF NICKEL-BASED THIN FILMS

Varun Sharma

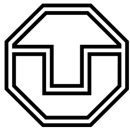

TECHNISCHE UNIVERSITÄT DRESDEN

Faculty of Electrical and Computer Engineering Institute of Semiconductors and Microsystems

Master Thesis

EVALUATION OF NOVEL METALORGANIC PRECURSORS FOR ATOMIC LAYER DEPOSITION OF NICKEL-BASED THIN FILMS

Submitted by:
Varun Sharma
born on March 24, 1988 in Ferozepur, India
Matriculation number: 3834614

for acquiring the academic degree
Master of Science (M. Sc.)

Supervised by:
Dr.-Ing. Christoph Hoßbach
M.Sc. Sascha Bönhardt
Responsible Professor:
Prof. Dr. rer. nat. Johann W. Bartha
Head of examination board:
Prof. Dr.-Ing. Thomas Mikolajick
Co-examiner:
Prof. Dr.-Ing.habil. W. J. Fischer

Submitted on:
Dresden, February 02, 2015

TECHNISCHE UNIVERSITÄT DRESDEN

Faculty of Electrical and Computer Engineering

Task assignment for a Master Thesis

Name des Studenten: Varun SHARMA **Born on: 24.03.1988**

Topic title: Evaluation of novel metalorganic precursors for Atomic Layer Deposition of nickel-based thin films

Topic description:

Nickel silicide (NiSi) features low resistivity of 14 µΩ·cm as well as low contact resistance. It is emerging as the material of choice for source and drain contact metallization for 28 nm technology node and beyond. There, the fabrication of three dimensional transistor devices requires technologies like Atomic Layer Deposition (ALD), which can deposit ultra-thin films with excellent step-coverage. A promising approach for NiSi contact formation is the ALD of pure or doped (e.g. with Pt or N) Nickel films on source and drain area in combination with a subsequent silicidation by Rapid Thermal Processing. However, so far, the number of ALD Nickel precursors and the resulting films qualities are limited. This master thesis addresses this issue and is about the evaluation of several novel Nickel precursors, which are provided by an industrial chemical supplier.

Subtasks:

- Literature survey on ALD and CVD of Nickel-based thin films
- Familiarizing with the custom-made ALD tool and measurement technologies
- Evaluation of selected Nickel precursors with focus on precursor, process and film properties
  - Development of a standard testing procedure
  - Process development
  - In-situ monitoring with Quartz Crystal Microbalance
  - Ex situ film characterization (e.g. Ellipsometry, Scanning Electron Microscopy, 4-probe electrical measurements as well as X-Ray Reflectivity, X-Ray Diffraction and X-Ray Photoelectron Spectroscopy)
- Feasibility study for nickel silicide formation
- Documentation and interpretation of precursor properties and experimental results
- Comparison with state of the art processes and precursors

Supervisors: Dr.-Ing. C. Hoßbach, M.Sc. S. Bönhardt
Starting date: 23.06.2014
Date of submission: 01.12.2014

Prof.Dr.-Ing T. Mikolajick	Prof. Dr. rer. nat. J. W. Bartha	Prof. Dr.-Ing.habil. W.J. Fischer
Head of examination board	Responsible faculty member	Co-examiner

DEDICATION

I would like to dedicate this Master thesis to my lovely wife *Maarja Sharma*, my parents *Varinder Sharma* and *Veena Sharma* as well as little sister *Vasudha*. They have always supported me during this period. Without their never-ending support and motivation, this thesis would not have been possible.

Explore, and explore.
Be neither chided nor flattered out of your position of perpetual inquiry.
Neither dogmatize or accept another's dogmatism.
Ralph Waldo Emerson

SELF DECLARATION

I hereby declare, that I have completed and submitted my Master thesis on "Evaluation of novel metalorganic precursors for Atomic Layer Deposition of Nickel-based thin films". I declare that this thesis was independently written by me. I have used no literature and quotations other than those specified in this report.

Dresden, February 02, 2015

Varun Sharma

CONTENTS

Lists of Abbreviations and Symbols VIII

Lists of Figures and Tables XIV

1 Introduction 1

I Theoretical Part 3

2 Nickel and Nickel Oxides 4

2.1 Introduction and Existence 5

2.2 Material properties of Nickel and Nickel Oxide 5

2.3 Application in electronic industry 5

3 Atomic Layer Deposition 7

3.1 History 8

3.2 Definition 8

3.3 Features of thermal-ALD 8

3.3.1 ALD growth mechanism – an ideal view 8

3.3.2 ALD growth behaviour 10

3.3.3 Growth mode 11

3.3.4 ALD temperature window 11

3.4 Benefits and limitations 12

3.5 Precursor properties for thermal-ALD 13

3.6 ALD & CVD of Nickel – A literature survey 13

4 Metrology 17

4.1 Thermal analysis of precursors 18

4.2 Film and growth characterization 21

4.2.1 Quartz Crystal Microbalance 21

4.2.2 Spectroscopic Ellipsometry 24

4.2.3 X-Ray Photoelectron Spectroscopy 28

4.2.4 Scanning Electron Microscopy 29

4.2.5 X-Ray Reflectometry and X-Ray Diffraction 29

4.2.6 Four Point Probe Technique 30

5 Rapid Thermal Processing 32

5.1 Introduction 33

5.2 Basics of RTP 33

5.3 Nickel Silicides-A literature survey 33

II Experimental Part 36

6 Methodologies 37
6.1 Experimental setup . . . 38
6.2 ALD process . . . 41
6.2.1 ALD process types and substrate setups . . . 41
6.2.2 Process parameters . . . 41
6.3 Experimental procedure . . . 42
6.3.1 Tool preparation . . . 42
6.3.2 Thermal analysis and ALD experiments from nickel precursors . . . 43
6.3.3 Data acquisition and evaluation . . . 44
6.3.4 Characterization of film properties . . . 46

7 Results and discussion 48
7.1 Introduction . . . 49
7.2 QCM verification with Aluminum Oxide ALD process . . . 49
7.3 ALD process from the reference precursor . . . 50
7.3.1 Introduction . . . 50
7.3.2 TG analysis for Ni(amd) precursor . . . 51
7.3.3 Thermal stability test for Ni(amd) . . . 51
7.3.4 ALD process optimization . . . 52
7.3.5 Film properties . . . 54
7.4 Evaluating the novel Nickel precursors . . . 55
7.4.1 Screening tests for precursor P1 . . . 55
7.4.2 Screening tests for precursor P2 . . . 62
7.4.3 Screening tests for precursor P3 . . . 66
7.4.4 Screening tests for precursor P4 . . . 70
7.4.5 Screening tests for precursor P5 . . . 72
7.5 Comparison of all nickel precursors used in this work . . . 74

8 Conclusions and outlook 77

References 83

III Appendix 101

A Deposition temperature control & Ellipsometry model 102

B Gas flow plan 105

LISTS OF ABBREVIATIONS AND SYMBOLS

LIST OF ABBREVIATIONS

4PP . . . . . . four-point probe
AFM . . . . . . atomic force microscopy
ALD . . . . . . atomic layer deposition
CMOS . . . . . complementary-metal oxide semiconductor
c-Si . . . . . . crystalline silicon
CVD . . . . . . chemical vapor deposition
DLI . . . . . . direct liquid injection
DRAM . . . . . dynamic random access memory
DSC . . . . . . differential scanning calorimetry
DTA . . . . . . differential thermal analysis
DTG . . . . . . differential thermogravimetry
EGA . . . . . . evolved gas analysis
EM . . . . . . electro magnetic
FAP . . . . . . Forschungs- und Applikationslabor Plasmatechnik GmbH
FCNT . . . . . Fraunhofer- Center Nanoelektronische Technologien (IPMS-CNT)
FDPC . . . . . frequency drop per cycle
FRAM . . . . . ferroelectric random access memory
FTIR . . . . . . fourier transform infrared spectroscopy
GI . . . . grazing incidence
GPC . . . . . . growth per cycle
HF acid . . . . hydroflouric acid
IC . . . . integrated circuit
IHM . . . . . . Institut für Halbleiter- und Mikrosystemtechnik
MBE . . . . . . molecular beam epitaxy
MFC . . . . . . mass flow controller
MIM . . . . . . metal-insulator-metal
ML . . . . monolayer
MS . . . . . . mass spectrometry
MSE . . . . . . mean squared error

natOx . . . . . native oxide; ≈ 2 nm SiO_2

$Ni(acac)_2$ . . . [Bis(acetyl-acetonate)]Nickel(II)

Ni(amd) . . . . [Bis(N,N'-ditertialbutylacetamidinato)]Nickel(II)

$Ni(Cp)_2$ . . . . [Bis(Cyclopentadienyl)]Nickel(II)

Ni(Cp)al . . . . [(Cyclopentadienyl)allyl]Nickel

$Ni(^tBu_2-DAD)_2$ [1,4-di-tert-butyl-1,3-diazabutadiene]Nickel(II)

$Ni(dmamb)_2$. [Bis(dimethylamino-2-methyl-2-butoxo)]Nickel(II)

$Ni(dmamp)_2$. [Bis(1-dimethylamino-2-methyl-2-propanolate)]Nickel(II)

$Ni(dmg)_2$ . . . [Bis(2,2,6,6-tetramethyl-3,5-heptandionato)]Nickel(II)

$Ni(EtCp)_2$ . . . $(Ethyl-cyclopentadienyl)_2$Nickel(II)

Ni(ηMDA) . . . [η^3-2-methylallyl N,N'-diisopropylacetamidinate]Nickel(II)

$Ni(hfip)_2$ . . . . [N2-hydroxyhexafluoroisopropyl-N1]Nickel(II)

$Ni(^iPrMeAMD)_2$ [Bis(N,N'-diisopropylacetamidinate)]Nickel(II)

$Ni(ktfaa)_2$ . . . [Bis(2-imino-pen-en-4triflouroacetylacetonato)]Nickel(II)

$Ni(MA)(^iPAMD)_2$ [(Methyl-allyl)(iso-propyl amidinate)]Nickel(II)

$Ni-(OCH)_2$ . . [Dimethylamino-2-propoxide]Nickle(II) ; $Ni-(OCHMeCH_2NMe_2)_2$

$Ni(PF_3)_4$ . . . . [tetrakis trifluorophosphine]Nickel(0)

$Ni[(t-Bu)_2Amd]_2$ Bis[di(tert-butyl)amido]Nickel(II)

$Ni(thd)_2$ . . . . [Bis(2,2,6,6-tetramethylheptane-3,5-dionato)]Nickel(II)

$Ni[(tta)_2]$tmeda [(2-thenoyl-trifluoroacetone)tetramethylethylendiamine]Nickel

NMOS . . . . n-channel-metal oxide semiconductor

OLS . . . . . . optical layer stack

PE . . . . plasma-enhanced

PMOS . . . . . p-channel-metal oxide semiconductor

PVD . . . . . . physical vapor deposition

QCM . . . . . quartz crystal microbalance

RRAM . . . . . resistive random access memory

RTCVD . . . . rapid thermal chemical vapor deposition

RTP . . . . . . rapid thermal processing

SEM . . . . . . scanning electron microscope

SiO_2 . . . . . . silicon dioxide

TA . . . . thermal analysis

TGA . . . . . . thermogravimetric analysis

thALD . . . . . thermal ALD

TMA . . . . . . trimethylaluminum

XPS . . . . . . x-ray photoelectron spectroscopy

XRD . . . . . . x-ray diffraction

XRR . . . . . . x-ray reflectivity/ reflectometry

LIST OF SYMBOLS

Constants

Z . . . . atomic number

h . . . . PLANCK's constant;
$h = 4,13566733 \cdot 10^{-15}$ eV s

R.T. . . . . . . room temperature;
R.T. = 20 to 26°C, an average of 23°C

Greek Symbols

θ . . . . angle of incidence

θ_B . . . . brewster angle

Δ . . . . phase difference

ϵ_r . . . . real part of complex dielectric function,
also: relative permittivity

κ . . . . extinction coefficient

ϕ . . . . work function

Ψ . . . . amplitude ratio

ρ . . . . complex reflectance ratio

$\vartheta_{\text{sublimator}}$ . . . sublimator temperature

$\vartheta_{\text{deposition}}$ . . . deposition temperature

ϑ_{TMA} . . . . . TMA source temperature

Symbols

C_p . . . . specific heat capacity

E_A . . . . activation energy

E_b . . . . binding energy

E_k . . . . kinetic energy

N_{cycles} . . . . . total number of cycles

n . . . . refractive index

t_{cycle} . . . . . . complete ALD cycle time

$T_{\text{thickness}}$ . . . total thickness

V_t . . . . threshold voltage

Units

A . . . . Ampere

Å . . . . Ångström

°C . . . . Degree Celsius;
0 °C = 273,15 K

eV . . . . electron volt;
1 eV = 1 e · 1 V

Hz . . . . Hertz

K . . . . Kelvin

kg . . . . Kilogram

m . . . . Meter

μm . . . . Micrometer or Micron

min . . . . . . Minute

mm . . . . . . milli-meter;
1 mm = 10^{-3}m

Ω . . . . Ohm

ppb . . . . . . parts per billion

ppm . . . . . . parts per million

ppt . . . . parts per trillion

s . . . . Second

V . . . . Volt;
1 V = 1 $\mathrm{kg\,m^2/A\,s^3}$

kV . . . . kilo-Volt;
1 kV = 10^3 V

LISTS OF FIGURES AND TABLES

LIST OF FIGURES

3.3.1 Schematic illustration of an ALD cycle. 8
3.3.2 The growth behaviour in Atomic Layer Deposition 10
3.3.3 Growth per cycle vs deposition temperature 12

4.2.1 Measuring principle of the Quartz crystal. 22
4.2.2 Schematic illustration of Colnatec™ type RC crystal. 24
4.2.3 The measuring principle of Spectroscopic Ellipsometry. 25
4.2.4 OLS and material models for Al_2O_3 and nickel-based films 26
4.2.5 Schematic of photoelectric effect in XPS. 28

5.3.1 Binary phase diagram of Nickel-Silicon. 34

6.1.1 Experimental setup for an ALD 38
6.1.2 Inside view of the tube reactor 39
6.1.3 Schematic of the experimental setup 39
6.3.1 Evolution of QCM frequency over the ALD process time. 45
6.3.2 Change in the frquency of RC-cut quartz crystal as a function of deposition temperature. 46
6.3.3 The approximate positions for various measurements on the silicon sample. 47

7.2.1 The thickness of AlO_x films versus number of ALD cycles. 50
7.3.1 TGA and DTG curves for Ni(amd) precursor. 51
7.3.2 Variation in the Ni(amd) exposure time. 52
7.3.3 Variation in the air exposure time. 53
7.3.4 XRR measurements for the film grown from Ni(amd)/air ALD process. . . . 54
7.3.5 SEM picture of the film grown from Ni(amd)/air process. 55
7.4.1 TGA and DTA curves for precursor P1. 56
7.4.2 Thermal stability tests for precursor P1 56
7.4.3 Variation in the P1 exposure time. 57
7.4.4 Variation in the H_2 exposure time. 58
7.4.5 Variation in the deposition temperature for P1/H_2 process. 59
7.4.6 SEM pictures of the films grown from P1/H_2 process 60
7.4.7 XPS analysis of the films grown from P1/H_2 process. 61
7.4.8 TGA and DTA curves for precursor P2. 62
7.4.9 Thermal stability tests for precursor P2 63
7.4.10 Deposition tests from P2/second-reactant process. 64

7.4.11 SEM picture of the film grown from P2/second-reactant process. 65
7.4.12 XPS analysis of the film grown from P2/second-reactant process. 66
7.4.13 TGA and DTA curves for precursor P3. 67
7.4.14 Thermal stability tests for precursor P3 67
7.4.15 Deposition tests from P3/H_2 processes. 68
7.4.16 SEM pictures of the film grown from from P3/H_2 process. 69
7.4.17 XPS analysis of the film grown from P3/H_2 process. 70
7.4.18 TGA and DTA curves for precursor P4. 71
7.4.19 Thermal stability tests for precursor P4m. 72
7.4.20 TGA and DTG curves for precursor P5. 73
7.4.21 Thermal stability tests for precursor P5. 74

A.1.1 Deposition temperature with respect to its corresponding voltage values . 103
A.2.1 General oscillator model parameters for NiX optical layer. 103
A.2.2 Optical constants for the parameterized Nix layer. 104

LIST OF TABLES

3.1 ALD growth of Ni-based thin-films from various precursors reported in the literature at the end of Nov, 2014. Deposition method indicates plasma or thermal-based ALD 15
3.2 CVD growth of Ni-based films from various precursors reported in the literature at the end of Nov, 2014. 16

4.1 Origin of peaks in DTA curve [adapted from Wendlandt 1974] 19

6.1 Comparison of nickel precursors obtained from the manufacturer 40
6.2 ALD process parameters 42

7.1 Various properties of the films grown from P1/H_2 process. 60
7.2 Comparison among nickel precursors used in this work. 76

1 INTRODUCTION

Nickel and nickel(II) oxide are widely used in advanced electronic devices [NASF 2014]. In microelectronic industry, nickel is used to form nickel silicide. The nickel mono-silicide (NiSi) has emerged as an excellent material of choice for source-drain contact applications below 45 nm node CMOS technology [Doering a. Nishi 2008; Kittl et al. 2005]. As compared to other silicides used for the contact applications, NiSi is preferred because of its low resistivity, low contact resistance, relatively low formation temperature and low silicon consumption [Chamirian et al. 2003]. Nickel is used in nickel-based rechargeable batteries and ferromagnetic random access memories (RAMs) [NASF 2014]. Nickel(II) oxide is utilized as transistor gate-oxide and oxide in resistive RAMs [Venter a. Botha 2011].

Atomic Layer Deposition (ALD) is a special type of Chemical Vapor Deposition (CVD) technique, that is used to deposit very smooth as well as homogeneous thin films with excellent conformality even at high aspect ratios [Knaut et al. 2013]. It is based on self-terminating sequential gas-solid reactions that allow a precise control of film thickness down to few Angstroms. In order to fabricate todays 3D electronic devices, technologies like ALD are required.

In spite of huge number of practical applications of nickel and nickel(II) oxide, a few nickel precursors are available for thermal based ALD [Knisley et al. 2013, p. 3226]. Moreover, these precursors have resulted in poor film qualities and the process properties were also limited [Knisley et al. 2013]. Therefore in this master thesis, the properties of various novel nickel precursors had to be evaluated. All novel precursors are heteroleptic (different types of ligands) complexes and were specially designed by the manufacturer for thermal based ALD of pure nickel with H_2 as a co-reactant.

In order to evaluate the novel precursors, a new methodology was designed to test small amounts (down to 2 g) of precursors in a very time efficient way. This methodology includes: TGA/DTA curve analyses of the precursors, thermal stability tests in which the precursors (< 0.1 g) were heated at elevated temperatures in a sealed environment for several hours, deposition experiments, and film characterizations. The depositions were monitored with the help of in situ quartz crystal microbalance, while application related film properties like chemical composition, physical phase, thickness, density, roughness and sheet resistance were investigated with the help of ex situ measurement techniques.

Prior to the evaluation of novel nickel precursors, a benchmark ALD process was developed from the reference nickel precursor (Ni(amd)) and air as a co-reactant. The main goal of developing and optimizing such benchmark ALD process was to extract standard process parameters like second-reactant exposure times, Argon purge times, total process pressure, starting deposition temperature and gas flows. These standard process parameters had to be utilized to shorten the process development task (thus saving precursor consumption) and optimize the sublimation temperature for each novel precursor. The ALD behaviour was checked in terms of growth rate by varying the nickel precursor exposure time, precursor temperature and deposition temperature.

I THEORETICAL PART

2 NICKEL AND NICKEL OXIDES

2.1 INTRODUCTION AND EXISTENCE

In 1700s, nickel (Ni) was known as '*kupfernickel*' and discovered in Saxony, Germany [Stimola 2007, p.4]. Ni has atomic number (*Z*) 28 and holds a position within a group of transition metals in a periodic table. In nature, pure nickel is rarely found [Sparrow 2005, p. 10 - 11]. Ni occurs most often in combination with Iron, Sulphur, Arsenic [Haynes et al. 2013]. Ni is widely employed in many industries like aircraft, automotive, power-electronic, semiconductor, memory, steel, rechargeable battery, glass and mint [Davis 2000, p.7-13].

2.2 MATERIAL PROPERTIES OF NICKEL AND NICKEL OXIDE

Nickel is silvery-white in color, hard, malleable and ductile in nature [Haynes et al. 2013]. It has bulk density of 8.9 g/cm^3 at R.T. with a *fcc* crystal structure [Haynes et al. 2013]. Ni has a relatively high melting point of 1,453°C [Davis 2000, p.3]. Ni is a very good conductor of heat and electricity [Cordente et al. 2001, p.567] [Davis 2000]. Pure nickel has a bulk resistivity value of 6.99×10^{-8} (Ω·cm) at R.T. [Haynes et al. 2013].

Nickel is known to form oxides like nickel monoxide (NiO), nickel dioxide (NiO_2) and dinickel trioxide (Ni_2O_3) [Haynes et al. 2013]. NiO is the most stable of all and is green in color with NaCl-type crystal structure. NiO has density of 6.7 g/cm^3 at R.T. and melting point of 1,955°C [Haynes et al. 2013]. The resistivity value for NiO has been reported in the range of 50 (Ω·cm) - 500 (Ω·cm) [Chen et al. 2005] [Venter a. Botha 2011].

At room temperature Ni is not very reactive and does not react readily with most acids and alkalis [Alchin 2014]. Nickel occurs mostly with an oxidation state of +2, but oxidation states from -1 to +4 have also been reported [Haynes et al. 2013]. On the other hand, nickel oxide (NiO) is soluble in acids but insoluble in hot and cold water because the formation of NiO prevents any further oxidation [Haugsrud 2003].

Optical properties of thin nickel and Nickel(II) oxide films are different from bulk material. Ni has a high absorption coefficient in the infra-red regime, and shows less absorption in ultra-violet region because of interband transitions. Pure nickel is a ferromagnetic below its curie-temperature [Chiaverina a. Lisensky 2014].

Nickel(II) oxide is p-type wide-band semiconducting material with a band-gap of 3.8 eV [Venter a. Botha 2011]. NiO is transparent in ultra-violet regime and visible in the near-infrared region [Venter a. Botha 2011]. It has some anti-ferromagnetic properties [Ismail et al. 2013]. Its dielectric constant (ϵ_r) is 10.7 and refractive index is 2.3 in infra-red regime [Chunli et al. 2010].

2.3 APPLICATION IN ELECTRONIC INDUSTRY

Ni is a very important material in electronics [Bradley 2011] [Nickel Institute 2014, p.1]. In microelectronic industry applications, nickel-silicide due to its low contact resistance

and less silicon consumption, has been adopted and integrated to CMOS technology [Lauwers et al. 2004] [Kittl et al. 2005]. It has been utilized for metal gates, schottky barrier source-drain and in nano-rod contact applications [Doering a. Nishi 2008][Léonard a. Talin 2011].

In electronics, many chips utilize Ni/Pd/Au coating for wire bondings and electroless nickel immersion gold (ENIG) as a diffusion barrier [Nickel Institute 2014, p.1]. ENIG also permits lead-free solder. ENIG process has made nickel a popular choice for mobile devices and high density interconnect applications [Lai et al. 2012, p.80] [Bui et al. 2010, p.305]. In magnetic hard disk drives, Ni coatings are applied to protect the disk surface from corrosion. Nickel ferrite has been used to make read-write heads [Hyie et al. 2014, p.797].

The other application of Ni is the development of Ni-metal hydride, nickel-cadmium, fuel cell batteries [Abu-Lebdeh a. Davidson 2013] and the anode material in Li-ion batteries [NASF 2014] [Lund et al. 2014].

Nickel(II) oxide is used as a gate-oxide in transistors, an oxide in dynamic random access memory (DRAM) and in making resistive as well as capacitive components [NASF 2014, p.1] [Venter a. Botha 2011]. Recently nickel(II) oxide has been utilized in resistive random access memory (RRAM), unipolar/bipolar resistance switches [Chunli et al. 2010], high performance super capacitors [Wang et al. 2012] and metal-insulator-metal (MIM) structures [Li et al. 2011]. Nickel(II) oxide is used in mobile touchscreens, computer displays, electrochromic display (ECD) devices [Anders Stenman 2013] [Nickel Institute 2014] and p-type transparent conducting films [Venter a. Botha 2011].

3 ATOMIC LAYER DEPOSITION

3.1 HISTORY

Prof. V. B. Aleskovskii was first to propose the concept of ALD in his Ph.D. thesis, in 1952 [Malygin 2013, p.61]. In 1964, the principle of ALD was published under the name of 'Molecular Layering' [Puurunen 2005]. Later in mid–1970s, a finnish scientist Dr. Tuomo Suntola developed a real ALD technology for thin–film depositions. Since 1980s, ALD technology was adopted and modified according to industrial needs [Parsons et al. 2013, p.050818-2].

3.2 DEFINITION

Atomic layer deposition is a thin film deposition technique that is based on sequential use of self–terminating surface reactions [Miikkulainen et al. 2013]. In ALD the gas phase chemical reactions take place on any activated surface. In order to deposit a layer of material and complete the surface reaction, minimum two reactant gases are required. In contrast to a chemical vapor deposition technique, an ALD uses two different gaseous reactant pulses each separated by purging or evacuating pulse.

3.3 FEATURES OF THERMAL-ALD

3.3.1 ALD growth mechanism – an ideal view

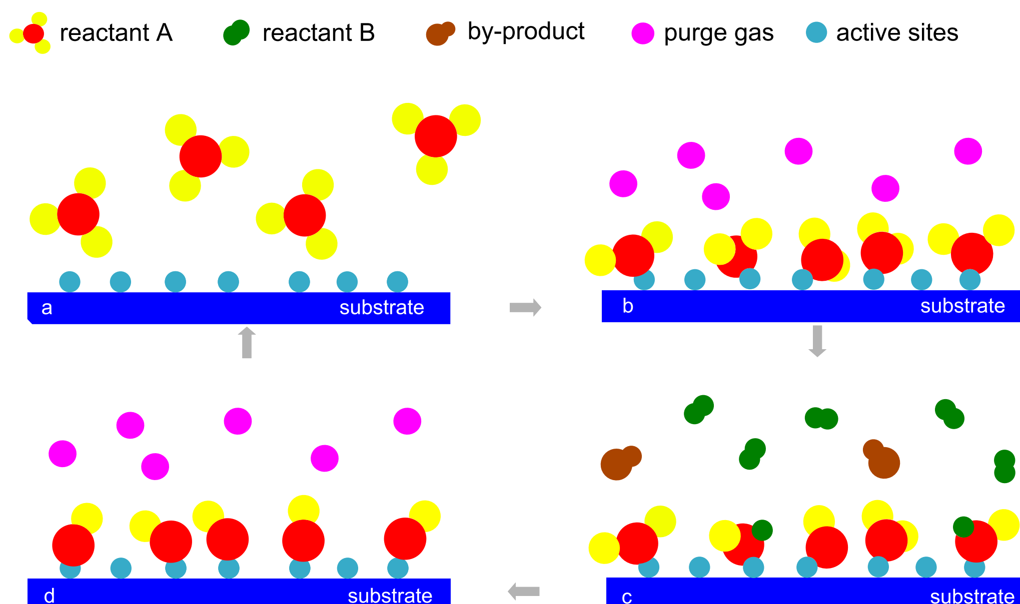

Figure 3.3.1 Schematic illustration of an ALD cycle: *a* and *d* denote the first step and the last step in an ALD cycle

The above figure 3.3.1 shows a four – step ALD growth mechanism and is repeated until a desired thickness of material is deposited. Most of the ALD processes are based on binary reaction mechanism where two surface reactions occur in a self – limiting sequential fashion [George 2010] and is described as follows :

1. **Exposure of the reactant A**: In this step the reactant A is introduced into the chamber. On exposure of reactant A an irreversible chemisorption reaction takes place on the surface of substrate and is shown in figure 3.3.1a. Three main classes of chemisorption mechanisms are ligand exchange, molecule dissociation and association [Puurunen 2005, p. 121301 - 24]. The exposure of reactant A is the first step towards a self-limiting growth mechanism. A self limited growth mechanism is due to the limited availability of active sites on the surface of substrate [George 2010, p.112]. For instance, in figure 3.3.1a there are seven active sites available which allow the chemisoprtion of maximum seven molecules of reactant A. The active sites are the sites on the surface of substrate that are terminated by reactive groups like -OH, -H, -SH etc. These reactive groups make a surface chemical reaction possible.

2. **Purging or evacuation**: After the exposure of reactant A a reaction chamber is purged or evacuated with the help of non-reacting gases like argon as shown in figure 3.3.1b. Inert gas acts as a purging or transport gas. This step is necessary to remove excessive non-reacted precursor molecules as well as the reaction by-products which prevents further incorporation of any contaminations and CVD like effects. A vacuum pump or other mean is required to draw all unnecessary products out of the reaction chamber.

3. **Exposure of the co-reactant B (such as O_3, H_2, NH_3) as shown in figure 3.3.1c**: During this step a co-reactant is introduced into the reaction chamber that allows to accomplish the surface reaction. This exposure further activates the surface for a chemisorption (or reaction) of the reactant A. The gaseous reaction by-products are formed during this step. A precise amount of activation energy (E_A) is required to accomplish above chemical reaction [George 2010, p.113]. This E_A can be obtained from thermal, radiation or enhanced by plasma etc.

4. **Purging or evacuation**: The by-products formed during the previous step are required to be removed from the reaction chamber to prevent any unnecessary surface contaminations as well as CVD like effects. This purging step is quite similar to the step 2 and is shown in figure 3.3.1d [Miikkulainen et al. 2013, p. 3].

This cycle of four steps is called an ALD cycle [Puurunen 2005, p. 121301 - 25][Sharma 2014, p.9]. After a saturated dose of each reactant and purge gas, a monolayer of material is deposited. Ideally, after each ALD reaction cycle a monolayer (ML) covers the activated (i.e. terminated by active sites) surface entirely and is known as the ideal growth per cycle (GPC). The ideal GPC should be constant over the number of ALD cycles. However, practically it is not the case, various phenomenons like: growth inhibition and growth enhancement can lead to different GPC over the number of ALD cycles. Therefore a cumulative GPC is calculated by dividing total thickness ($T_{\text{thickness}}$) obtained over the total

number of ALD cycles (N_{cycles}) and is given by equation 3.1 [Puurunen 2005, p. 121301 - 38].

$$\text{cumulative GPC} = \frac{T_{thickness}}{N_{cycles}} \tag{3.1}$$

The time required to accomplish one ALD cycle (t_{cycle}) can be denoted as 3.2.

$$t_{cycle} = t_{rA} + t_{P1} + t_{rB} + t_{P2} \tag{3.2}$$

Where t_{rA}, t_{P1}, t_{rB}, t_{P2} are: exposure time of reactant A, purge time after exposure of reactant A, exposure time of reactant B and purge time after exposure of reactant B, respectively.

3.3.2 ALD growth behaviour

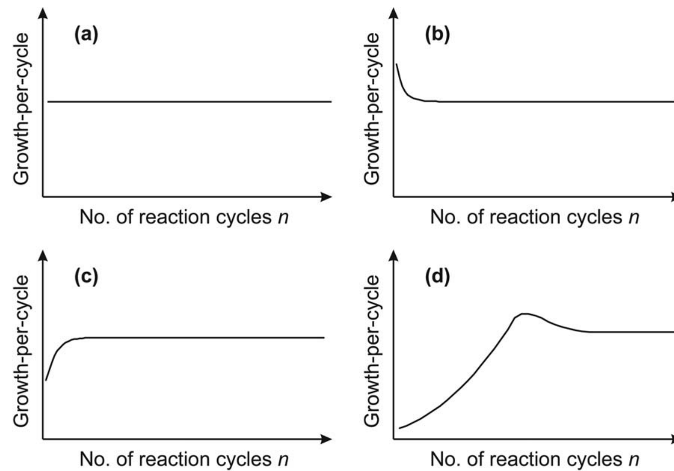

Figure 3.3.2 ALD growth behaviour: (a) linear growth, (b) substrate-enhanced growth, (c) Type 1 substrate-inhibited growth, and (d) Type 2 substrate-inhibited growth [Puurunen 2005]

Based on the variation of GPC with number of ALD reaction cycles, ALD growth behaviour over the number of ALD cycles can be classified into four categories. In above figure 3.3.2, actual GPC is expected to settle to a constant value after sufficient number of ALD reaction cycles. In linear growth, GPC is constant over the number of reaction cycles and is known as steady state growth regime. Linear growth can occur, e.g. if the number of reactive sites on the surface does not change with the cycle number [Puurunen 2005, p. 121301 - 26].

In figure 3.3.2 (b) substrate-enhanced growth, the GPC is higher at the beginning (known as transient regime) than the steady state growth regime. Substrate-enhanced growth can occur, if the number of reactive sites on the substrate is higher than on the ALD-grown material [Puurunen 2005, p. 121301 - 26].

Figure 3.3.2 (c) and (d) shows the growth inhibition of Type 1 and Type 2. In Type 1

the GPC is lower at the beginning of the growth than the steady state growth regime. In Type 2 the GPC reaches to a maximum value before settling. Substrate-inhibited growth is caused by a lower number of reactive sites on the substrate than on the ALD grown material. In substrate-inhibited growth of Type 2 island growth further seems to occur [Puurunen 2005, p. 121301 - 27].

3.3.3 Growth mode

Growth mode is defined by the way a material is arranged on the surface during ALD growth [Puurunen 2005, p. 121301 - 27]. Several growth modes are possible in ALD. In 2-D growth mode (layer-by-layer, Frank-van der Merwe), new material is deposited on the lowest possible unfilled state of the material layer and one ML covers the substrate completely [Puurunen a. Vandervorst 2004, p.7688] [Lüth 2010].

In island growth (Volmer-Weber growth) mode, new material prefers to deposit on already grown ALD material [Puurunen a. Vandervorst 2004, p.7688].

Random growth mode is based on statistical model, where the probability of new material units to grow on all surface sites is equal. Because of self-terminating reactions, random deposition causes smoother layers in ALD than in continuous deposition processes [Puurunen 2003, p.328] [Puurunen 2005, p. 121301 - 27].

3.3.4 ALD temperature window

For an ALD process, it is very important to define a temperature regime where deposition temperature has almost no influence on GPC [Miikkulainen et al. 2013]. Figure 3.3.3 shows a plot, in which GPC is recorded as a function of deposition temperature. In case of an ideal ALD process the GPC remains constant with variation in deposition temperature, and is marked as *b*. Al_2O_3 ALD process from TMA and H_2O is one example of nearly ideal ALD process [George 2010, p.127]. Most of ALD processes diverge from this ideal ALD behaviour. Some ALD systems tend to follow non self-limiting behaviour because the surface species may decompose at higher temperatures (marked by *c*) and shows CVD like effect, while desorption of reactants can lead towards a decreased growth rate marked by *e*.

At lower deposition temperatures, non-ideal behaviour can still exist, e. g. condensation or physisorption of precursor molecules (marked by *a*) [Puurunen 2005]. In case of *d*, decomposition can occur, even at the minimum temperatures required for the surface reactions [George 2010, p.127]. Some ALD processes may never accomplish complete surface reaction. An incomplete surface reactions can be due to limited number of reactive surface groups, insufficient activation energy and steric-hinderance [Hurle 1994]. In case of *f*, the actual ALD window is not possible and the GPC is dependent on tem-

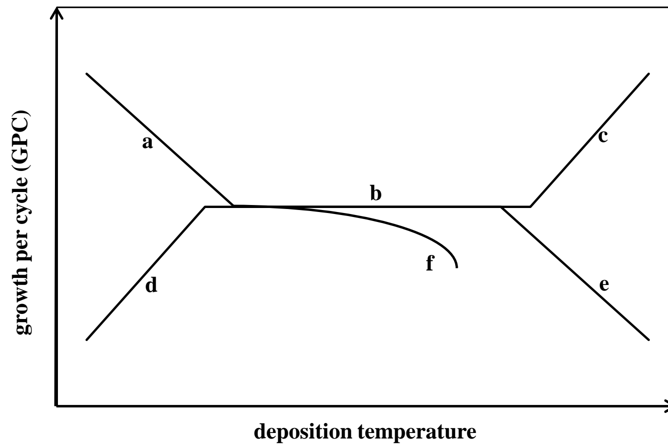

Figure 3.3.3 Growth per cycle vs deposition temperature

perature. This can be due to decrease in number of reactive sites on the surface or incomplete reactions at higher temperatures [Puurunen 2005].

3.4 BENEFITS AND LIMITATIONS

ALD has many advantages over other thin film deposition techniques. The main advantage of ALD over CVD, PVD and sputtering is that an ALD offers a good control over film thickness down to few Angstroms. Depositions done with ALD can have better step coverage and side wall coatings. The properties of the films grown by ALD can be reproduced. ALD can allow high density, low defect density, uniformity and homogeneity over large wafers. In some cases, the physical state of films like amorphous and crystallinity can be controlled by varying the process parameters like substrate temperature [NanoTech 2011]. ALD requires less reactant flux as compared to CVD. ALD gives a choice to grow heterogeneous, graded index and doped layers of different materials. Due to availability of various precursors in the market, it is possible to grow almost all materials used in semiconductor industry [Nalwa 2002, p. 116 - 119] [Puurunen 2005].

Also, in combination of PE-ALD and Flash-ALD, depositions at lower temperature can be achieved especially for substrates like polymers [Henke et al. 2014]. Films grown with the help of ALD can be of low stress due to molecular self-assembly.

The major limitation of ALD is the poor quality of the films due to incorporation of residues (like C, N, H, O etc.) as well as deviation of growth behaviour from an ideal self-limiting reaction mechanism. The residues come predominately from the precursors or other gases. Designing a good precursor for an ideal ALD behavior is very hard, this effects the ALD process the most. Many important materials like Si, Ge, Si_3N_4, noble metals (Ag), several multi-component oxides, cannot be deposited currently by ALD in a cost-effective way [Emslie et al. 2013, p. 3283] [Nalwa 2002]. Recently to overcome this difficulty, many precursors have been designed to deposit Si, Ge, Si_3N_4, SiO_2 films but still it is required to improve the film qualities [Miikkulainen et al. 2013]. Sometimes

the depositions performed by ALD can lead to poor homogeneity over the complete wafer. Low temperature depositions (below 100°C) are very rare for thermal based ALD systems.

For film thickness more than 20 nm, ALD can be more time consuming as compared to other widely used deposition techniques like PVD, CVD and MBE. However, innovative roll-to-roll, spatial and batch ALD processes have been introduced to mitigate low yield and throughput problem [Maydannik et al. 2014].

3.5 PRECURSOR PROPERTIES FOR THERMAL-ALD

The properties of precursors for thermal ALD (thALD) are different from plasma-based or flash-based ALD systems. As in case of plasma-based ALD, the low reactive precursors can also produce good results but in case of thALD, the precursors should possess the following properties [Niinisto et al. 2014, p.222] [Dussarrat 2014, p.234]:

1. **Volatility**: they must posses high volatility below 200 °C.
2. **Thermal stability**: they must not self decompose, neither while delivering nor at deposition temperatures.
3. **Reactivity**: should be highly reactive towards co-reactants and enough reactive for chemisorption to take place on initially pre-treated substrates.
4. **State**: preferably liquid, to prevent clogging inside the gas lines and handling problems. Also the impurity levels in precursors should be low.

Recently, a trend has been seen towards the development of heteroleptic (different ligands) precursors for ALD based systems. The heteroleptic precursor design offers higher reactivity, volatility, better thermal stability and low melting point over the homoleptic class of precursors [Niinisto et al. 2014, p.224]. They also improve the ALD process window, GPC, step coverage and conformality [Blasco a. Girard 2014]. Sometimes heterolepetic precursor adds an extra bulky ligand that can decrease the GPC by introducing the steric-hinderance [Dussarrat 2014].

3.6 ALD & CVD OF NICKEL – A LITERATURE SURVEY

A brief literature review is devoted to this section, that covers only a small part of the entire work done on nickel-based thin films. According to the previous research done, various precursors for both CVD as well as ALD have been adopted to deposit nickel-based thin films. As a summary, some of the main precursors for ALD and CVD of nickel-based films have been listed in Tables 3.1 and 3.2. In general, nickel metal films are obtained by two different approaches and are as follows [Utriainen et al. 2000, p.151]:

1. **Direct method (DM) of metal deposition**: In DM, nickel metal was deposited directly from sequential surface based chemical reactions on different substrates.

2. **Indirect method (IDM) of depositon for nickel-based thin films**: In IDM, no pure metal was deposited but in the form of Ni−X, where X is either nitrogen, oxygen, carbon or silicon atom. In order to obtain pure metal film, a reduction step is required. A reduction of NiX based thin films into pure Ni film can be achieved by hydrogen, ammonia etc. The various deposition methods for IDM approach are, ALD, CVD, MOCVD, DLI-CVD and pulsed-CVD.

However, in the later case, reduction of denser NiO causes the structure deformation and pinholes in the resulting Ni metal-film [Utriainen et al. 2000, p.157]. Carbon and nitrogen were also left inside the film after reduction, that caused increase in the resistivity [Li et al. 2010, p.3061].

Recently, two patents have been granted for the development of new nickel-organic precursors for thALD, PEALD and CVD [Lansalot-Matras et al. 2014] [Winter et al. 2014]. Unfortunately, no publication data on such precursors have been found so far. Also, two heteroleptic precursors $Ni(MA)(^{i}PAMD)_2$ and Ni(Me−allyl)(PCAI) have been chosen for nickel-based thin film depositions by thALD and PEALD processes [Blasco a. Girard 2014]. Recent review articles on nickel-based thin films have been studied and only the most frequently and widely used Ni-precursors have been discussed in this section [Cloud et al. 2014] [Emslie et al. 2013] [Knisley et al. 2013].

Table 3.1 ALD growth of Ni-based thin-films from various precursors reported in the literature at the end of Nov, 2014. Deposition method indicates plasma or thermal-based ALD

Mat. Depo.	Depo. method	Prec_1/ prec_2	Substrate/s	Depo. temp. (°C)	Growth rate	Prec. temp. (°C)	Comments	References
Ni	PEALD	$Ni(MA)(^{i}PAMD)_2/NH_3$	Si	200-240	0.7 Å/cyc	50	fine, conformal, metallic and low C contaminations	[Blasco a. Girard 2014]
Ni	PEALD	$Ni(\eta MDA)/\ NH_3$; H_2	SiO_2	300	1.2Å/cyc	50	high purity and conformal Ni film	[Yokota et al. 2013]
Ni	PEALD	$Ni(dmamb)_2$ /NH_3-plasma; H_2-plasma	Si,SiO_2	200 ,250	0.5, 0.8 Å/cyc	70	use of NH_3-plasma as co-reactant leads in low C contamination and resistivity	[Lee et al. 2010]
Ni	thALD	$Ni(dmamb)_2$ /NH_3	SiO_2, Si, OTS	300	0.64 Å/cyc	70	Low O, N, C contaminations	[Kim et al. 2011]
Ni	thALD	$Ni{-}(OCH)_2$ /N_2H_4,HCOOH	Si	175	0.5	95	low temp th-ALD	[Knisley et al. 2011] [Winter et al. 2014]
Ni	thALD	$Ni(hfip)_2$ /H_2	Si Poly-Si	220	1.87 Å/cyc	-	low C contaminations	[Ha et al. 2010] [Yang et al. 2007]
Ni	thALD	$Ni(^{i}PrMeAMD)_2$ /H_2	SiO_2, C, glass, WN	250	0.04 Å/cyc	55	very low growth	[Lim et al. 2003a] [Lim et al. 2003b]
Ni	thALD	$Ni(dmamb)_2$ /H_2	Si	200-250	1.21 Å/cyc	70	Ni_3C formed, decreases the resistivity	[Do et al. 2006]
NiO to Ni	thALD	$Ni(acac)_2$/ O_3; H_2-plasma	Si(100),Al, Ti, glass	250	0.62 Å/cyc	155	reduction causes pinhole and structure deformation	[Utriainen et al. 2000]
NiO_X to Ni	thALD	$Ni(amd)/H_2O$;later reduced in H_2	Si,SOI ,SiO_2,Si_3N_4, glassy-carbon	200	1 Å/cyc	80	low temperature anneal leads to smooth and conductive Ni film	[Li et al. 2011]
NiO	thALD	$Ni(dmamb)_2$ /H_2O	SiO_2,glass	100-140	1.4 Å/cyc	-	low C contamination with controllable Ni atom Conc.	[So et al. 2007] [Chung et al. 2011] 100-140
NiO	thALD	$Ni(dmamp)_2$ /H_2O	Si	100-170	0.8Å/cyc	90	smooth NiO film, no C contamination	[Yang et al. 2005]
NiO	thALD	$Ni(thd)_2$/ H_2O	Si, MgO	260	0.4Å/cyc	165	rough and granular film, 12% C contamination	[Lindahl et al. 2009a]
NiO	thALD	$Ni(thd)_2/H_2O$; NH_3	Si	250	0.4Å/cyc	165	amorphous NiO film	[Lindahl et al. 2010]
NiO	thALD	$Ni(Cp)_2$,$Ni(EtCp)_2$ /O_3	Si(100)	150-300	3.2,0.9 Å/cyc at 150°C	40,80	dense, granular and rough NiO films	[Lu et al. 2008]
Ni_3N	ALD	$Ni(^{t}Bu_2{-}DAD)_2$/ $NH_2{-}NMe_2$	Si	220-240	0.7 Å/cyc	50	fine Ni film, low C contamination	[Knisley 2012]
NiN_X	PEALD	$Ni(amd)/NH_3$ remote plasma	SiO_2	125-175	0.9 Å/cyc	85	highly pure, dense and continuous film	[Clendenning 2010]

Table 3.2 CVD growth of Ni-based films from various precursors reported in the literature at the end of Nov, 2014.

Mat. Depo.	Depo. method	Prec_1/ prec_2	Substrate/s	Depo. temp. (°C)	Growth rate	Prec. temp. (°C)	Comments	References
Ni_9N	CVD	$Ni[(t{-}Bu)_2Amd]_2$ $/NH_3$	Si	150-300	2.8nm /min	52	C contaminated film	[Cloud et al. 2014]
Ni_xN	DLI-CVD	Ni(amd)/ NH_3;$NH_3{-}H_2$ gas	Si,SOI, SiO_2	160-200	5nm/min at 200°C	80	smooth, conformal, continuous film	[Li et al. 2010]
Ni_3N	CVD	$Ni(thd)_2$ $/NH_2$	Si Poly-Si	205-290	1.1nm /min	160	initial-island growth	[Lindahl et al. 2009b]
$NiSi_x$	CVD	$Ni(PF_3)_4$ $/Si_3H_8$-H_2	Si	180-250	130nm /min at 200°C	50	conformal, dense film	[Ishikawa et al. 2007]
NiO	CVD	$Ni(Cp)_2$,$Ni(EtCp)_2$ $/O_2$	Si	400	4.5nm /min	60	good quality NiO film	[Yang et al. 2014] [Yeh a. Matsumura 1997]
NiO nanorods	CVD	$Ni[(tta)_2]$tmeda $/O_2$	alumina-template	500	3.3nm /min	-	very dense, thick NiO nanorods	[Malandrino et al. 2007]
NiO	CVD	$Ni(ktfaa)_2$/ H_2-pyrolysis	Cu, Ni	250-350	-	190	good adhession of Ni on Cu plate	[Bakovets et al. 2005]
NiO	CVD	$Ni(dmamb)_2$/ O_2	Si, SiO_2,Pt	230-410	-	30	low C content	[Min et al. 2007]
NiO	CVD	$Ni(acac)_2$ $/H_2O$	ITO, glass BSG	250-400	2.1nm/min at 280°C	200	amorphous NiO film	[Maruyama a. Tago 1993] [Maruyama a. Arai 1993]
NiO	CVD	$Ni(Cp)_2$/ O_2	Si	200-500	3.3nm /min	60	amorphous NiO film	[Kang a. Rhee 2001]
Ni	CVD	$Ni(EtCp)_2$/ H_2-Ar	Si	446-597	2nm/min at 597°C	97	low C (< 2 at.%) content	[Alexandrov a. Protopopova 2011]
Ni	CVD	Ni(Cp)al $/H_2$	SiO_2,Si	80-200	13nm/min at 120°C	25	low C content	[Kada et al. 2005]
Ni	CVD	$Ni(Cp)_2$/ H_2	BSG	200-	1.3nm /min	60	higher purity, crystallinity, lower resistivity film	[Kang a. Rhee 2000]
Ni	CVD	$Ni(dmg)_2$ $/H_2$	Si, quartz	300-600	2.9nm/min at 450°C	220-250	granular, rough film	[Becht et al. 1995]

4 METROLOGY

4.1 THERMAL ANALYSIS OF PRECURSORS

4.1.1 Introduction

Thermal analysis (TA) is a term used to describe analytical experimental techniques, in which the sample behaviour is investigated as a function of temperature [Hatakeyama a. Liu 1998, p.3]. In 1945, the commercial thermogravimetry was developed [Hatakeyama a. Liu 1998, p.3]. Since then TA techniques like thermogravimetric analysis (TGA), differential scanning calorimetry (DSC) and differential thermal analysis (DTA) are widely used to analyse the physical properties of materials. The use any TA technique alone may provide insufficient information to understand the thermal behaviour of material. Therefore, TA techniques in combination with other methods like evolved gas analysis (EGA), fourier transform infrared spectroscopy (FTIR) and mass spectrometry (MS) are used to analyze the physical and chemical properties of material as a function of temperature [Hatakeyama a. Liu 1998, p.3].

4.1.2 Principal techniques for thermal analysis

Thermogravimetric analysis (TGA)

TGA is an experimental analytical technique in which the mass m of a sample is measured and continuously monitored as a function of temperature T or time t and can be described as $\Delta m = f(T,t)$ [Gabbott 2008, p.88]. The mass (typical range 0.1 μg – few mg) is placed in a tiny vessel (closed, perforated or open and can be made up of alumina, glass, ceramic etc.) on a thermobalance [Gabbott 2008, p.90]. The sample is heated at a constant heating rate (so-called dynamic measurement) or held at a constant temperature (isothermal measurement), but may also be subjected to non-linear temperature programs such as those used in sample controlled TGA experiments [Gabbott 2008, p.88].

The TGA curve is plotted between mass loss Δm and T or t. This mass loss can be negative as well as positive indicating the decrease or increase in mass. This resulting curve gives information concerning the thermal stability of original sample, intermediate compounds and residue [Hatakeyama a. Liu 1998, p.4]. TGA does not provide information about melting, crystallization and glass transition because such thermal events do not bring any change in the mass of sample. On the other hand, TGA provides information such as decomposition, sublimation, reduction, desorption, absorption and vaporization [Hatakeyama a. Liu 1998, p.17].

Sometimes, differential thermogravimetry (DTG) is used to interpret the TGA curve. DTG is a method in which a first derivative of thermogravimetric curve with respect to T or t is plotted and can be given by relation $\frac{dm}{d(T,t)} = f(T,t)$. DTG curve provide information regarding the rate of change of mass and area under the peak in a DTG curve shows

the total mass change of the sample [Wendlandt 1974, p.27]. Sometimes, the higher derivatives of TG curve are required to resolve multiple phenomenons that are overlapping. The most frequently used higher derivative of TG is the double derivative of TG curve (DDTG) [Gabbott 2008, p.5].

Differential thermal analysis (DTA)

Differential thermal analysis is a technique in which a temperature difference ($\Delta T = T_{reference} - T_{sample}$), that is associated with physical or chemical properties of material with respect to the reference material is recorded as a function of temperature or time [Hatakeyama a. Liu 1998, p.4]. The ΔT causes either endothermic or exothermic peaks and can be related to various phenomenons that can occur (as shown in table 4.1) [Wendlandt 1974, p.230]. The area under such endo/exo-thermic peaks gives an important information regarding different enthalpies (ΔH), such as enthalpy of decomposition, sublimation, fusion, melting and chemical reaction etc.

Table 4.1 Origin of peaks in DTA curve [adapted from Wendlandt 1974]

Phenomenon	**Enthalpy change**	
	Endothermic	Exothermic
Physical		
Sublimation	X	
Desorption	X	
Absorption	X	
Adsorption		X
Crysatalline transition	X	X
vaporization	X	
Chemical		
Decomposition	X	X
Oxidation		X
Dehydration	X	

Differential scanning calorimetry (DSC)

DSC is a dynamic thermal analysis technique where the heat flux between sample and a reference material is measured, whilst reference and sample materials are subject to controlled temperature program [Hatakeyama a. Liu 1998]. In a DSC curve, heat flux ($\frac{dQ}{dt}$) is plotted against temperature T or time t. Sometimes DSC is more advantageuos over DTA because it is more sensitive in determining various enthalpies and specific heat capacities (C_p).

4.1.3 Combining TA techniques with other analysis methods

In general, TGA/DTG analysis alone do not provide a complete understanding of material behaviour as a function of temperature. Thermogravimetry technique can provide us the information about various phenomenons like decomposition, sublimation, reduction, desorption, absorption and vaporization but it cannot distinguish among such phenomenons [Hatakeyama a. Liu 1998, p.17]. For instance in many cases it is almost impossible to distinguish sublimation from decomposition by TGA/DTG alone. Therefore, TGA with MS or TGA with EGA analysis is required to perform better thermal analysis of a material, this method helps to highlight the decomposition from sublimation.

4.1.4 Thermal analysis of novel Nickel precursors - theoretical aspects

Nickel precursors (P1 to P5) in this work have been evaluated, in terms of thermal curve analysis. The thermal curves include TGA, DTG and DTA analysis. All TA measurements were performed on a thermobalance from NETZSCH TG-209F1 under N_2 atmosphere. Depending on precursor type either Al_2O_3 or stainless steel open-cup type crucibles were used. For all analysis, a constant heating rate of 10°C/min at atmospheric pressure was applied to heat the samples, starting from 21°C to 860°C approximately.

Prior to thermal curve analysis, some of the important definitions, terminologies and points of interest are explained below:

1. **Sublimation**: sublimation is a physical transition of a material that happens directly from solid to gaseous phase without going through an intermediate liquid state. Sublimation is an endothermic process, that leads to smooth and uninterrupted exponential mass loss in TGA curve [Yu et al. 2014, p.5] [Sean Barry 2014a, p.1].

2. **Decomposition**: Here, decomposition is defined as the thermal degradation of a substance. T_{decomp} indicates the approximate temperature for decomposition. T_{decomp} point is evaluated by superimposing two factors; non-exponential mass-loss behaviour and exothermic peak in DTA curve. It is well established in literature, to relate an exothermic peak to decomposition or partial ligand loss [Arockiasamy et al. 2010] [Bakovets et al. 2005].

3. **Differentiating sublimation from decomposition**: Any exothermic peak in DTA/DSC, that is caused during the mass loss in TGA curve can be due to decomposition, oxidation or other chemical break down pheneomenon, while any endothermic peak indicates sublimation [Wendlandt 1974] [Sean Barry 2014b]. Moreover, after a thermal treatment if the residue is more than 5% of initial mass indicates no clean sublimation but a thermal decomposition [refer to TGA examples in Blasco a. Girard 2014; Sean Barry 2014b].

4. **Melting**: causes a sharp and symmetric endothermic peak that occurs in DTA/DSC with no noticeable mass loss in TGA curve [Gabbott 2008]. However, in some cases melting can cause some tiny wobblings in TG curve.

5. **Pressure adjustment**: the entire TGA curve subject to shift towards lower temperatures at lower pressures [Lansalot-Matras et al. 2014].

6. **Onset point**: the onset points are marked by an intersection of two tangents drawn from the different slopes in TGA curve [more description in Gabbott 2008, p.104]. In this report for a subliming material $T_{5\%\ \mathrm{mass\ loss}}$, $T_{\mathrm{onset_1}}$, and $T_{\mathrm{onset_2}}$ indicate the temperature value at which a 5% of the mass, 2% of the mass and almost complete mass is lost, respectively. In order to define $T_{\mathrm{onset_1}}$ point, a tangent was drawn on a TGA curve where 2% mass loss was visible. The goal for defining $T_{\mathrm{onset_1}}$, was to set the final temperature point boundary, beyond that $\vartheta_{\mathrm{sublimator}}$ was never raised to prevent fast dissipation of mass. The sublimator temperature value was extracted from $T_{\mathrm{onset_1}}$ point and is given by a relation 4.1.

$$\vartheta_{\mathrm{sublimator}} \approx T_{\mathrm{onset_1}} - 50°\mathrm{C} \tag{4.1}$$

4.2 FILM AND GROWTH CHARACTERIZATION

4.2.1 Quartz Crystal Microbalance

Introduction

In late 18th century, Jacques and Pierre Curie demonstrated the piezoelectric effect [Jacques Curie a. Pierre Curie 1880, p.294]. They showed that if a mechanical stress is applied to certain crystals like quartz (α-SiO_2), a corresponding electric field is developed across the crystal and vice-versa [Manbachi a. Cobbold 2011]. In 1959, Sauerbrey used the term quartz crystal microbalance (QCM) and demonstrated the dependence of quartz oscillating frequency on the change in surface mass [Sauerbrey 1959, p.206]. For many years, QCM has been valued for its use as in situ growth monitoring and probing the surface chemistry in ALD [Rocklein a. George 2003, p.4975].

Working principle

The operating principle of QCM is based on a resonace property of piezoelectric material. As shown in figure 4.2.1, an alternating electric field is applied to a crystal through metallic electrodes such as gold, silver, nickel and aluminum [Colnatec 2014a]. An applied electric field (or high frequency *f*) allows the piezoelectric crystal to experience a longitudinal mechanical strain. On removal of applied field, the crystal tends to restore its original orientation. The alternating electric field causes a crystal to swing in a shear-mode. The swinging in shear-mode causes a crystal to vibrate with a resonant frequency

f_0. The f_0 is a function of total mass m of the crystal and is dependent on the crystal thickness d, density ϱ_q of quartz crystal, at particular orientation, shear modulus μ_q and is given by formula 4.2 [Smith a. Shirazi 2005, p.203].

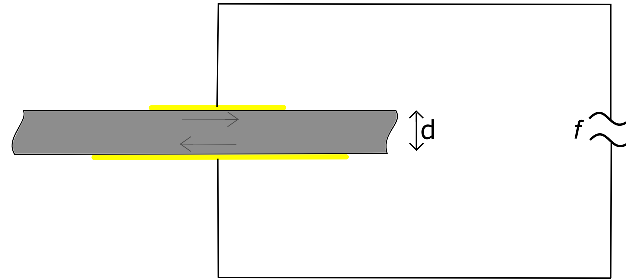

Figure 4.2.1 Schematic side view of Quartz crysal microbalance with gold electrodes: d is the crystal thickness, f is alternating high frequency

$$f_0(m) = \frac{1}{2d}\sqrt{\frac{\mu_q}{\varrho_q}} \tag{4.2}$$

Mass of the crystal per unit active area A can be translated in the form of crystal density and thickness and is given in relation 4.3.

$$M = \frac{m}{A} = d \cdot \varrho_q \tag{4.3}$$

From formula 4.2 and formula 4.3, $f_0(M)$ can be written as 4.4.

$$f_0(M) = \frac{\sqrt{\mu_q \varrho_q}}{2M} \tag{4.4}$$

However, $f_0(M)$ starts to dampen by factor Δf_0 if a small mass ΔM is deposited on active unit area A; e. g. on completion of each ALD cycle [Sauerbrey 1959, p.208] and is give in 4.5.

$$f_0(M) + \Delta f_0 = \frac{\sqrt{\mu_q \varrho_q}}{2(M + \Delta M)} \tag{4.5}$$

By subtracting 4.4 from 4.5, gives us change in frequency corresponding to change in mass and can be formulated as 4.6.

$$\Delta f_0 = -\frac{\Delta M \sqrt{\mu_q \varrho_q}}{2M(M + \Delta M)} \tag{4.6}$$

From 4.4 and 4.6, Δf_0 can be written as 4.7

$$\Delta f_0 = -\frac{f_0(M)\Delta M}{M(1 + \frac{\Delta M}{M})} \tag{4.7}$$

Now assume for very thin film depositions, where $\frac{\Delta M}{M} >> 1$, and $f_0(0)$ is the resonant frequency with no mass deposited on active area a. Thus the formula 4.7 for Δf_0 can be

written as function of Δm, with S as sauerbrey's constant [Sauerbrey 1959].

$$\Delta f_0 = -\left[\frac{f_0(0)}{ad\varrho_q}\right]\Delta m = -S\Delta m \tag{4.8}$$

Sauerbrey's equation 4.8 cannot be applied to inelastic subjects such as bio-cells and any viscoelastic films. Moreover, if the mass change is more than 2% of the crystal mass then there is a no linear relationship between Δf and Δm [Vashist a. Vashist 2011, p.1]. To overcome this limitation QCM with dissipation was developed [König et al. 2014]. The other limitation of correct interpretation of change in frequency Δf with mass uptake Δm is due to non-linear dependencies like change in the surface area, temperature, pressure, stress build-up, on deposition after each ALD cycle [Grimshaw 2013, s.6,10] [Colnatec 2014a].

Quartz crystal orientations

A quartz crystal plate is cut out from a bulk material to a specific orientation, that allows an acoustic wave propagation perpendicular to the crystal surface [Vashist a. Vashist 2011, p.1]. A quartz crystal can be cut into many orientations such as AT, BT and IT etc. and each cut has a specific vibrational mode. The AT-cut is cut at angle of 35°15' from its main crystal axis and it has a shear vibrational mode.

Applications

QCM sensor has many applications in various fields of science. It is utilized in monitoring the growth behaviour and surface chemistry in thin film technology [Rocklein a. George 2003] [Lu a. Czanderna 1984, p.63,197] e.g. in ALD, CVD and MBE [Colnatec 2014a]. QCMs are used in sensing bio-molecules, micro-organisms and screening of drugs and biomaterials [Cheng et al. 2012, p.1951] [Johannsmann 2014] [Marx 2003, p.1099]. QCM sensors have been employed in the analysis of gaseous species, humidity analysis, analysis of an etching rate of various corrosive species like argon or hydrogen plasma radicals, volatile compound and composition analysis [Vashist a. Vashist 2011, p. 2 - 8] [Lu a. Czanderna 1984]. It has been widely applied in electrochemistry industry [Arbuckle-Keil 2002].

QCM sensors and software used in this work

In this thesis work, two types of quartz crystals were used: standard AT-cut quartz crystal from company Inficon and RC-cut quartz crystal from company Colnatec™. AT-cut quartz crystal was only used in the early stage of process development and to test the operation of tube-reactor ALD tool. An AT-cut crystal is very sensitive to temperature changes above 50°C [Martinson et al. 2014, p.1]. Therefore it was discarded for ALD experiments

above 150°C. For all experiments mentioned in this work, RC-cut crystal was adopted due to its insensitivity towards temperature and film stress changes between 20°C and 250°C temperatures [Colnatec 2014b]. RC-cut crystal has a plano-convex contour to keep crystal vibrations at the center of active area [Grimshaw 2013, s.8]. It has gold-plated electrodes as shown in figure 4.2.2 with an active area of 33 mm^2 and is 0.025 mm thick [Grimshaw 2013, s.7]. RC-cut crystal has a fundamental frequency in the range of 5.975–5.993 MHz. The resistance between the gold electrodes is $< 40\ \Omega$ [Colnatec 2014a].

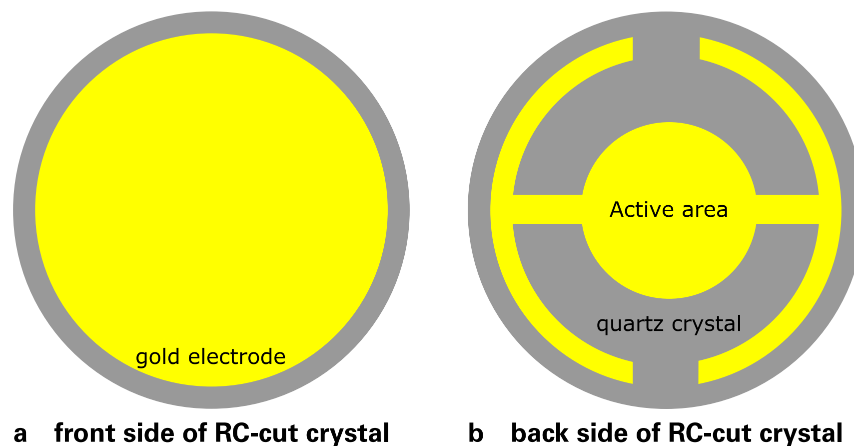

Figure 4.2.2 Schematic of Colnatec™ type RC crystal [Colnatec 2014a, model number: CNT06RCIG]

EON™ process control system software and controller were used to monitor the frequency, temperature and rate with time. The sampling rate of 0.3 s was used, which means after an interval of 0.3 s the data values were logged into a .csv file. The sampling rate between 0.1 s and 1 s can be selected.

4.2.2 Spectroscopic Ellipsometry

Introduction

Ellipsometry was first defined mathematically and prototyped by Paul Drude in 1887. In the last century, ellipsometry has been extensively developed and still the research is going on to make it better [Fujiwara 2007, p. 8] [Accurion 2013]. Ellipsometry is an optical technique used for surface analysis, imaging and metrology of almost every material [Accurion 2013]. Ellipsometry is mainly used to determine film properties like thickness and optical constants. It is also implemented to characterize composition, crystallinity, roughness, doping concentration, and other properties that are related to change in optical response of the material [Sharma 2014]. The term 'ellipsometry' comes from the fact that polarized light upon reflection with sample gets elliptically polarized and spectroscopy comes from the measurements that are carried out in the wide range of

electro magnetic (EM) spectrum e. g. (200nm to 1700nm approx.) [Fujiwara 2007, p. 1]. SE technique can be deployed to in situ and ex situ measurements [Sharma 2014, p. 18].

Measuring principle

In Ellipsometry, the incident light beam with a known polarization state falls on a sample. On reflection, the polarization state of the light beam is changed. The change in the polarization state of an incident light is dependent on film or stack properties like thickness, optical constant and roughness. This is the basic idea of ellipsometry and is described briefly as below with the help of figure 4.2.3.

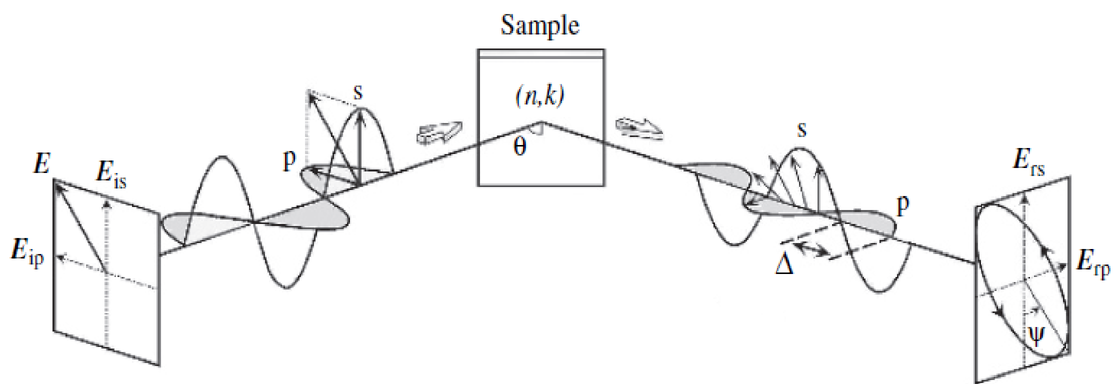

Figure 4.2.3 Schematic illustration of the measuring principle of Spectroscopic Ellipsometry [taken from Fujiwara 2007, p.82]; figure shows the incident light with known polarization state and after reflection the polarization has been changed

The coordinates of p and s (the s component is parallel, the p-component is perpendicular to the sample surface) polarizations describe the polarization state of a light. A ratio of fresnel amplitude reflection coefficients (r_p, r_s) for p and s polarized light is defined by $\rho = \frac{r_p}{r_s}$. This ratio is expressed in terms of measured Ψ, Δ values where Ψ is the amplitude ratio and Δ is the phase difference between the reflected s and p wave components [Fujiwara 2007, p. 81 - 84].

In figure 4.2.3 a linearly polarized light beam E strikes the sample at incident angle θ. E contains both parallel (E_{ip}) and perpendicular (E_{is}) polarized wave components. For a linearly polarized light beam $E_{is} = E_{ip}$ because the amplitudes of p and s polarizations are the same and the phase difference between the polarizations is also zero. The reflected beam has corresponding s and p wave components shown as E_{rs} and E_{rp} in figure 4.2.3. Now these reflected wave components, undergo a significant change in its amplitude and phase for both p and s polarized states [Fujiwara 2007, p.82]. This change in polarization is measured and is commonly written as:

$$\rho \equiv \left[\frac{E_{rp}}{E_{ip}}\right]\left[\frac{E_{rs}}{E_{is}}\right] = \tan(\psi).\, \mathrm{e}^{\,i\Delta} \tag{4.9}$$

An accurate ellipsometry measurement is done when an incident light beam is irradiated onto a sample at the brewster angle (as the difference between r_p and r_s is maximized at brewster angle θ_B, hence the measurement sensitivity is maximum too).

The measured Ψ and Δ values are used to calculate film thickness and optical parameters [Dale E. Morton et al. 2002, p.3] [Fujiwara 2007, p.40]. Particularly, when a sample structure is simple, the Ψ is characterized by the refractive index n and Δ represents light absorption described by the extinction coefficient κ. In this case, the n and κ can be determined directly from the Ψ and Δ obtained at particular wavelength [Fujiwara 2007, p.84].

Modelling and fitting the film parameters

In ellipsometry, film properties like thickness, optical constants and roughness etc. can be described indirectly with the help of an accurate SE model. In general, models are of two types: optical layer stack (OLS) model and material model. OLS models consist of layers of different materials e. g. single or multi layer etc. These layers can be further elaborated with roughness and graded indices. Figure 4.2.4 shows different fit parameters t_1 and t_2 that must be evaluated. A specific OLS model depends on a best assumption made according to a specific deposition process [Sharma 2014, p. 20]. For instance, in this research Al_2O_3 and nickel-based thin film was deposited on silicon substrate (with $\approx$ 2 nm of native oxide) as shown in figure 4.2.4.

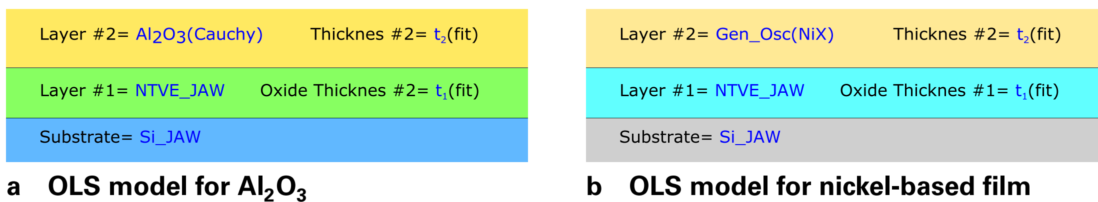

a OLS model for Al_2O_3 **b OLS model for nickel-based film**

Figure 4.2.4 Optical layer stack and material models for Al_2O_3 and nickel-based films

The material model represents the optical properties of material and film thickness. According to the optical properties of sample an appropriate dielectric function model is selected from the material database or developed by using oscillator functions. The various dielectric function models are Lorentz, Sellmeier, Cauchy, Tauc-Lorentz, and Drude models. Basically, all these models are derived from the Lorentz oscillator model [Fujiwara 2007, p.160]. In figure 4.2.4(b), a similiar material model was built for nickel-based (NiX) films from a general oscillator, that is described more in appendix A.2. The material models used in this work were: NTVE_JAW from [Herzinger et al. 1998] for natOx, Si_JAW [proposed by Jellison and modine] and for Al_2O_3 a cauchy model was used.

After defining the accurate stack model, fit parameters like thickness and optical constants are fitted by using some algorithms e.g. Levenberg-Marquardt method [J.A. Wool-

lam Co. 2011, p.3-42]. Fitting is performed to improve the agreement between the measured and model generated SE data [J.A. Woollam Co. 2011, p.3-42]. The quality of fit is defined by the mean-squared-error.

MSE definition

During the SE data evaluation, it is necessary to minimize the mean-squared-error (MSE). MSE describes the fit quality, between model-originated and the measured Ψ and Δ values. Mathematically, MSE is defined by equation 4.10 [Himcinschi et al. 2001, p.808].

$$MSE = \sqrt{\frac{1}{2L-K}\sum_{i=1}^{L}\left[\left(\frac{\Psi_i^{mod}-\Psi_i^{exp}}{\sigma_{\Psi,i}^{exp}}\right)^2+\left(\frac{\Delta_i^{mod}-\Delta_i^{exp}}{\sigma_{\Delta,i}^{exp}}\right)^2\right]} \quad (4.10)$$

Where L is number of experimental duplets (Ψ, Δ), K is number of fit parameters and σ is the standard deviation on the experimental data points [Himcinschi et al. 2001, p.808]. For a very good and unique fit, the MSE value is the lowest value possible [J.A. Woollam Co. 2011, p.3-45]. For accurate determination of model parameters, MSE should be constant over the desired range of wavelength and should be minimum among various allowed OLS models for a particular deposition [J.A. Woollam Co. 2011, p.3-44][Dale E. Morton et al. 2002, p.1].

Advantages and limitations

Spectroscopic ellipsometry has many advantages over conventional techniques based on reflection and absorption. Firstly, SE is a ratio based measurement technique, therefore the intensity fluctuations in the light source has almost no effect on the measurements [Dale E. Morton et al. 2002, p.1]. Thus SE allows estimation of the film thickness and optical constants with high precision [Fujiwara 2007, p.136]. Secondly, SE can determine the film thickness with high resolution (< 1 nm) and accuracy. It is fast in measurement and the delay can also be introduced (in case of triggered measurements). Third, it can be incorporated to measure a real time in situ growth rates [Fujiwara 2007, p.3]. Provided that light reflects from the sample surface, ellipsometry can be used to measure a wide variety of thin films including dielectrics, semiconductors, metals, organics, and composites of materials etc. [Dale E. Morton et al. 2002]. Spectroscopic ellipsometry can even be applied to multilayer structures, with films of different materials. Moreover, substrate temperature, quality, absorption and desorption of material can also be measured [B. Johs et al. 1999].

However, SE has few limitations including the necessity of sophisticated accurate optical models for analyzing the data. A characterization of optical constants for a low absorption materials is very difficult [Siah et al. 2013, p.452]. Thickness measurements for very rough films can include many erors, due to scattering of the light from a rough

surface [Dale E. Morton et al. 2002], but this can be corroborated with the help of other surface analysis techniques like SEM and AFM. The upper thickness limit for SE measurement depends on the material and wavelength used e. g. for metals and absorbing films, the upper detection limit is below 50 nm which is dependent on extinction coefficient (κ) [Hilfiker et al. 2014]. In combination with array scan technique, it is possible to analyze the whole wafer surface area of 300 mm or more but at the expense of time.

4.2.3 X-Ray Photoelectron Spectroscopy

Introduction

X-ray photoelectron spectroscopy (XPS) is a type of an electron spectroscopy. XPS allows the quantitative and sensitive chemical surface analysis. XPS provides information regarding the elemental composition, chemical state and empirical formula of the elements present in top 1-3 nm thick sample surface. XPS also allows the depth profiling of the material. XPS is widely used to analyze various materials like: inorganic, organic, semiconductor, polymer, ceramic, bio-material [Andrade 1985, p.106].

XPS mechanism

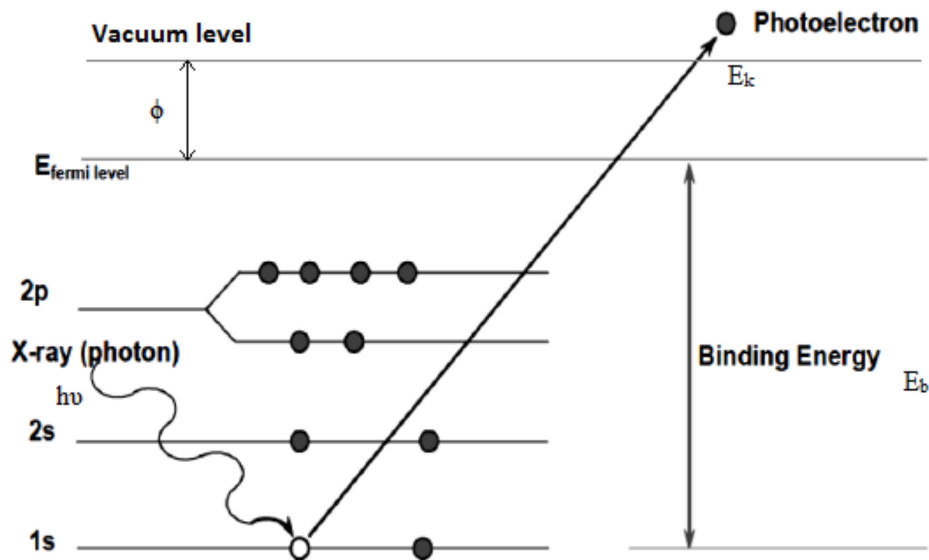

Figure 4.2.5 Schematic of photoelectric effect in XPS [adapted from CoreTech 2014]

The mono-energetic X-rays are irradiated on a surface. These X-rays with energy $h\nu$, interact with atoms on the upper few nanometers of the surface by photoelectric effect as shown figure 4.2.5. These atoms upon excitation, emits photoelectrons with kinetics energy (E_k) given by equation 4.11.

$$E_k = h\nu - E_b - \phi \quad (4.11)$$

Where, E_b is binding energy of atomic orbital from which electron originates and ϕ is known as work function [Wagner a. Muilenberg 1979, p.4]. XPS detector detects, the kinetic energy and number of electrons that had escaped from the surface of the material upon interaction with X-rays. XPS detector is composed of an array of electrostatic plate detectors and hemispherical analyser.

XPS analysis in this work

For all experiments, XPS tool used was from Omicron Nanotechnology Gmbh. An AlKα X-ray source, with an excitation energy of 1486.6 eV and pass-energy of 30 eV was used. The samples were brought in contact with clean-room (of class-1000 type) environment before transferring into the XPS tool. Therefore, surface cleaning step was required. A surface cleaning step was done by sputtering the sample surface with 0.6 keV of argon ion-beam, for 4 min. The surface etching was done at 4 keV of argon ion-beam energy, for 0.5 min to 3 min, depending on the thickness of deposited material.

4.2.4 Scanning Electron Microscopy

Scanning electron microscope (SEM) is a technique that utilizes a focused electron beam (typically 1 μm in diameter) to produce an image of a sample by scanning its surface [Egerton 2005, p.126]. The beam of electrons is controlled, focussed and accelerated upto 30k eV by using electro magnetic (EM) lenses and is irradiated onto a specimen [Zhou a. Wang 2007, p.9]. These electrons interact with atoms in the sample. Two major interactions that occur are: elastic interactions that cause electrons to back-scattered and are detected by a detector, where inelesatic interactions cause generation of secondary electrons. The other emitted signals are x-rays, x-ray continuum and auger electrons [Zhou a. Wang 2007, p. 3 - 8]. These signals contain information about the surface topography and composition of specimen. A complex detector and imaging system further transforms these signals into an image. SEM can be untilized to obeserve the sample in high vacuum, low vacuum, cryogenic and elevated temperatures conditions [Egerton 2005].

In this report all samples were analysed at Fraunhofer IPMS-CNT, Dresden. The SEM equipment used was a S-5000 from Hitachi. This particular tool has a field-emission cathode as a source and an in-lense scanning electron detector. A high voltage of 10 kV was used to accelerate the beam of electrons.

4.2.5 X-Ray Reflectometry and X-Ray Diffraction

X-Ray Reflectometry (X-ray reflectometry) is a non-contact and non-destructive way to determine thickness, roughness, density and interfacial information for single as well as

multilayer thin films,deposited on smooth substrates [Windover et al. 2014, p.1] [Gupta 2010, p.388]. In XRR measurements, a sample is irradiated with an X-ray beam at very low incidence angles. Total reflection occurs at or below a specific angle known as critical angle θ_c. In general, θ_c is very small and depends on the density of material. Now, either the sample or detector (or both) is rotated through a range of angles and the scattered intensity is monitored [Bernd O. Kolbesen 2003, p.440]. As the angle of incident θ is gradually increased beyond θ_c, the reflectivity of the X-rays from the sample starts to decrease rapidly. The oscillations are induced due to an interference between the reflected X-rays from the top surface and the underlaying layer or interface. The thickness and roughness values for the sample surface are determined by periodicity and slope of the oscillations. The density of the surface is calculated from the amplitude of oscillations and the position of a critical angle [Yasaka 2010].

In X-Ray Diffraction (XRD), a diffraction pattern is obtained when the X-rays interact with a crystal structure [more details can be found in Birkholz et al. 2006]. From the diffraction pattern, it is possible to determine the crystal phase, structure, orientation, grain-size of film surface. Every crystal structure produces unique diffraction pattern.

All samples were analysed in analytics lab at Fraunhofer IPMS-CNT, Dresden. XRR measurements were performed on equipment 'D8 Discover' from Bruker AXS. This particular tool has a copper anode tube (operated at 40 kV, 40 mA) with a fine focus, as a source. X-rays were irradiated onto the sample via primary-optics that was composed of 60 mm Göble mirror, and were detected via 0.35° Soller slit as a secondary-optics. The measurements performed for GI-XRD were with an incidence angle of 0.65° and the detector angle 2θ was varied from 10° upto 90°. For XRD measurements, 2θ was varied from 0° to 10°, with a step size of 0.01° in a step interval of 0.3 s for each step.

4.2.6 Four Point Probe Technique

The four-point probe (4PP) method is commonly used to measure the resistivity in semiconductors, directly without any calibration [Schroder 2006, p.2]. As the name suggests, in 4PP method four probes are arranged next to another at equal distance in collinear fashion. In general, current is passed through the outer two probes and a potential difference is measured between the inner two probes, this allows to measure the resistivity of conductive surface [Bullis 1977, p.7]. For an arbitrarily shaped sample significantly larger than the tip setup, the resistivity ρ can be given by equation 4.12 [Schroder 2006, p.7].

$$\rho = 2\pi F s \frac{V}{I} \tag{4.12}$$

Where F is a correction factor, s is the spacing between any two adjacent probes, V is the measured potential difference and I is the applied current. F depends on several factors like probe location, sample diameter, sample thickness t and sample temperature etc. For samples thinner than probe spacing s, the correction factor can be calcualted

independently from each other [Schroder 2006, p.8]. For very thin samples (where t « s), ρ and sheet resistance $\rho_\square$ can be given by equation 4.13.

$$\rho_\square = \frac{\rho}{t} = 4.532\frac{V}{I} \tag{4.13}$$

To measure the resistivity of sample, it is mandatory to know the sheet resistance and the thickness of thin films. 4PP is a contact technique that can damage the surface of the sample [Schroder 2006, p.2].

In this thesis, the 'ResMap 178' tool from company CDE (Creative Design Engineering, Inc.) was used to measure the $\rho_\square$ (ohms per square) of thin films. The probe spacing s was 1 mm. The maximum measurement value for this model is 5 MΩ per square. The resistance of silicon samples used in this work was in the range of 25 to 30 ohms per square.

5 RAPID THERMAL PROCESSING

5.1 INTRODUCTION

Rapid thermal processing (RTP) is a very important technique used in the fabrication of modern integrated circuit (IC), with a wide range of applications such as, metal nitride and silicide formation, ion implantation damage annealing and activation, contact annealing, stress relief annealing, FRAM/magnetic film annealing, dielectric formation and reflow of deposited oxides [MacKnight et al. 2004, p. 26 - 27]. With shrinking device dimensions, the application of RTP has been recently extended to the gate dielectric formation and rapid thermal CVD (RTCVD) [Doering a. Nishi 2008, p11-1]. Main components of any RTP tool include heating furnace and elements, quartz chamber, vacuum system and various gases like N_2, H_2 and Ar [Doering a. Nishi 2008, p.11-5]. There are many commercialised RTP system configurations available, that include hot plate and hot wall RTP system, linear lamp RTP and arc lamp RTP. In section 5.3, the formation of nickel silicide by RTP will be discussed.

5.2 BASICS OF RTP

In RTP technique, the silicon wafers are heated at high temperatures (up to 1200°C or more) for a short duration of time (0.01 s to few 100 s) [MacKnight et al. 2004, p.31]. The wafers are kept under vacuum in quartz envelope and heated from many sides with the help of tungsten-halogen lamps [Doering a. Nishi 2008, p.11-5]. The quartz envelope is continuously cooled down with the help of jet streams of air or cold water [Doering a. Nishi 2008, p.11-4]. The wafers must be cooled down slowly in order to prevent some cracks, defects due to thermal shock.

5.3 NICKEL SILICIDES-A LITERATURE SURVEY

5.3.1 Introduction

There are more than 180 silicides known, which are chemical compounds of silicon with different metals from the periodic table [Borisenko 2000, p.VI]. Depending upon the element X and Si:X ratio, these silicides can be metallic, semiconducting or insulating [Borisenko 2000, p.VI]. Nickel silicide is one example among various metallic silicides and is used in current state-of-the-art logic devices[Doering a. Nishi 2008, p.10-1]. The desired properties of metallic silicides for IC are: low resistivity, low thermal budget, low Si consumption, easy to form and etch, thermally stable, non-oxidizable, good adherence, low stress [Murarka 1995, p.174]. A brief literature review is devoted to this section, that covers only small part of the entire work done on NiSi phase. In last decade, the silicidation of nickel has been studied extensively.

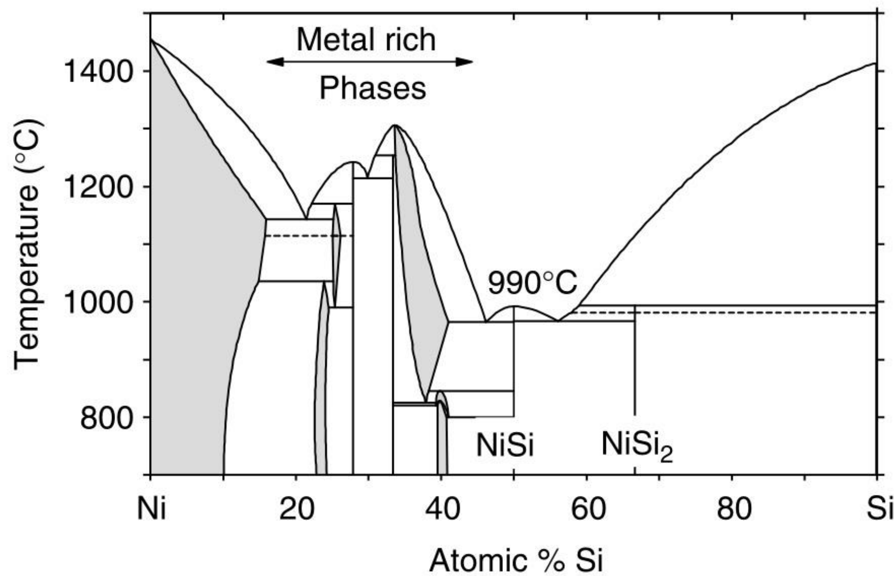

Figure 5.3.1 Binary phase diagram of Nickel-Silicon [taken from Doering a. Nishi 2008, p.10-18]

5.3.2 Formation steps of Nickel Silicide

The above figure 5.3.1 shows a complex formation of Ni-Si compounds with upto 11 phases [Doering a. Nishi 2008, p.10-18]. Only six out of eleven phases are thermodynamically stable at room temperature. From the binary phase diagram it can be seen that rich metal phases can be formed at higher temperatures (> 800°C). The desired low resistivity NiSi phase has relatively low melting point of 990°C, which is the primary cause of morphological instability of NiSi [Van Bockstael et al. 2009]. Also, $NiSi_2$ phase is more thermodynamically stable than all other phases [Doering a. Nishi 2008, p.10-18].

In a typical process, approximately 10 nm of pure nickel metallic film is required on top of silicon in order to start the silicide formation process [Van Bockstael et al. 2009][Van Bockstael 2010][Foggiato et al. 2004, p.56]. The formation of nickel silicide depends on several factors and temperature is a major factor. At low temperatures first Ni-rich phases are formed [Kittl et al. 2005, p.443]. These phases are $Ni_{31}Si_{12}$, Ni_3Si_2, Θ-Ni_2Si, Ni_2Si; and Ni_2Si phase is the dominant phase at low temperature range (170°C-300°C) [Kittl et al. 2005, p.443][Foggiato et al. 2004, p.56][Fouet et al. 2014, p.139]. The Ni_2Si phase is a foundation step for a desired low resistitivity [Kulkarni a. Canale 1991, p.311][Bhaskaran et al. 2009, p.100]. At 260°C, a Θ-Ni_2Si phase was detected by bragg peak [Fouet et al. 2014, p.140]. As the temperature is increased from 300°C- 650°C, the nickel monosilicide phase is formed [Chamirian et al. 2003, p.202]. The resisitivity of the nickel monosilicide phase is constant over the range 300°C–550°C, above 550°C the agglomeration starts and resistivity increases [Foggiato et al. 2004, p.57]. At temperatures exceeding 750°C the high resistivity $NiSi_2$ forms and agglomerates [Foggiato et al. 2004, p.58].

5.3.3 Issues in the formation of nickel monosilicide

There are several issues that have been reported during the formation of desired nickel monosilicide phase. The issues are: scaling issues due to degradation of thin films including agglomeration and lateral diffusion of NiSi that causes stress in the film, leakage current due to NiSi/Si rough interfaces, low thermal stablity of NiSi phase [Foggiato et al. 2004, p.57][Chamirian et al. 2003, p. 201 - 207][Lauwers et al. 2004, p.40][Doering a. Nishi 2008, p.10-19].

However, many solutions have been found in the literature, that mitigate the agglomeration in NiSi phase formation, for instance introduction of refractory metals like W, Ti and Ta, introduction of caping layers, implantation of nitrogen or hygrogen or BF_2 that retards the agglomeration [Doering a. Nishi 2008, p.10-30][Deduytsche et al. 2007] and foramtion of thin epitaxial films [Van Bockstael 2010, p.23]. The nucleation and film stress issues that are caused due to high temperature (approx. 650°C) anneal step, can be reduced by adding Pt or Pd [Doering a. Nishi 2008, p.10-30][Van Bockstael 2010, p. 70 - 79][Mangelinck et al. 1999][Lee et al. 2005]. The dual-step annealing process has improved the formation of nickel monosilicide [Foggiato et al. 2004, p.58].

5.3.4 Applications of Nickel Silicides

Recently in last decade, the applications of NiSi in microelectronic industry have been increased. It has been adopted in ohmic contact application [Zhang a. Smith 2004, p.1361][Gambino a. Colgan 1998, p.103]. NiSi has recently replaced $CoSi_2$, for metal gates, schottky barrier source-drain contact applications [Doering a. Nishi 2008, p.10-38]. NiSi has been easily integrated in CMOS technology for 45 nm node and below, because it provides a good control over threshold voltage V_t of PMOS and NMOS devices, without using two different metals [Lauwers et al. 2004] [Kittl et al. 2005, p.442] [Qin et al. 2001][Iwai et al. 2002]. Recent application of NiSi has been reported as a contact in nano-wire silicon solar cells [Ren et al. 2013], magneto-resistance device [Kim et al. 2013], contacts for nano-rods [Léonard a. Talin 2011] and Li-ion batteries [Lund et al. 2014].

II EXPERIMENTAL PART

6 METHODOLOGIES

6.1 EXPERIMENTAL SETUP

In this Master work, all experiments were performed on a MOCVD tool from Forschungs- und Applikationslabor Plasmatechnik GmbH (FAP), Dresden. The MOCVD tool has been equipped with one tube reactor and one MOCVD chamber. The tube reactor was designed to perform thALD experiments and the MOCVD chamber had been modified to perform PEALD experiments. Only the tube reactor that was used during this thesis work will be discussed here and has been shown in figure 6.1.1.

6.1.1 Reaction chamber

The tube reactor consists of a process chamber and a load lock chamber. Both of the chambers are separated from each other with the help of hand valve. The ALD chamber is a hot-wall tube reactor with cross-flow type of gas exposure and is shown in figure 6.1.1. A gas diffusor was used, to ensure the uniform supply of reactants and purge gases over the complete substrate holder because a better flow dynamics may lead to faster growth with better conformality, homogeneity, quality and less contaminations [Kim et al. 2003, p.734]. The chamber walls are heated with the help of resistive heaters controlled by a DC voltage source (from company Manson HCS-3102 with output range 0-36V and 0-5A). The substrate holder has been designed to mount substrates of size $7.5 \times 2.5\ cm^2$. Two thermocouples were attached to the tube reactor to monitor and control the temperature of the chamber. There is only one gas inlet for both the reactants as well as purge gas. The tube reactor is equipped with a detachable QCM arm, that allows in situ growth and process monitoring with the help of QCM sensor (QCM sensor described in 4.2.1). The heat insulator around the tube reactor was made of glass fibre composite.

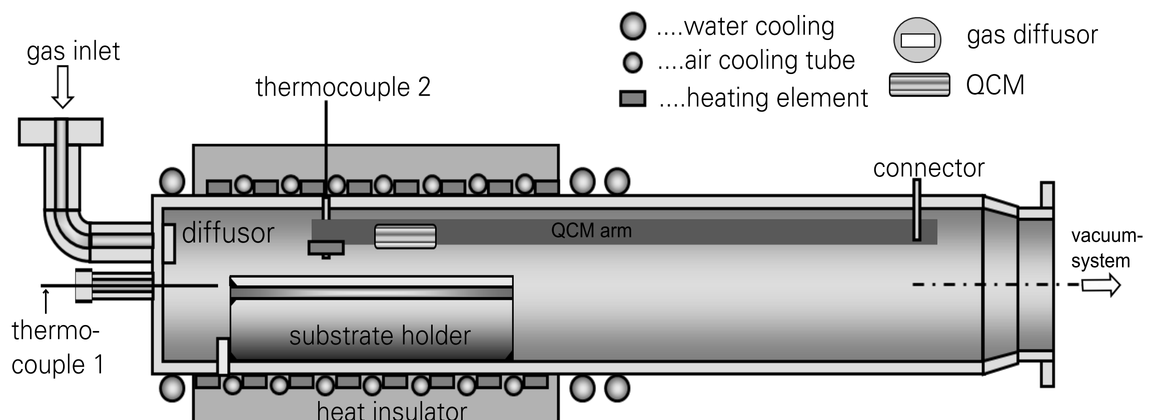

Figure 6.1.1 Experimental setup for an ALD

6.1.2 Position of QCM inside the reaction chamber

In figure 6.1.2, shows the approximate position of QCM with respect to the substrate and substrate holder. The QCM is placed almost 10 cm away from the gas inlet. The thermocouple is inserted from the inlet named as thermocouple 1 and is close to the quartz crystal (shown as yellow ring in the figure 6.1.2). The figure is not according to the scale.

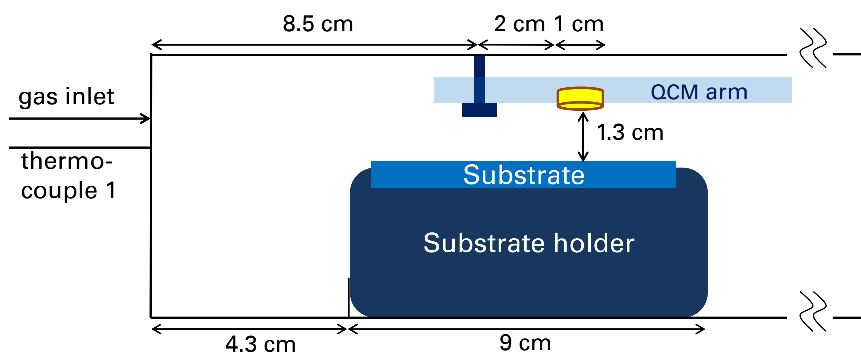

Figure 6.1.2 Inside view of the tube reactor

6.1.3 Experimental schematic

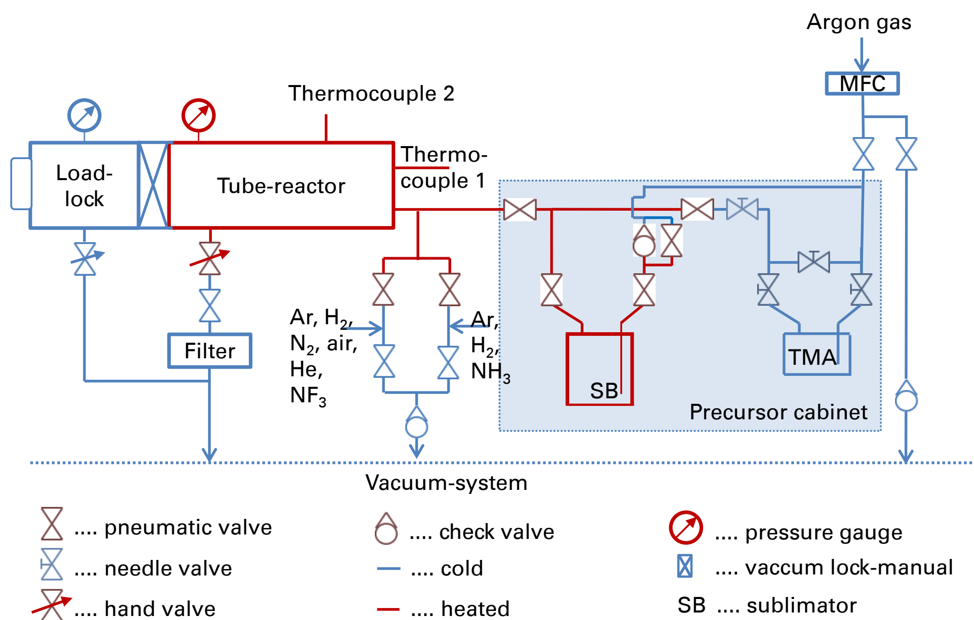

Figure 6.1.3 Schematic of the experimental setup

A schematic of the experimental setup used during all thALD experiments in this work is shown in figure 6.1.3. The tube reactor has one inlet for nickel precursors, trimethylaluminum (TMA) precursor, reactant and purge gases. The reactant gases used for thALD

process, for depositing nickel-based thin films were H_2, NH_3, and air (source for water).

The inert gases like Ar, He and N_2 were filtered by using gas purifiers from the company Gatekeeper with an outcome of H_2, CO and CO_2 levels below 1 ppb as well as H_2O and O_2 levels below 100 ppt. For reactive gases like NH_3 and H_2 the O_2, CO_2 and H_2O contamination levels were below 1 ppb. The flow of gases was controlled with the help of MFCs. The supply of gases was controlled by pneumatic valves, that in itself were controlled with help of system software from company FAP. Ar was used as a carrier gas (CG) to transport nickel precursor molecules into the reaction chamber and to purge the tube reactor and the gas lines. Both precursor sources were kept in a closed cabinet. The gas lines were heated with the help of resistive heaters, that were controlled by a power source. At some positions, check valves were used in the gas lines, in order to prevent the back flow of gases (see figure 6.1.3).

To measure the pressure in the tube reactor, a pirani gauge was used. A dry-pump was used to evacuate the tube-reactor. A particle filter was used to filter out the residual molecules from the chamber, to prevent the vacuum system from clogging. A more detailed version of the gas flow schematic plan can be found in the appendix section B.

6.1.4 Precursors and precursor sources

In this thesis work, precursors for nickel (Ni(amd) as reference precursor, P1, P2, P3, P4, P5) and TMA were used. TMA precursor is a colourless liquid at room temperature (R.T.) and atmospheric pressure, with a melting point of 15.4°C. TMA (98% pure) used, was bought from company Strem Chemicals, Inc.. Ni(amd) precursor was bought from Dow Chemical Co., and it comes in the form of black solid crystal chunks. The comparison among nickel precursors $Pn|_{n\in\{1,2,3,4,5\}}$, is given in the table 6.1.

Table 6.1 Comparison of nickel precursors obtained from the manufacturer

Precursor	*Confidential data, any use is denied*	Type	Color
P1		heteroleptic	yellow
P2		heteroleptic	yellow
P3		heteroleptic	red-orange
P4m,P4t		heteroleptic	yellow
P5		heteroleptic	dark-red

Confidential data, any use is denied

Two kind of precursor sources were used in this thesis work. One was a usual steel container from company ATMI, and other was a sublimator from company SMI. The steel container was used for TMA and nickel precursor P2. TMA source temperature (ϑ_{TMA}) was set to R.T. and TMA has s high vapor pressure at R.T., and no career gas was used to transport TMA molecules to the reaction chamber. The amount of TMA precursor

molecules were controlled with the help of a needle valve attached at the outlet of TMA bubbler.

The sublimator was especially designed to facilitate the transport of low vapour pressure solid precursor molecules into the chamber. It has in total four shelves, three of which are with meshed bottom to ensure the proper flow of carrier gas and other is like a closed cup to capture any melted precursor or residues. The shelves were tightly screwed to a tube. The tube serves the purpose of CG inlet. The sublimator is sealed by copper sealing of type CF-40.

6.2 ALD PROCESS

6.2.1 ALD process types and substrate setups

In this work, three types of thALD processes were used that are categorized on the basis of type of material deposited and are as follows:

1. *AlOx depositions*: Aluminum oxide (AlOx) depositions were performed by thALD technique from TMA and air. In each experiment crystalline silicon (c-Si) sample with native oxide (natOx) was used. AlOx was deposited on silicon samples and later the AlOx thickness was measured with the help of spectroscopic ellipsometer. The change in the QCM frequency was associated with the thickness measurements. AlOx depositions were also performed to passivate the QCM and reaction chamber as well as to verify the change in QCM surface area or roughness.

2. *NiO_x depositions*: the surface reactions for nickel oxide (NiO_x) ALD process were accomplished by two reactants: a reference precursor Ni(amd) and air. NiO_x depositions were performed on either HF–last silicon or c-Si substrates with natOx. NiO_x thin films were deposited to test the reference precursor, test sublimator source and to derive the standard ALD process parameters (results in section 7.3.5.1).

3. *NiX depositions*: depositions for NiX were carried out by using any nickel precursor from P1, P2, P3 and P5 either with H_2 or NH_3 or air as a second reactant. Substrates on which the NiX depositions were carried out are either HF–last silicon or c-Si with natOx. Evaluation of novel nickel precursors were done under this process type.

6.2.2 Process parameters

An ALD process can be affected by many process parameters. The ALD process parameters that were taken into account are: deposition temperature $\vartheta_{\text{deposition}}$, sublimator temperature $\vartheta_{\text{sublimator}}$, TMA source ϑ_{TMA}, total process pressure P_{total}, carrier gas flow f_{CG}, co-reactant gas flow f_{rB} and purge gas flows f_{P1} as well as f_{P2}. Other ALD process

parameters are: precursor exposure time t_{rA}, Ar purge time after precursor exposure t_{P1}, co-reactant exposure time t_{rB} and Ar purge time after co-reactant exposure t_{P2}, for the above mentioned process types.

The thALD process for AlOx depositions was already optimized and the ALD process parameters are provide in table 6.2. The thALD processes for nickel-based thin films have some fixed parameters and some parameters were varied in order to optimize the ALD process and to test the reactivity towards different co-reactants. The parameters that were varied will be dicussed relevantly in chapter 7. Table 6.2 shows the ALD process parameters.

Table 6.2 ALD process parameters

Process type	ϑ_{TMA}, $\vartheta_{sublimator}$ (°C)	$\vartheta_{deposition}$ (°C)	t_{rA} (s)	t_{P1} (s)	t_{rB} (s)	t_{P2} (s)	f_{CG} (sccm)	f_{P1} (sccm)	f_{rB} (sccm)	f_{P2} (sccm)	P_{total} (Pa)
AlOx	R.T.	180	1	5	10	5	-	200	100	200	200
NiO_x	95	200	varied	15	varied	15	50	200	100	200	180, 200
NiX	varied	varied	varied	30	varied	30	50	200	100 for air; 700 for H_2; 100 for NH_3	200	200

6.3 EXPERIMENTAL PROCEDURE

The whole experimental procedure can be divided into following parts: tool preparation, thermal analysis and ALD experiments for nickel precursors, data acquisition as well as data evaluation and characterization of thin films.

6.3.1 Tool preparation

6.3.1.1 Substrate and pre-treatment

During all experiments, c-Si with natOx and HF-dipped Si substrates were used. The size of substrate samples used, were approximately 2 cm $\times$ 7 cm and 1 cm $\times$ 7 cm, respectively. The samples were cut into small coupons from original 4-inch Si-wafers. The 4-inch wafers were 500 μm thick and lightly doped (3.16 $\times$ 10^{-15}cm^{-3}) with boron atoms. The c-Si samples with native oxide were cleaned with the help of AID process, before loading into the ALD chamber. AID stands for acetone, isopropanol and de-ionized (DI) water. First, the samples were dipped in acetone for 30 s and then rinsed with DI water. Then the samplese were dipped in isopropanol for 30 s and later washed with DI water. The AID cleaning was performed to remove the organic contaminations from the substrate surface.

In order to etch natOx from the surface, samples were dipped in 0.5% hydroflouric acid (HF acid) for 2 min. At last the sample surface was washed with DI water.

6.3.1.2 Chamber and QCM passivation

AlOx ALD processes were performed to passivate the chamber as well as the QCM. AlOx is an insulator that prevents the QCM from getting short-circuited. According to the experience, the QCM life was significantly increased after passivating it with 500 ALD cycles of AlOx process. In this way, the chamber was also passivated with aluminum oxide, that might help to reduce any contaminations from previously executed ALD processes.

6.3.1.3 Chemical cleaning of components and filling the vaporizers

The components from the ALD tool like tube reactor, substrate holder, QCM arm, gas lines and ALD pneumatic valves as well as the sublimator, were cleaned in the chemistry lab at Institut für Halbleiter- und Mikrosystemtechnik (IHM), Dresden. The chemical cleaning process was carried out with the help of strong acids and bases e.g. residues from nickel precursors were cleaned by using HNO_3 ($\approx$ 35% by vol.), 10% aqueous solution of KOH was used to clean the AlOx coatings. Later the components were washed with acetone and ethanol. Before loading the sublimator, it was heated upto 120°C in the oven to get rid of water molecules. All, precursors used in this work were filled in a glovebox from company 'MBraun', under N_2 environment with H_2O and O_2 contamination levels below 0.1 ppm.

6.3.2 Thermal analysis and ALD experiments from nickel precursors

The ALD experiments were planned initially with the help of TGA/DTA curve anlysis. These curves can provide rough information regarding some ALD process parameters. In this work, the following measures were taken for a particular ALD process e.g. $\vartheta_{\text{sublimator}}$ temperature was never raised beyond $T_{\text{Onset_1}}$ (and will be relevantly discussed in chapter 7) to prevent the risk of losing all precursor in a very short time. The $\vartheta_{\text{deposition}}$ temperature was kept below the thermal decomposition of the precursor T_{decomp} in order to prevent CVD like effects or self decomposition of precursor. Nickel precursors were also evaluated in terms of decomposition, melting, change in color and texture, at different temperatures. These thermal stability tests were performed in a 2-inch steel ampoules. A steel ampoule was a normal VCR component with blind caps on each side. The temperature range for thermal stability tests was between 40°C and 200°C. All the samples were left for overnight (approximately 20 hours) in the oven at particular temperature. Next day the ampoules were opened in a glovebox and precursors were analysed. After TGA/DTA curve analysis and thermal stability tests, some idea about the initial temperature of sublimator and deposition can be obtained.

In order to obtain other process parameters like ALD pulse times, total process pressure and flow of the gases for nickel-based thin films, the reference ALD process (from Ni(amd) and air) was used. The process parameters from an optimized reference ALD

process were utilized to define the standard process conditions. The standard process conditions were required to set the sublimator temperature without losing too much precursor. For the standard ALD process, a first reactant was any nickel precursor among $Pn|_{n\in\{1,2,3,4,5\}}$ and H_2 as a second reactant. Initially, in order to know the value of $\vartheta_{\text{sublimator}}$, a standard ALD process was started and everytime the $\vartheta_{\text{sublimator}}$ was kept at 40°C, approximately. After some ALD cycles (50-100 cycles) if no deposition was seen then the value of $\vartheta_{\text{sublimator}}$ was increased in steps of 5 or 10°C depending on a precursor. Finally the $\vartheta_{\text{sublimator}}$ was set to a particular value at which some significant deposition was observed. At already high enough (according to the equation 4.1) $\vartheta_{\text{sublimator}}$ value, where no deposition was found at standard ALD process conditions, then the same ALD experiments were also tested at different $\vartheta_{\text{deposition}}$ and with other co-reactants (e.g. air or NH_3). In the case of significant deposition, ALD behaviour was examined by looking at exposure time variation for both the reactants and ALD temperature window.

For all standard ALD processes the temperature of precursor lines and $\vartheta_{\text{sublimator}}$ was set according to the relation 6.1. The precursor lines were always kept at 20°C higher than $\vartheta_{\text{sublimator}}$ in order to prevent any precursor condensation in the lines.

$$T_{\text{precursor_lines}} = \vartheta_{\text{sublimator}} + 20°\text{C} \tag{6.1}$$

6.3.3 Data acquisition and evaluation

6.3.3.1 In situ growth monitoring

QCM measurement technique was used to monitor the in situ growth of ALD process. The frequency change in hertz (Hz), deposition rate, $\vartheta_{\text{sublimator}}$ and $\vartheta_{\text{deposition}}$ with respect to time were monitored. The logging of data was extended by a period of 10 min before starting and after accomplishing each ALD process. This extra logging was performed to attain a constant stable frequency level as shown in figure 6.3.1. This figure shows the change in frequency with ALD process time. To evaluate the frequency drop per cycle (*FDPC*) two methods were used: a slope method and total frequency change method (level method). Both methods are mathematically described by equations 6.2 and 6.3. A slope method is valid only if change in frequency with respect to ALD process time is linear.

$$FDPC_{slope} = \left|\frac{\Delta y}{\Delta x}\right| \times t_{\text{cycle}} \tag{6.2}$$

$$FDPC_{level} = \frac{|f_b - f_a|}{N_{\text{cycles}}} \tag{6.3}$$

Where, f_a, f_b, N_{cycles} and t_{cycle} are frequency value at level (marked by red line) *a* in above figure, frequency value at level (marked by red line) *b* in figure 6.3.1, total number of ALD cycles and complete ALD cycle time, respectively. In ALD process software

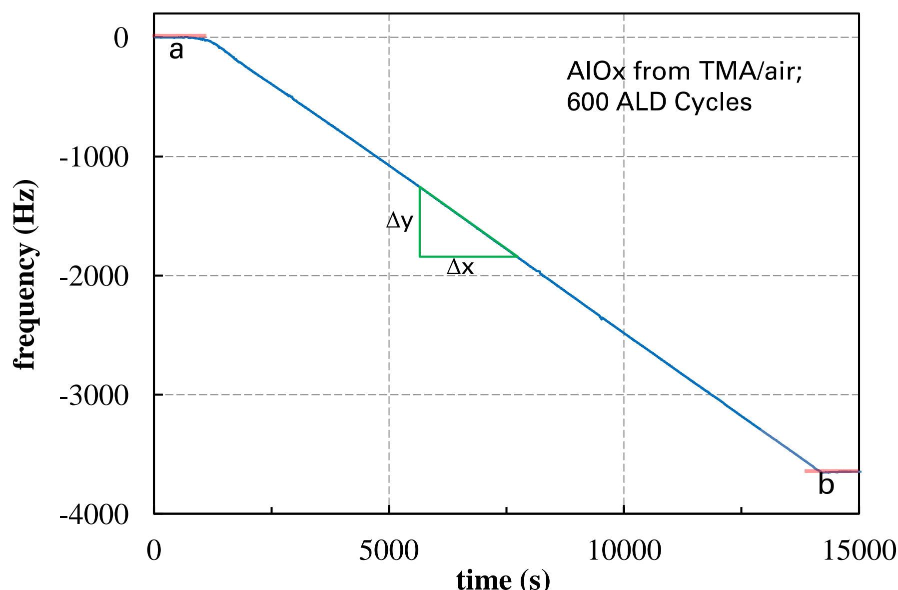

Figure 6.3.1 Evolution of QCM frequency over the ALD process time. The figure indicates how △X and △Y were calculated for a linear slope to evaluate *FDPC*.

from FAP, every time there was a small delay introduced due to switching of an ALD valve. This delay was calculated by using simple stop watch and it came out to be approximately 0.3 s. The total delay for a complete ALD cycle depends on the number of ALD valves and therefore depends on a process recipe. For instance, in TMA/air, Ni(amd)/air and Ni(amd)/H_2 ALD processes the delay was around 1.2 s, 1.2 s and 1.5 s per cycle, respectively. In general, if n is the total number of valves switching and t_{delay} is the delay caused by switching of an ALD valve, then a corrected form of cycle time is given by equation 6.4.

$$t_{corrected_cycle} = t_{cycle} + n \times t_{delay} \tag{6.4}$$

6.3.3.2 Temperature compensation for RC™ type quartz crystal

QCM is very sensitive to temperature changes therefore it is prone to erroneous results. In case of the ALD process that utilizes H_2 as second reactant, a significant frequency shift was caused by the H_2 pulse during the first ALD cycle that could have been misinterpreted as some deposition. But this frequency shift had started to saturate at some level after 15-20 min. Therefore to avoid this effect, every ALD process with H_2 as one of the reactants was commenced and finished with 15 blind ALD cycles. In blind ALD process no precursor was consumed during the precursor pulse. Instead of the precursor pulse, Ar was used to purge the chamber continuously and rest of the ALD process parameters were same as in case of normal ALD process.

The frequency shift due to the temperature changes can be compensated by monitoring the QCM temperature [Grimshaw 2013]. Temperature related QCM frequency shift Δf for a complete ALD process can be evaluated by knowing the temperature coefficient

$T_{coeff.}$ around $\vartheta_{deposition}$ and the temperature change ΔT during an ALD process and is given by equation 6.5.

$$\Delta f = \Delta \mathrm{T} \times \mathrm{T}_{coeff.} \tag{6.5}$$

The corrected form of frequency drop per cycle can be calculated as shown in 6.6:

$$FDPC_{temp_comp.} = FDPC \pm \Delta f \tag{6.6}$$

The figure 6.3.2 a, was used to calculate the $T_{coeff.}$ around the $\vartheta_{deposition}$ of 178°C. The green ellipses show an overshooting in heating, due to a manual control of the voltage source for the tube reactor. In figure 6.3.2 a, the $\vartheta_{deposition}$ was varied from 178°C to 165°C and back to 178°C, then from 178°C to 192°C. The respective change in frequency was recorded and the temperature coeffecients for cooling and heating were calculated. $T_{coeff.}$ for cooling by approximately 10°C and for heating by approximately 10°C were calculate as +9.4 Hz/°C and -10.3 Hz/°C, respectively and these calculated values were close to those found in the literature (±10 Hz/°C) [Martinson et al. 2014, p.7]. In figure 6.3.2 b the temperature as well as frequency change settles to a particular value.

Figure 6.3.2 Change in the frquency of RC-cut quartz crystal as a function of deposition temperature: figure a is used to calculate the $T_{coeff.}$ around 178°C and b shows the evolution of QCM frequency with respect to deposition temperature. In figure b the frequency and temperature tends to saturate to a particular value and is approximately marked by a green vertical line.

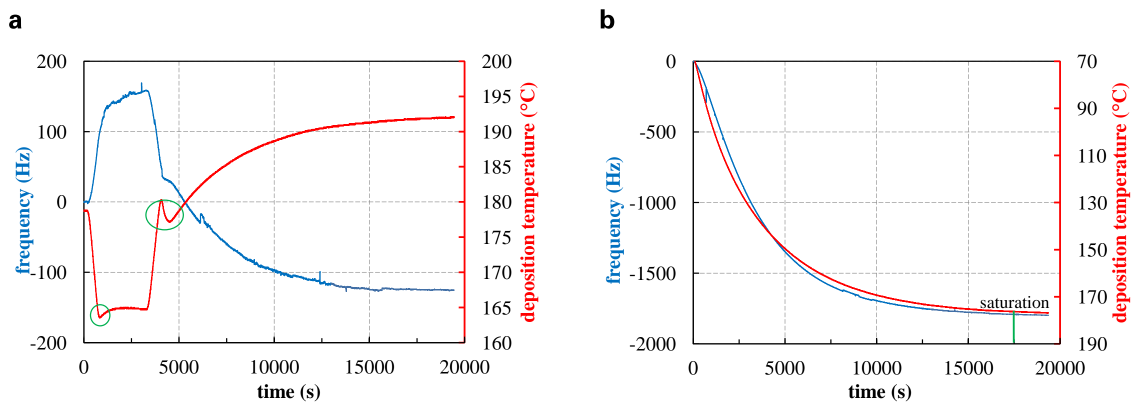

6.3.4 Characterization of film properties

The thickness and density measurements were mainly carried out by XRR. Ex situ SE was also used to evaluate the thickness. The thicknesses obtained from SE measurements were considered as rough values due to lack in solid information regarding the film composition. Moreover, no material model that could match with the optical constants of the grown films was available in the software library. Therefore a methodology for ex situ SE measurements was adopted to fit the thickness values. This methodology is based on general assumption i.e. the deposited material is isotropic with Si/SiO_2/NiX

interlayer structure. B-spline mathematical material model was used as a starting model to fit thickness and optical constants. Multi-sample analysis and 3-angle measurements were performed to increase the number of duplet (Ψ, Δ) values. After having the rough approximation of fit parameters Kramer Krönig co-relation was used to fit ϵ_2 - ϵ_1 relation. Later the B-spline layer was parameterized with Lorentz-ian oscillator because the lorentz oscillator has more physical significance than the B-spline material model.

The grown films by thALD process were analysed with the help of SEM, XRD, XPS and 4PP methods. XRD measurement technique was utilized to analyze the crystal structure and phase. SEM was used to study the surface roughness and quality. The sheet resistance was determined with the help of 4PP method. The chemical composition of grown material was analysed with the help of XPS measurements. The sample piece for XPS measurement was taken from the gas inlet side of the reaction chamber, then the priority was given to SEM (more detail in figure 6.3.3).

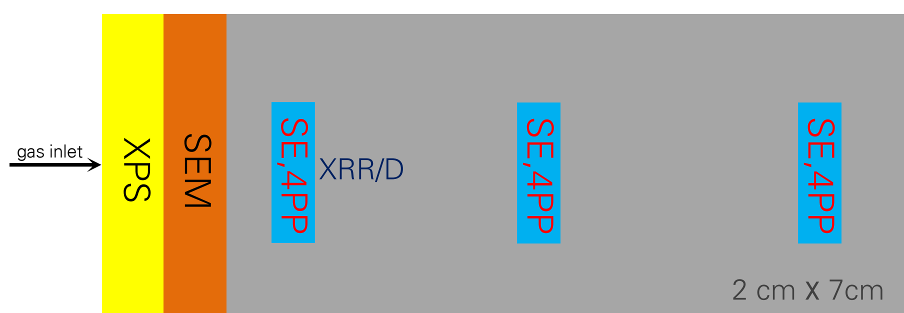

Figure 6.3.3 The approximate positions for various measurements on the silicon sample. The 4PP and SE measurements were performed at three different positions on the sample to check the film homogeneity over the sample length. The figure gives an idea of where the measurements were performed and is not to scale.

7 RESULTS AND DISCUSSION

7.1 INTRODUCTION

In this work, many experiments have been performed in order to examine ALD growth behaviour and the thermal stability of various precursors. ALD characteristic curves depict the dependency of growth behaviour on the exposure time for both the reactants and purge gases as well as the amount of gases [Sharma 2014]. The results presented in following sections evaluate the novel nickel precursors. The evaluation of such precursors was done by looking into ALD characteristic curves and ALD temperature window. The TGA/DTA curve analysis, thermal stability and thermal decomposition tests for precursors were also done. The thermal stability tests were performed in accumulated fashion, where the ampoules were not always refilled with new precursor. Moreover the film properties were analysed with the help of SEM, XRR/D, XPS, SE and 4PP techniques.

The verification of QCM sensor was done by AlOx ALD process and has been discussed in section 7.2. In section 7.3, a benchmark ALD process was established from a reference nickel precursor. Later the same approach was used to evaluate novel nickel precursors and the results of such screening experiments have been discussed in section 7.4. In the end, a table 7.2 compares the results obtained from evaluation of reference and the novel nickel precursors.

For the simplicity, the order of four pulse times (as described in section 3.3.1) for every ALD process described in this chapter is written in $t_{rA}/t_{P1}/t_{rB}/t_{P2}$ format.

7.2 QCM VERIFICATION WITH ALUMINUM OXIDE ALD PROCESS

Al_2O_3 ALD process from TMA/H_2O is an example of an ideal ALD process with a growth rate upto 1.3 Å per ALD cycle is possible [Groner et al. 2004] [George 2010]. Several similar ALD processes were performed to passivate the QCM surface. A performance of the QCM and the verification any change in the surface of QCM active area. The AlOx ALD process was also performed to passivate inner walls of the tube reactor, in order to reduce a risk of incorporating the elements like carbon into the films based on nickel from previous experiments.

ALD process parameters for already optimized AlOx process with TMA and air are: 1 s of TMA exposure time, 10 s of Ar purge after TMA exposure, 5 s of air exposure time, 10 s of Ar purge after air exposure, 200 Pa process pressure, at $\vartheta_{\text{deposition}}$ of 200°C. The frequency drop per cycle for an already optimized aluminum oxide ALD process tends to saturate around 6 Hz [similar to that found in Grimshaw 2013, s.26]. In the saturation regime, the proportionality of this frequency drop per cycle was evaluated in terms of thickness.

The AlOx film thickness was extracted with the help of VASE ellipsometer. The AlO_x film thickness with respect to number of ALD cycles has been plotted in figure 7.2.1. The samples were coated with 50, 100, 200, 500 and 600 total ALD cycles from TMA/air

process. The figure shows that in saturation regime the AlOx film thickness was very relevant to number of ALD cycles with GPC value of approximate 1 Å. The same GPC was assumed to take place on the QCM surface, therefore giving a good control over thickness for the passivation purpose. The major goal for the whole procedure was to verify any non-uniformity obtained during nickel-based depositions. For instance if the FDPC obtained during AlOx ALD right after nickel-based ALD was more than 6 Hz, this would have indicated an increase in QCM surface.

The homogeniety of samples coated with AlOx was also checked in terms of thickness. The thickness non-uniformity between two points on each sample, that were 3 cm apart was less than 0.3 nm.

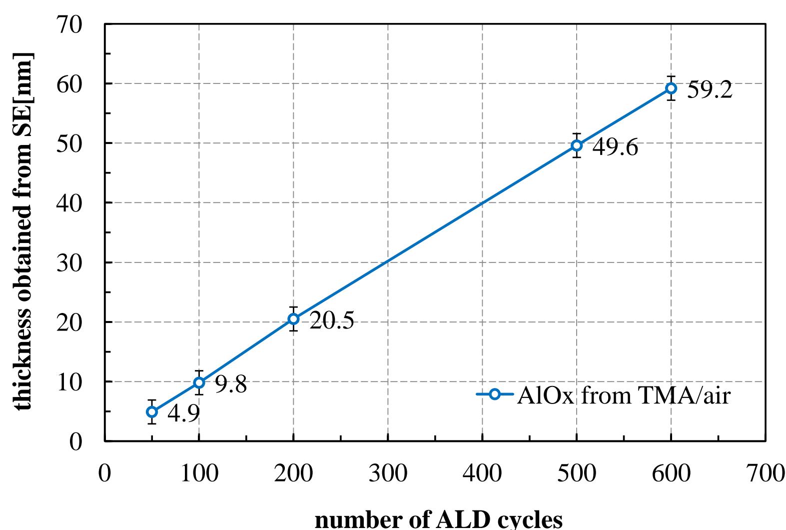

Figure 7.2.1 Film thickness obtained by SE from AlO_x ALD process versus number of ALD cycles. ALD pulse times are 1 s/5 s/10 s/5 s. At deposition temperature of 200°C and process pressure of 200 Pa.

7.3 ALD PROCESS FROM THE REFERENCE PRECURSOR

7.3.1 Introduction

The reference precursor used was Ni(amd). The TGA curve and thermal stabilty analysis of Ni(amd) precursor will be done in following sections. The main goal of performing ALD experiments with Ni(amd)/air was to develope a benchmark ALD process and define standard process parameters. The standard process parameters were required to save time and the precursor amount that might consume during setting the sublimator temperature. Moreover, a benchmark ALD process was required to compare the deposition tests from other nickel precursors used, in terms of ALD behaviour, growth rate, FDPC and film properties. A benchmark ALD process was optimized with the help of in situ growth monitoring.

7.3.2 TG analysis for Ni(amd) precursor

Thermogravimetric analysis for Ni(amd) precursor was performed by the manufacturer in an open crucible of AlOx. The figure 7.3.1 plots an exponential mass loss of Ni(amd) precursor with temperature. It can be seen that approximately 99% of the mass is lost as a single step process with temperature. The $T_{5\%\ mass\ loss}$ is around 175°C. A first derivative DTG curve has also been plotted, which is very smooth and shows a peak at approximately 250°C. TGA of Ni(amd) shows no indication for any decomposition. The sublimator temperature was calculated according to the equation proposed in 4.1, and was set around 95°C in order to draw enough vapors into the chamber.

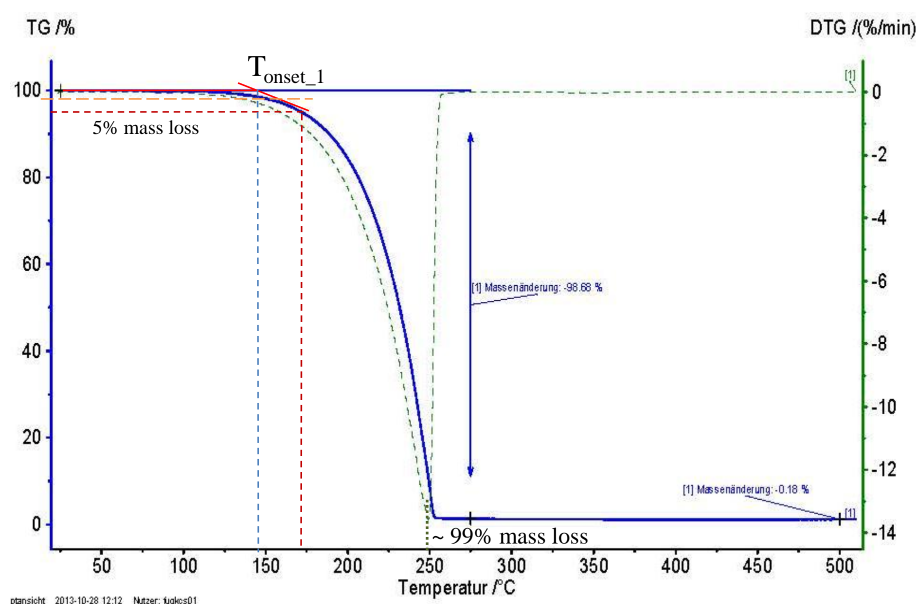

Figure 7.3.1 **TGA and DTG curves for Ni(amd) at atmospheric pressure and under N_2 gas environment. Around 250°C, about 99% of the mass is lost and is indicated by a blue horizontal arrow. At 500°C, approximately 1% of the original mass is left as residue.**

7.3.3 Thermal stability test for Ni(amd)

According to the results from TGA, a thermal stability test was performed for Ni(amd) reference precursor. For that less than 0.1 g of precursor was filled in a steel ampoule and sealed with blind caps. The ampoule was heated at 150°C for 20 hours in the oven and the oven was kept in clean room environment. Later the ampoule was opened and analysed inside the glovebox. It was found that precursor was melted and later solidified at R.T. The color of the precursor was unchanged and it was reactive when brought in contact with air in the chemistry lab. The color changed from black to light green within few seconds of contact with air. This test might indicate the thermal stability of Ni(amd) precursor at 150°C.

7.3.4 ALD process optimization

In order to test the self limiting growth characteristics for Ni(amd)/air process, the exposure time for both the reactants was varied. The following curves were obtained on NiO coated QCM.

Variation in the Ni(amd) exposure time

In figure 7.3.2, the frequency drop per cycle with respect to Ni(amd) exposure time has been plotted. Ni(amd) exposure time was varied from 5 s to 30 s. The air exposure time was kept at 20 s. The Argon purge times were kept at 15 s each. Each data point in the figure 7.3.2 was extracted from complete 100 ALD cycles. It has been found that the frequency drop per cycle tends to saturate after 15 s of Ni(amd) exposure, at the level of approximately 7 Hz. *FDPC* was calculated with both slope as well as level methods (described in section 6.3.3.1), and no observable difference was found among both methods. The temperature compensated data points (red) were also calculated to see if there is a significant difference from non compensated data points. The main advantage of subtracting temperature effects from QCM frequency change over the ALD process time is to neglect any misapprehended depositions (also described in section 6.3.3.2).

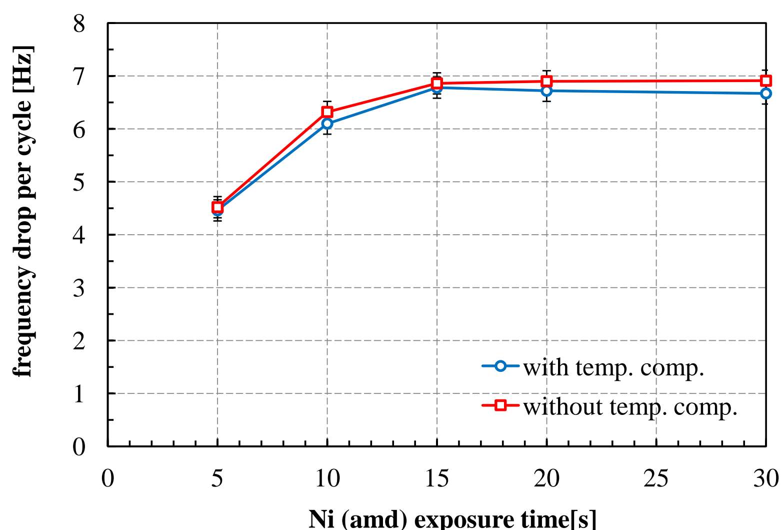

Figure 7.3.2 Variation in the Ni(amd) exposure time. The figure shows frequency drop per cycle tends to saturate around 7 Hz, right after 15 s of Ni(amd) exposure time. The process parameters like $\vartheta_{deposition}$, $\vartheta_{sublimator}$ and P_{total} were: 180°C, 95°C and 200 Pa, respectively. The $T_{coeff.}$ of 2 Hz/°C was used to compensate *FDPC* as described by equation 6.6.

Variation in the air exposure time

Air exposure completes the second half reaction and the NiO_x film is obtained during this step. Figure 7.3.3, indicates the minimum amount of air exposure needed to accomplish a complete reaction with all the Ni(amd) adsorbates on the surface. All the ALD process parameters were same as described in previous subsection, except Ni(amd) exposure time was set to 15 s and the air exposure time was varied between 5 s to 30 s. In figure 7.3.3, it can be seen that *FDPC* tends to saturate right after 10 s of air exposure time. The saturation level was again achieved around 7Hz. Thus the amount of air dose needed is atleast 10 s, in order to have self-limited chemical reaction on the substrate surface.

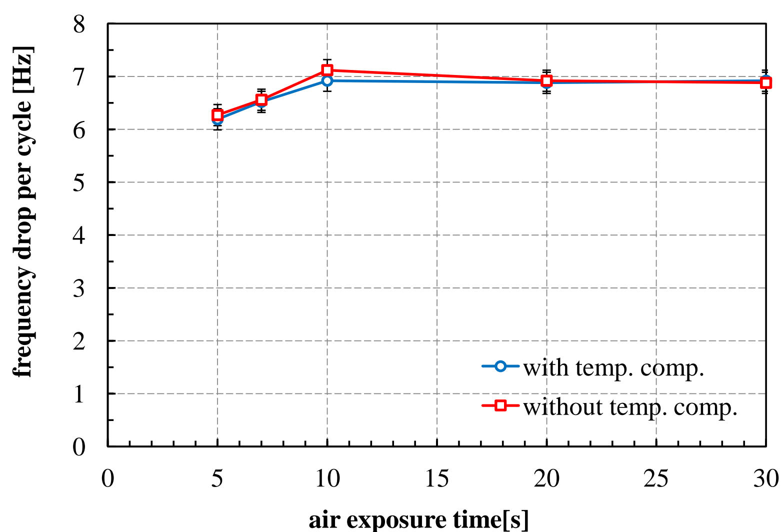

Figure 7.3.3 Variation in the air exposure time. The figure shows frequency drop per cycle tends to saturate around 7 Hz, right after 10 s of air exposure time. The process parameters like $\vartheta_{deposition}$, $\vartheta_{sublimator}$ and P_{total} were: 180°C, 95°C and 200 Pa, respectively. The $T_{coeff.}$ of 2 Hz/°C was used to compensate *FDPC* as described by equation 6.6.

It must be noted here that sometimes the short purgings might lead to CVD like effect, that manifests as increased growth rate and thickness non-uniformities [Nalwa 2002, p.140]. Therefore, ALD process with 15 s/30 s/20 s/30 s of pulse times was also performed to see any effect of variation in the purge times on *FDPC*. This experiment showed no noticeable change in *FDPC* and thus 15 s of both the argon purge times was assumed to be enough to purge the reaction chamber.

Self decomposition test for Ni(amd) precursor at 200°C of deposition temperature

Deposition tests from Ni(amd) without any co-reactant gas were also performed. In total 50 ALD cycles, with 15s of Ni(amd) exposure time, 20s of Ar purge instead of second reactant exposure time and 20s for both purging steps were used. No growth was found during this test which indicates that after a monolayer formation of adsorbed Ni(amd)

precursor molecules, no adsorption or reaction was possible without any reactant. This experiment indicated that Ni(amd) precursor undergoes no self decomposition at deposition temperature of 200°C.

7.3.5 Film properties

The grown nickel-based thin-films were analysed with the help of XRR, XRD, XPS, SEM, SE and 4PP. The figure 7.3.4 shows the thickness, density and roughness measurements from XRR fit-curve. A total of 100 cycles were performed on HF-dipped silicon samples as initial substrates. The ALD pulse times were fixed to 15 s/30 s/20 s/30 s. Other ALD process parameter like: $\vartheta_{deposition}$, $\vartheta_{sublimator}$ and P_{total} were kept at 180°C, 95°C and 200 Pa, respectively. The thickness, density and roughness values were 9.8 nm, 4.4 g/cm^3 (with respect to the literature value of 6.7 g/cm^3) and 1.6 nm, respectively. The XRR fit was performed for NiO. A 0.5 nm of SiO_2 has been shown by XRR meaurements, and could might have come from air exposure step during ALD experiments.

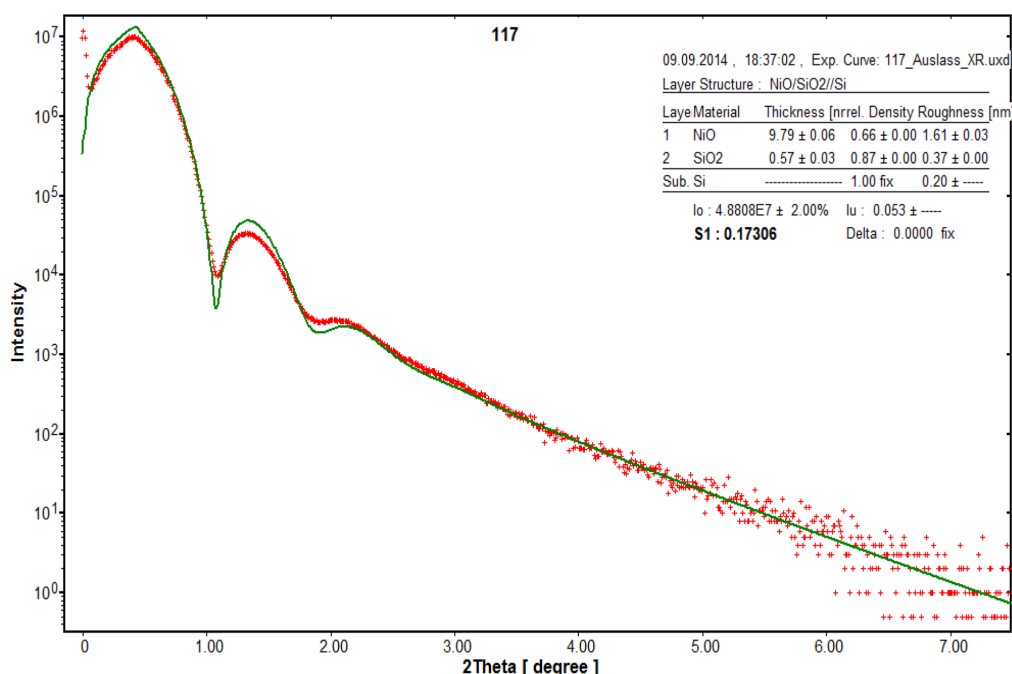

Figure 7.3.4 XRR plot reveals the thickness, roughness and density of NiO film grown from Ni(amd)/air ALD process. Si/SiO_2/NiO layer structure was used. XRR measurement was done in the air atmosphere.

The thickness measurement from XRR was also cross-checked by VASE ellipsometer. The ellipsometer model used is already described in section 4.2.2. The measured thickness from ellipsometer was 10.4 nm.

SEM picture of the surface for the above sample was also taken and can be seen in figure 7.3.5. From SEM it can be speculated that the film is rough, less dense and there are some pinholes on the surface.

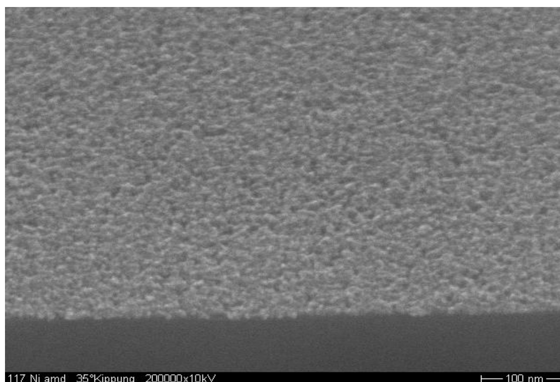

Figure 7.3.5 SEM picture of the film grown from Ni(amd)/air process. Light region shows nickel-based film and the dark grey region is silicon substrate. Film may have less density and is little rough with some pinholes on the surface.

XPS analysis for this sample was not done because the focus of this experiment was to extract the ALD cycle parameters and develope standard deposition conditions for further testing of other novel nickel precursors. 4PP measurements showed the sheet resistance value was beyond a detection limit of the tool, thus more than 5 MΩ/□.

7.3.5.1 Summary from the reference ALD process

The results obtained from Ni(amd)/air ALD process were used to define the standard process parameter conditions. The standard process parameters will be used as starting process parameters for nickel-based thin film depositions from novel nickel precursors. The standard process parameter values for nickel-based ALD process are 10 s/30 s/30 s/30 s of ALD pulse times. The $\vartheta_{\text{deposition}}$ and P_{total} are: 180-200°C and 200 Pa.

7.4 EVALUATING THE NOVEL NICKEL PRECURSORS

7.4.1 Screening tests for precursor P1

7.4.1.1 Introduction

First of all the TG/DT curve analyses of P1 will be done followed by thermal stabilty test for P1. The growth behaviour and film properties will also be discussed in next sections.

7.4.1.2 Thermal analyses of precursor 1

Confidential data, any use is denied

Figure 7.4.1 Thermal analysis curves for precursor P1 performed at atmospheric pressure under N_2 environment. The endothermic and exothermic peaks belong to DTA curve. The onset points are calculated from tangents drawn on TG curve [more detail in Gabbott 2008].

7.4.1.3 Thermal stability test for P1

The thermal stability test for P1 was done at three different temperatures as shown in figure 7.4.2. All three samples were kept at particular temperature for 18 hours.

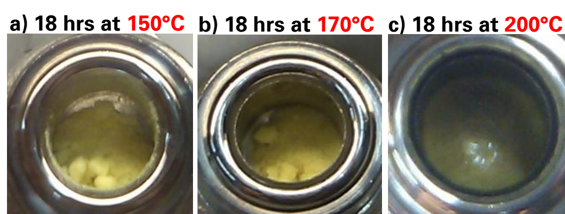

Figure 7.4.2 Thermal stability tests performed for precursor P1 at 150°C, 170°C and 200°C. The sealed ampoule was heated in the oven that was kept in clean room environment. The ampoule was opened under N_2 atmosphere in the glovebox.

At 150°C and 170°C, P1 shows no visible change in color and texture if compared to the original picture. At 200°C, precursor has melted and a black residue can be seen

on inner walls of ampoule in fig 7.4.2c. This black residue might indicate the thermal decomposition of P1 at 200°C or below.

7.4.1.4 Deposition experiments with P1

The exposure time for both the reactants and deposition temperature were varied, to observe any ALD behaviour for P1. The c-Si samples with native oxide on them were used as initial substrates. The $\vartheta_{deposition}$, $\vartheta_{sublimator}$ and P_{total} were set to 180°C, 144°C and 200 Pa, respectively. The choice for H_2 as a second reactant was set by the manufacturer. Each experiment was performed with 100 ALD cycles on AlOx coated QCM surface.

Variation in the P1 exposure time

In figure 7.4.3, the P1 exposure time was varied. The air exposure as well as both Ar purge times were kept at 30 s. The P1 exposure time was varied from 3 s to 30 s, and a linear *FDPC* relation was found. This linear change in frequency per cycle upto 30 s of P1 exposure time, shows no self limited growth behaviour which can be an indication for CVD like growth behaviour. At 30 s of P1 exposure the *FDPC* was found to be around 18Hz (it is maybe too much for a layer by layer growth behaviour, in case of AlOx and NiOx ALD processes the *FDPC* was approximtely 6 Hz and 7 Hz, respectively). A linear dependency of change in frequency can be due to self decomposition, under saturated chemisorption of the precursor during precursor pulse.

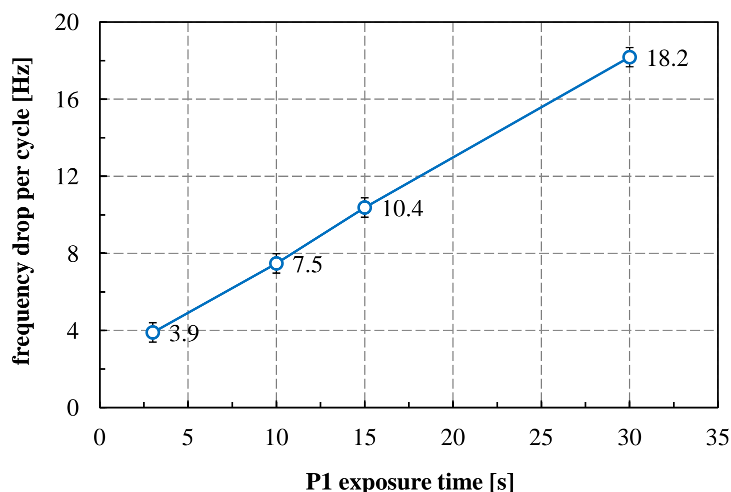

Figure 7.4.3 Variation in the P1 exposure time. The figure shows a linear dependency of *FDPC* on P1 exposure time. The process parameters like $\vartheta_{deposition}$, $\vartheta_{sublimator}$ and P_{total} were: 180°C, 144°C and 200 Pa, respectively.

Variation in the Hydrogen exposure time

From figure 7.4.3, P1 exposure time cannot be said to accomplish a self-limited chemisorption surface reaction. Therefore, for obtaining a curve for H_2 exposure time variation, a standard ALD process with 15 s of P1 exposure time was used. In figure 7.4.4 H_2 exposure time was varied from 10 s to 60s, and it was found that *FDPC* saturates at a level of approximately 10.8 Hz right after 30 s exposure time. The figure shows that 30 s of H_2 exposure time is sufficient for a complete reaction to take place with adsorbed P1 precursor molecules on QCM surface.

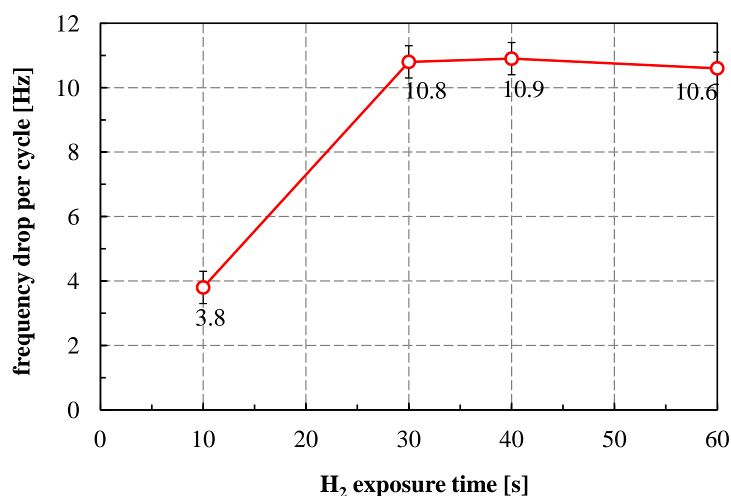

Figure 7.4.4 Variation in the H_2 exposure time. The *FDPC* tends to saturate around 10.8 Hz, right after 30 s of H_2 exposure time. The process parameters like $\vartheta_{deposition}$, $\vartheta_{sublimator}$ and P_{total} were: 180°C, 144°C and 200 Pa, respectively.

Variation in the deposition temperature

The dependency of *FDPC* was also obsereved at different deposition temperatures and is shown in figure 7.4.5. In a range from 200°C to 240°C the *FDPC* is found to be nearly unaffected by the $\vartheta_{deposition}$ and is around 12 Hz. This nearly constant *FDPC* may suggest that the precursor molecule can be stable in this temperature regime or the activation energy required to accomplish the surface reaction is suficient. At 270°C, the *FDPC* was around 18 Hz, indicating higher growth rate at this temperature. This higher growth rate can be due to CVD like effects, precursor decomposition and a different reaction mechanism than at lower deposition temperatures. The lower *FDPC* around 160°C, may be due to less surface activation energy.

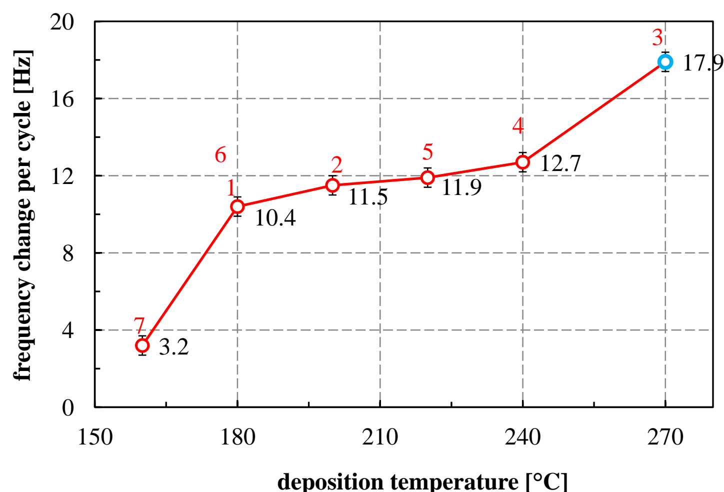

Figure 7.4.5 Variation in the deposition temperature. The deposition temperature was varied from 160°C to 270°C. The process pressure was 200 Pa. All data points in red were obtained by repeating corresponding experiments twice except the blue data point, that was run only one time. The numbers represent an order of experiment runs.

Self decomposition test for P1 at 170 and 180°C of deposition temperature

The ALD process from P1 and without any co-reactant was also carried out. Instead of H_2, a 200 sccm of Ar was used during the second reactant pulse. The ALD pulse times were 15 s/30 s/30 s/30 s at standard deposition conditions. This deposition experiment was performed to see if P1 shows any thermal decomposition on the QCM surface. Interestingly, the *FDPC* was found to be around 4.2 Hz and 1.5 Hz, on the QCM surface that was coated with AlOx and nickel-based film grown previously by P1/H_2 ALD process, respectively. In both cases, total of 50 ALD cycles were performed at 170°C and 180°C. This growth behaviour was reproduced more than 2 times. Moreover, no leak was found in the reaction chamber or gas lines. Chamber was also verified by AlOx ALD process without air as second reactant and no growth during this process was found.

7.4.1.5 Film properties

All samples at different $\vartheta_{\text{deposition}}$, were grown with 100 cycles of P1/H2 ALD process with standard process parameter set but with 15 s of P1 exposure time. A c-Si sample with native oxide on top was used. The thickness, roughness and density values for samples deposited at temperatures below 180°C were measurable with XRR. The films grown at deposition temperatures more than 200°C were: thick, porous, rough, inhomogeneous and more in Ni content. The film properties of samples grown at different temperatures are summarized in table 7.1.

The samples grown at temperatures above 210°C were conductive and the sheet resistance values were also uniform ($\pm$ 1$\Omega/\square$) throughout the sample length ($\approx$ 7 cm).

Table 7.1 Evaluation of the film properties by XRR, XRD, SEM, SE and 4PP. The films were grown from P1/H_2 ALD process at deposition temperatures of 160°C, 180°C, 210°C, 240°C and 270°C.

$\vartheta_{deposition}$ (°C)	t_{SEM} (nm)	t_{XRR} (nm)	t_{SE} (nm)	$roughness_{XRR}$ (nm)	$density_{XRR}$ (g/cm^3)	R_S (Ω/□)	Comments (XRD)
160	14	14	15	0.7	4.1	high	amorphous, high C contamination
180	32	32	32	0.6	4.2	high	amorphous, high C contamination
210	109	-	-	-	-	9.6	hexagonal lattice, Ni_3C,Ni_3N,Ni_2H
240	276	-	-	-	-	5.3	hexagonal lattice, Ni_3C,Ni_3N,Ni_2H
270	356	-	-	-	-	6.2	very inhomogeneous, peaks for fcc Ni

The $\vartheta_{deposition}$ below 200°C did produce very high sheet resistance, that was more than 5 MΩ/□ (refer to table 7.1).

Figure 7.4.6 SEM pictures of the films grown from P1/H_2 process with standard parameters, except the P1 exposure time was 15 s and deposition temperature was 160°C, 180°C, 240°C and 270°C.

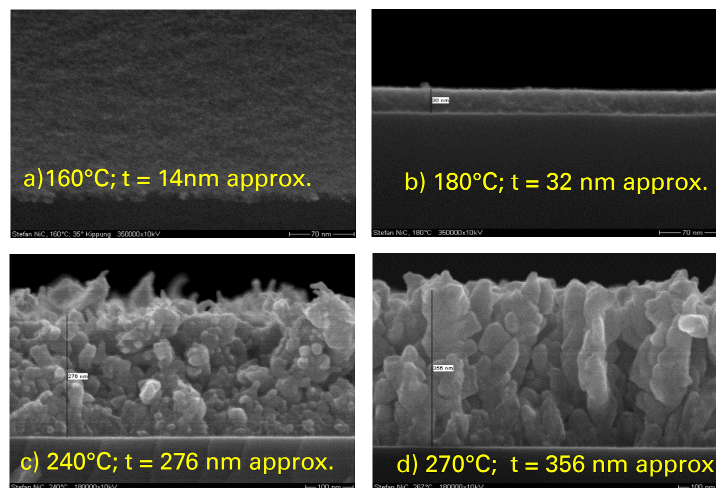

SEM pictures for samples at $\vartheta_{deposition}$ of 160°C , 180°C , 240°C , and 270°C have been shown in figure 7.4.6. It can be seen that the higher deposition temperatures have indeed produced films with very high roughness, low density and large grains.

XPS chemical analysis was also done for the samples grown at 160°C, 180°C and 270°C deposition temperatures and has been shown in figure 7.4.7. XPS measurements were done for initial condition (after deposition), surface-clean and surface-etch as described earlier in section 4.2.3. In general, it can be seen that at $\vartheta_{deposition}$ of 270°C, the overall nickel content was more, carbon and oxygen content were low as compared to low deposition temperatures.

The elemental constituents at initial conditions for the samples deposited at different temperatures were almost similar, meaning the atomic percent levels for Ni2p3, O1s

and C1s were almost identical for all samples. The similar content levels can arise from the identical oxidation process of the surface. After surface-etch step for the sample at 270°C, nearly 80 atomic % of Ni2p3 content was visible and this increase in nickel content validates the XRD results (shown in table 7.1), the oxygen level reduced to almost zero and this may indicate that oxygen atoms did not come from the chamber but from oxidation in an atmosphere. In all cases, high amount (approximately 40%) of carbon was seen for the initial condition. The evolution of carbon content for samples at 180°C and 270°C was nearly similar, and almost 20-27% carbon was present after clean and etch steps, this may indicate the incorporation of the C atoms from precursor itself. After the surface-etch step for the sample at 160°C, the initial substrate became visible and this indicates that the film was thin (validate the results revealed by XRR, SE and SEM analysis).

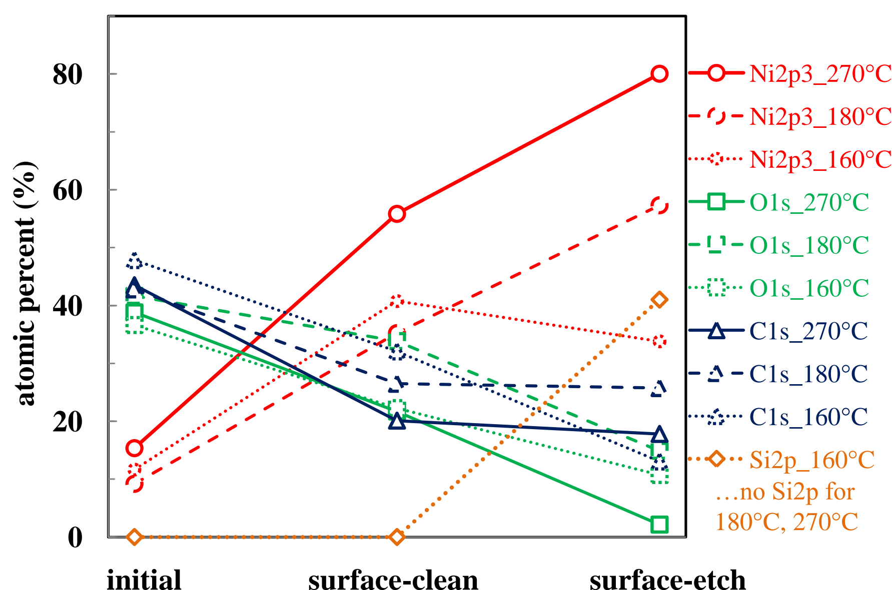

Figure 7.4.7 **XPS analysis of the films grown from P1/H_2 process. The initial condition is the condition where sample surface was intact. In surface-clean and surface-etch steps the sample surface (5 $\times$ 5 mm^2) was sputtered by 0.6 keV and 4 keV of argon ion-beam energy, for 4 min and 1 min, respectively.**

7.4.1.6 Remarks on precursor P1

The results obtained during the evaluation test for precursor P1, indicates that P1 and H_2 deposition process does not show self limiting growth behavior. From the deposition tests, the decomposition of P1 starts already at 160°C for the precursor. This may corroborate with TGA evaluation in section 7.4.1.2, which had suggested the first shallow endothermic peak at 154°C can be due to partial decomposition.

7.4.2 Screening tests for precursor P2

7.4.2.1 Introduction

In this chapter, the TG/DTA curve analysis and thermal stability test of precursor P2 will be discussed. The results from deposition experiments of P2/second-reactant have been discussed in section 7.4.2.4. The second reactants used are: H_2, NH_3, air. Later, the properties of films deposited from P2/second-reactant processes have been discussed.

7.4.2.2 Thermal analyses for precursor P2

Confidential data, any use is denied

Figure 7.4.8 Thermal analysis curves for precursor P2 performed at atmospheric pressure under N_2 environment. The endothermic and exothermic peaks belong to DTA curve. The ordinates for DDTG curve are plotted with respect to right vertical axis. The onset points are calculated from tangents drawn on TG curve [more detail in Gabbott 2008].

7.4.2.3 Thermal stability test for P2

Thermal stability test for precursor P2 was not performed because all precursor (initial weight of 2g) was consumed during the deposition tests and no precursor was left later for this test. However, equivalent results can also be obtained by looking inside the precursor container. Figure 7.4.9a, is the initial state of precursor P2 at R.T. The figure 7.4.9b indicates that P2 was melted and turned into brown at 100°C. The figure 7.4.9c shows that P2 was melted and turned into black at 150°C. The black color of P2 around 150°C may indicate some decomposition around this temperature. In figure 7.4.9b and c, the container was opened in the glovebox at room temperature, this can be a reason of solidification of P2.

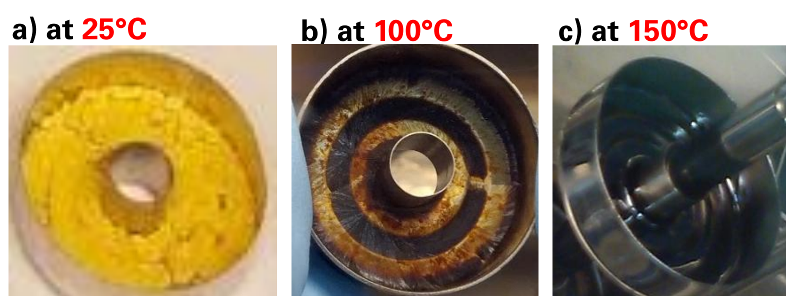

Figure 7.4.9 Change in color and texture of the P2 after handling the precursor container at 100°C and 150°C. A subfigure a) shows the original state, b) and c) indicates P2 was melted and later solidified as well as crystallized. The container was opened at room temperature in the glovebox environment.

7.4.2.4 Deposition experiments for P2

In this section, deposition tests from P2/H_2 have been performed, in order to see if P2 shows any self-limiting growth behaviour. ALD process parameters were: 15 s/15 s/20 s/15 s of ALD pulse times, 140°C of precursor-container temperature and 250°C of deposition temperature. Figure 7.4.10, shows the frequency drop in 100 ALD cycles was almost 25 times less as compared to the frequency drop in 100 ALD cycles from P1/H_2 process at $\vartheta_{deposition}$ of 240°C. Therefore due to significantly low frequency drop, a choice towards other reactants was made. The same experiment was repeated with P2/air and P2/NH_3, in order to see the reactivity trend towards such reactants. It can be seen from the figure 7.4.10 that the frequency drop in 100 ALD cycles was almost similar for both the cases and was around 45 Hz.

According to the manufacturer the precursor molecules are very sensitive towards air exposure and thus more reactive with air. This independency of frequency drop in 100 ALD cycles over the choice of second reactant created a doubt on the thermal stability of the precursor. Therefore, the same experiment as described in this paragraph was repeated without any second reactant (marked as X in figure 7.4.10) and the frequency

drop in 100 cycles was quite similar to that found in case of P2/air, P2/H_2, P2/NH_3 processes (shown in figure below). The growth from P2/X process might indicate towards a self-decomposition of the precursor at 250°C of $\vartheta_{deposition}$. The same P2/X process was also repeated at 200°C and 170°C of deposition temperature, inorder to mitigate the self-decomposition of the precursor. Figure 7.4.10, shows that P2 already grows without any second reactant at $\vartheta_{deposition}$ of 170°C.

Therefore a choice of second reactant and $\vartheta_{deposition}$ has not made much difference to the frequency change in 100 cycles, this might indicate that the films were grown during the P2 pulse itself. The frequency change in 100 cycles in all the cases is around 45-55 Hz. From the results it can be assumed that P2 shows self-decomposition or CVD like behaviour in the deposition temperature range of 170°C and 250°C.

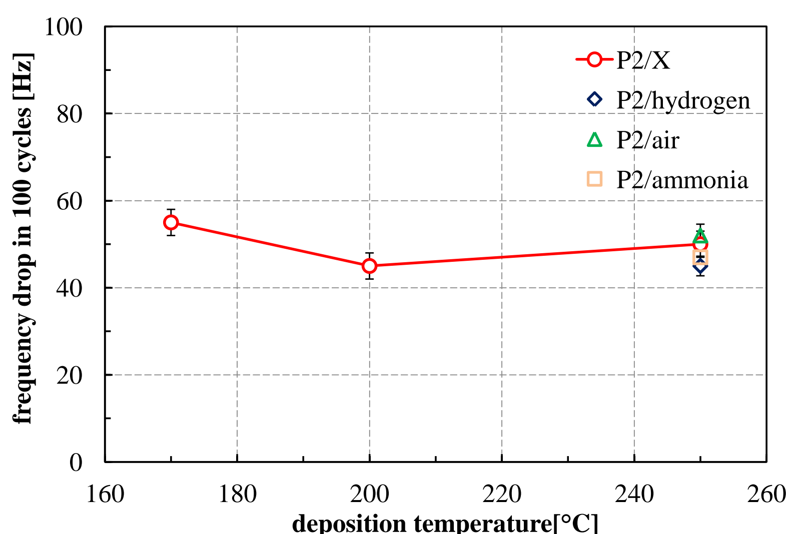

Figure 7.4.10 Deposition tests from P2/air, P2/H_2, P2/NH_3 and P2/X processes. The deposition temperature was 170°C, 200°C and 250°C. The other process parameters like ALD pulse times, precursor-container temperature and P_{total} were: 15 s/15 s/20 s/15 s, 140°C and 200 Pa, respectively.

7.4.2.5 Properties of the films grown from the depositions described in the previous section

The c-Si sample with native oxide was coated with 200 cycles of AlOx ALD process from TMA/air. This substrate was used as initial surface to grow nickel-based film in order to have similar surface conditions as on QCM. Total of 800 ALD cycles were performed in this order: 200, 100, 100 and 400 ALD cycles from P2/air, P2/H_2, P2/NH_3 and P2/X process, respectively. The thickness and density values for top nickel-based film are around 7.8 nm and 4.9 g/cm^3, respectively. Two layer model was used to fit the thickness of top nickel-based layer and underlaying AlOx film together. The underlaying AlOx thickness was around 20 nm with density of 3.6 g/cm^3 and roughness of 0.5 nm. The roughness value of top layer (NiX) was around 3 nm.

The 4PP measurements for this sample had shown the sheet resistance in the range of 550-650 Ω/□, approximately. The conductivity of the sample was very inhomogeneous (±100 Ω/□), throughout the sample length.

SEM pictures for the same sample has been taken and is shown in figure 7.4.11. From SEM picture it can be seen that the total thickness is also around 28 nm as revealed by XRR measurements. SEM picture shows the top film was rough and granular.

Figure 7.4.11 SEM pictures of the film grown from from P2/air, P2/H_2, P2/NH_3 and P2/X process on AlOx coated sample. The The ALD process parameters were: 15 s/15 s/20 s/15 s of ALD pulse times, 140°C of precursor-container temperature. The deposition temperature was: 170°C, 200°C and 250°C.

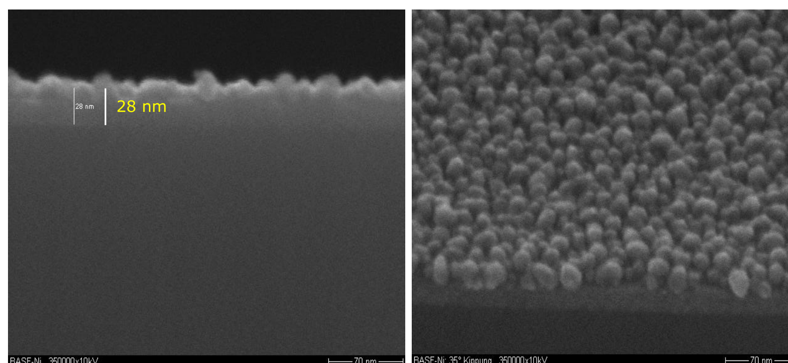

The XPS measurement for this sample was also performed and the results are shown by the figure 7.4.12. It can be seen from the figure that the nickel-based film was either oxidised after getting in contact with clean room air environment or from P2/air process. Large quantities of flourine and carbon were also present on initial surface conditions with only 6.8 atomic % of nickel content. After cleaning the surface, flourine and oxygen atomic % levels were tremendously decreased to 0.5 and 2.5, respectively. The high carbon content (almost 44.6%) might indicate towards precursor decomposition (relies with in situ deposition, TGA and thermal stability tests). After surface-etching for 30 s, the flourine content was increased to 3.4 atomic %. XPS results did not show any Ni-O peak (may be due to incomplete surface reactions during air exposure pulse in P2/air process), but C-C or Ni-C chemical bindings can be suggested. After performing surface-etch steps with 1, 2 and 3 minutes of sputter time, correspondingly showed the visibility of underlaying AlOx film.

7.4.2.6 Remarks on precursor P2

All the experiments performed for precursor P2, indicate towards the self-decomposition above 170°C. The occurence of decomposition in case of P2 is similar to that for P1, but in case of P1 the decomposition was less visible around 160°C. This similarity can arise from their alike molecule structure, the only difference is one of the ligands has been replaced by the other.

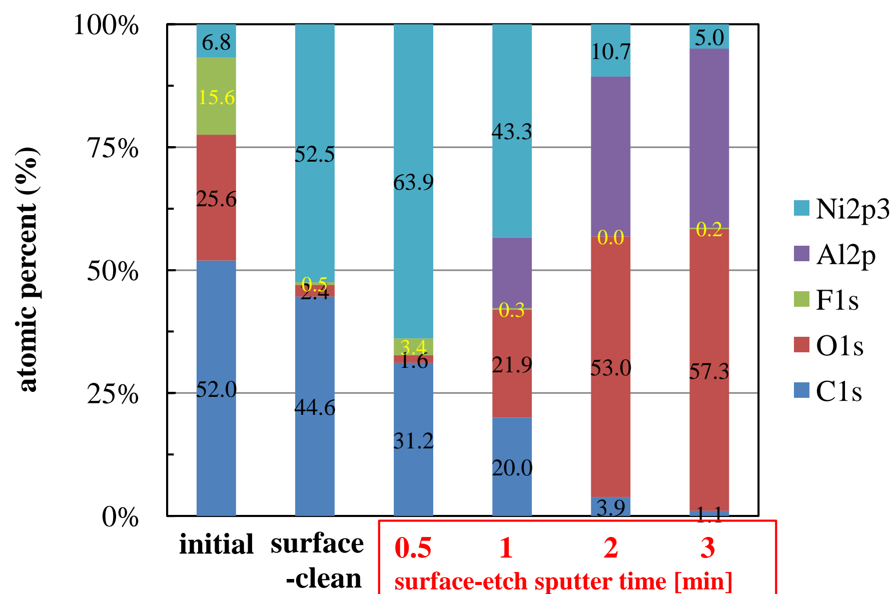

Figure 7.4.12 **XPS analysis of the film grown on AlOx coated sample from P2/air, P2/H_2, P2/NH_3 and P2/X process. In total 800 ALD cycles were performed. The initial condition is the condition where sample surface was intact. In surface-clean and surface-etch steps the sample surface (5 $\times$ 5 mm^2) was sputtered by argon-ion beam of 0.6 keV and 4 keV energy, for 4 min and 0.5-3 min, respectively.**

7.4.3 Screening tests for precursor P3

7.4.3.1 Introduction

In this chapter, the TG/DTA curve analysis and thermal stability test of precursor P3 will be discussed. The results of the deposition experiments from P3/H_2 process has been shown. Later the properties of deposited films have been discussed.

7.4.3.2 Thermal analyses of precursor P3

Confidential data, any use is denied

Figure 7.4.13 Thermal analysis curves for precursor P3 performed at atmospheric pressure under N_2 environment. The endothermic and exothermic peaks belong to DTA curve. The onset points are calculated from tangents drawn on TG curve [more detail in Gabbott 2008].

7.4.3.3 Thermal stability test for P3

Thermal stability test for precursor P3 was not performed because all precursor was consumed during the deposition tests. However, equivalent results can also be obtained by looking into the sublimator. The figure 7.4.14a, shows the initial state of precursor P3 at room temperature, 7.4.14b shows the black residue left after heating the sublimator to maximum of 90°C. In figure 7.4.14c, the $\vartheta_{\text{sublimator}}$ was set to 100°C after refilling the cleaned sublimator and the repetition had shown the same effect.

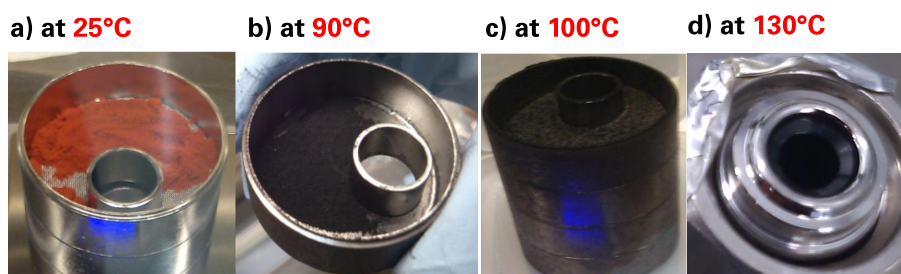

Figure 7.4.14 Change in color and texture of P3 after handling the sublimator at 90°C, 100°C and 130°C. Figure a) shows the original state, b) and c) indicates that P3 remained in powder form but turned to black and d) shows that precursor outlet line kept at 130°C was coated in black. The sublimator was opened at room temperature in the glovebox environment.

In both subfigures b) and c), similar results were obtained and no melting was seen upto 100°C (corroborates the TG analysis). Figure 7.4.14d), shows the direct outlet from a sublimator and it was set to a maximum of 130°C. In figure 7.4.14d, no second reactant was passed through outlet line and the thick black coating may indicate thermal decomposition of P3 at 130°C.

7.4.3.4 Deposition experiments for P3

The amount of P3 obtained was 2 g as compared to 10 g of P1. Therefore in ALD experiments, the P3 exposure time was set to 5 s in order to run reasonable number of ALD cycles and accomplish the evaluation task. The H_2 exposure time and both Ar purges were kept at 30 s. At $\vartheta_{\text{sublimator}}$ of 90°C, a very little change in *FDPC* was observed. Next the $\vartheta_{\text{sublimator}}$ was increased in steps of 5°C in order to increase the vapor pressure of the precursor and achieve higher *FDPC* value.

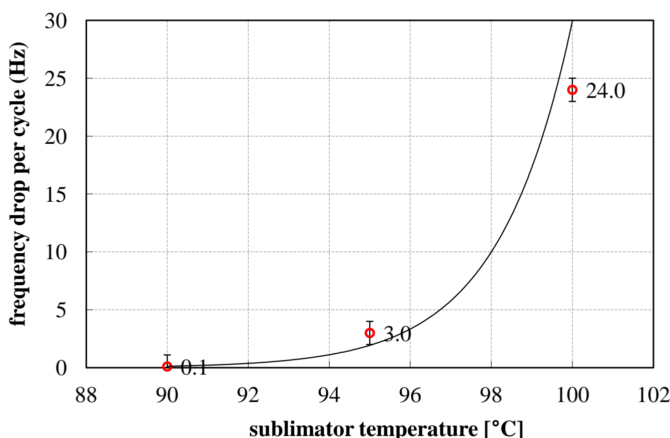

Figure 7.4.15 Deposition tests from P3/H_2 processes. The sublimator was kept at 90°C, 95°C and 100°C. A black line in this figure shows an exponential trendline. The deposition temperature and P_{total} were: 180°C and 200 Pa, respectively.

A figure 7.4.15, shows the $\vartheta_{\text{sublimator}}$ was varied from 90°C to 100°C in step of 5°C and a significant increase in the *FDPC* was observed at 100°C. The results revealed by in situ QCM measurements were fitted by an exponential curve and can be seen by black curve in figure 7.4.15. A tremendous increase in *FDPC* with just 5°C increase in sublimator temperature can be due to some decomposition or undersaturation where the film growth depends dominantly on the precursor exposure time or precursor vapour pressure. According to the results obtained in previous sections, this 24 Hz of *FDPC* can be interpreted as approximately 3-4 Å of growth increment per cycle, depending on the density. For every varied parameter, a total of 50 ALD cycles were performed with standard parameters.

7.4.3.5 Film properties

The initial substrate used was a c-Si sample with 1.8 nm of native oxide on top. In total of 200 ALD cycles were run with P3/H_2 process at 180°C of deposition temperature. The XRR results showed that a two layer model was necessary to fit the thickness, density and roughness of nickel-based film. Top layer was fitted as NiO with thickness, roughness and density values around 2 nm, 5 nm and 2.8 g/cm^3, respectively. The underlaying layer

was fitted as Ni with thickness, roughness and density values around 55 nm, 3 nm and 6 g/cm^3, respectively.

The 4PP measurements for this sample had shown the sheet resistance value in the range of 10-60 Ω/□, approximately. The sheet resistance of the sample was very inhomogeneous being 10 Ω/□ near to the gas inlet side and 60 Ω/□ on the other side.

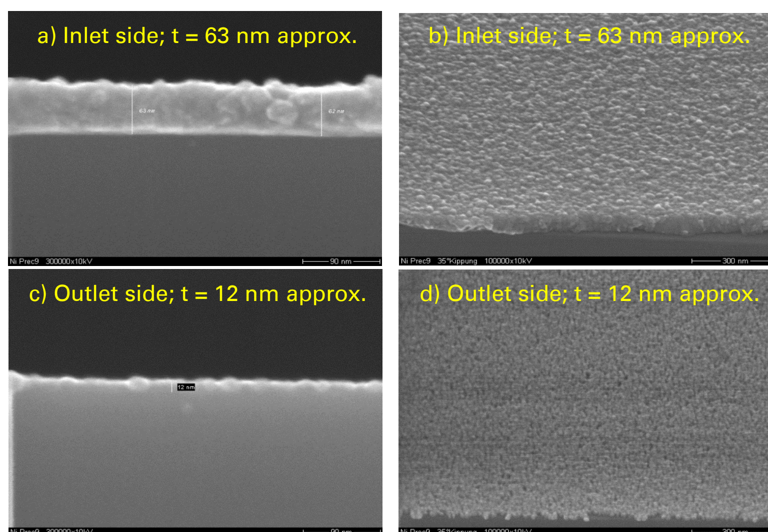

Figure 7.4.16 SEM pictures of the film grown from from P3/H_2 process. The ALD process parameters were: 5 s/30 s/30 s/30 s of ALD pulse times, total of 200 ALD cycles, 90-100°C of the sublimator temperature. The deposition temperature was 180°C. The inlet side is close and outlet side is far from the gas inlet.

In figure 7.4.16, the SEM pictures for the inlet and outlet side of the substrate has been taken, to see the inhomogeniety of the film grown throughout the sample length. The pictures 7.4.16a and 7.4.16b show, the films are very thick, rough and dense as compared to the outlet side (7.4.16c and 7.4.16d).

In figure 7.4.17, the XPS results for the inlet side of a same sample have been evaluated. A 48% of Ni and almost 30 % of oxygen was present at the intial condition. The high amount of oxygen and carbon (20%) might have come from the air exposure because the sample was brought in contact with air before transferring to XPS tool. After performing the surface-clean step, the oxygen content level was dropped to 5% and the carbon level was increased to 24%. After etching the surface for 1 and 2 minutes no significant change in atomic concentration level has been seen for nickel, carbon, oxygen and nitrogen. This may indicate a uniform distribution of elements within the film. A nickel content of almost 70% was seen with considerably high amount of carbon (around 25%). The presence of substantial amount of contaminations like carbon and nitrogen most probably indicate towards thermal decomposition of precursor P3 at 180°C of deposition temperature because according to the manufacturer the precursor molecule contains N and C atoms.

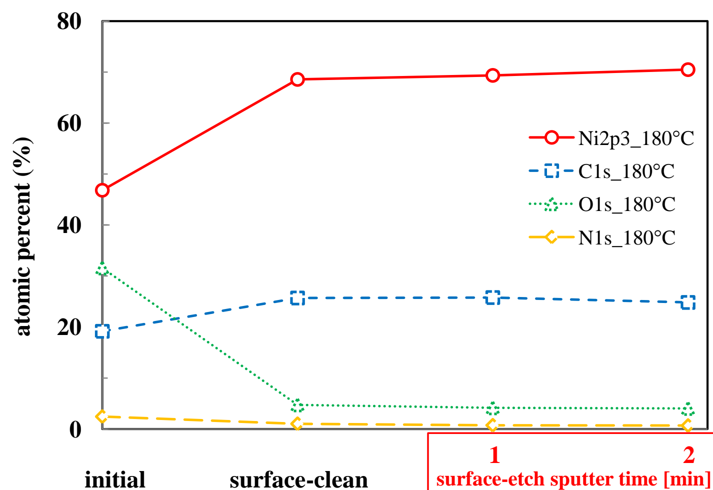

Figure 7.4.17 XPS analysis of the film grown from P3/H_2 process at 180°C of deposition temperature. In total 200 ALD cycles were performed. The initial condition is the condition where sample surface was intact. In surface-clean and surface-etch steps the sample surface (5 × 5 mm^2) was sputtered by argon-ion beam of 0.6 keV and 4 keV energy, for 4 min and 1-2 min, respectively.

7.4.3.6 Remarks on precursor P3

All the experiments performed for precursor P3, indicates toward decomposition or non-ALD behaviour of the precursor from 130°C onwards.

7.4.4 Screening tests for precursor P4

7.4.4.1 Introduction

The class of P4 precursor had two enantiomers and were named as: P4m and P4t. In this chapter, the TG/DTA curve analysis of precursor P4 will be discussed. According to the manufacturer, the TGA and DTA curves for P4m and P4t are same.The deposition experiments were not performed from P4m because it did not pass thermal stability test.

7.4.4.2 Thermal analyses of precursor P4

Confidential data, any use is denied

Confidential data, any use is denied

Figure 7.4.18 Thermal analysis curves for precursor P4 performed at atmospheric pressure under N_2 environment. The exothermic peak belongs to DTA curve. The ordinates for DTG curve are plotted with respect to right vertical axis. The onset points are calculated from tangents drawn on TG curve [more detail in Gabbott 2008].

7.4.4.3 Thermal stability test for P4m

Thermal stability test for P4m was performed to check the stability of precursor over the time. The figure 7.4.19, shows that the temperature of the precursor was increased from a room temperature (original state) to 150°C (follow the red line). In 7.4.19c, the change in color of pecursor at temperature of 80°C was observed. The color was changed to light brown from yellow. The color became even darker at higher temperatures and became completely black after 100°C and remained black until 150°C. This may indicate the thermal degradation of P4m at temperatures above 80°C. This test showed that precursor 4m is not stable at higher temperatures and thus the deposition tests were not performed.

7.4.4.4 Remarks on precursor P4m

The thermal stability of the P4m is questionable at temperatures above 80°C. The results from TGA analysis also indicate towards thermal decomposition behaviour. According

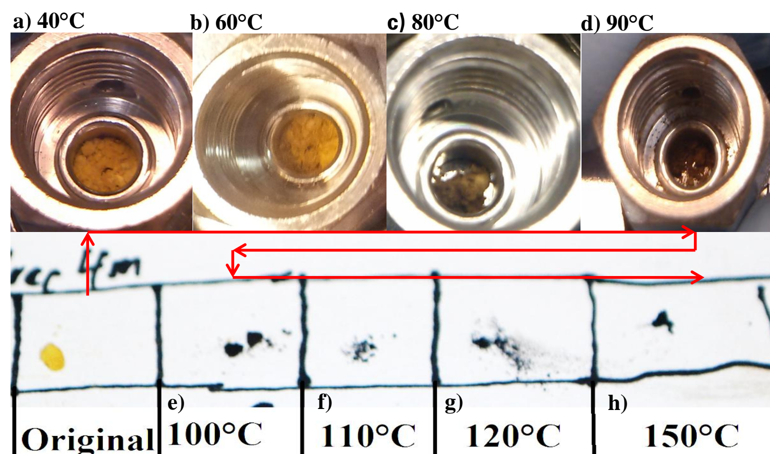

Figure 7.4.19 Change in color and texture of P4m after heating the precursor at different temperatures. The sealed ampoule was heated in the oven that was kept in clean room environment. Later the ampoule was opened in the glovebox environment at room temperature. From subfigures e) to h), a tiny amount of the precursor powder was taken out of the ampoule and placed on a white paper (always kept in the glovebox). From 80°C onwards the precursor showed visible change in the color.

to the same TGA curve a similar behaviour for P4t is expected. Therefore P4 class of precursors may not be suitable for thermal based ALD.

7.4.5 Screening tests for precursor P5

7.4.5.1 Introduction

In this chapter, the TG/DTG curve analysis and thermal stability tests for precursor P5 will be discussed. The results of deposition experiments performed from P5/H_2 and P5/air as well as the film properties have been discussed.

7.4.5.2 Thermal analyses of precursor P5

Confidential data, any use is denied

Confidential data, any use is denied

Figure 7.4.20 Thermal analysis curves for precursor P5 performed at atmospheric pressure under N_2 environment. The onset points are calculated from tangents drawn on TG curve [more detail in Gabbott 2008].

7.4.5.3 Thermal stability test for P5

Thermal stability test for precursor P5 was performed in a temperature range of 100°C - 150°C. The figure 7.4.21a), shows the initial state of precursor P5 at room temperature. Figure 7.4.21c), shows the precursor state at 110°C, no change in the structure as well as color was seen upto this temperature. The precursor P5 was slightly melted at temperature around 120°C but it is hard to see in the figure 7.4.21d). 7.4.21e) shows the melting completed at temperature around 150°C. The similar results were obtained by looking into the sublimator (see 7.4.21f) and it was subjected to maximum temperature of 134°C. At room temperature, the melted precursor did not solidify back. Overall, the color change was not observed with respect to the original state. This irreversible change in the phase was also predicted in section 7.4.5.2. All thermal stability test shown in 7.4.21a) to 7.4.21d) were performed in accumulated fashion. The experiment in figure 7.4.21e) was repeated for the same precursor with new ampoule directly at 150°C, to verify the melting.

7.4.5.4 Deposition experiments for P5

The deposition tests with P5 as the first reactant and H_2 as well as air as the second reactant were also performed. All experiments for P5 were performed with ALD pulse times of 5 s/30 s/30 s/30 s. The sublimator temperature was varied from 50°C to 168°C. The deposition temperature was also varied from 140°C to 270°C, depending on the sublimator temperature. Each parameter variation was tested by running atleast 50 ALD

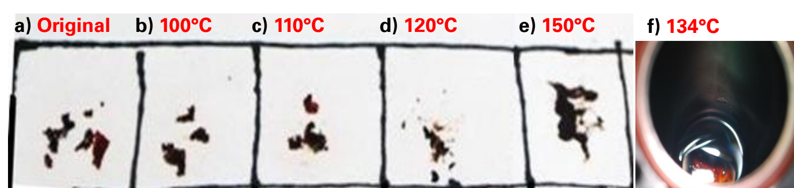

Figure 7.4.21 **The color and texture of P5 after heating the precursor at 100°C, 110°C, 120°C, 134°C and 150°C. In subfigure a) P5 is in its original state, b) and c) P5 remained in a chunk form with no visible color change, d) the P5 went soft and no longer in the chunk form, e) P5 was melted and did not solidify, f) P5 is in the melted form inside the sublimator. The sealed ampoule was heated in the oven that was kept in clean room environment. The containers were opened in the glovebox environment at room temperature.**

cycles, and in some cases atleast 100 ALD cycles were performed. A similar methodolgy was followed as described in previous sections. Despite all the above measures, no change in the frequnecy was revealed by in situ QCM measurements. The QCM was coated with AlOx from atleast 500 ALD cycles of TMA/air process.

7.4.5.5 Film properties

A c-Si sample with native oxide was used as initial substrate. In total of 900 ALD cycles were run and the sample was analysed with the help of XPS. The XPS results showed absence of nickel-based film on the surface but only silicon with little amount of native oxide was present. Some carbon contaminations were also present on the surface, presumably they did arise after getting in contact with clean room environment.

7.4.5.6 Remarks on precursor P5

From all the results, it can be concluded that P5 underwent a permanent structural change at temperature around 134°C. The mass loss in TGA is most probably due to decomposition phenomenon. Therefore making it as a unfit candidate for thermal based ALD experiments.

7.5 COMPARISON OF ALL NICKEL PRECURSORS USED IN THIS WORK

The properties of all nickel precursors used in this work have been summarised and compared in the table 7.2. In general, CVD kind of behaviour was observable from P1, P2 and P3 while only the reference precursor did show ALD charactersistics. Unfortunately, a thermal decomposition was observable for P1, P2 and P3. In general, precursor P1 and P3 had shown significantly higher growth rates as compared to P2 and the reference precursor. Precursor P4m showed thermal degradation around 80°C and was not suitable

for thALD. P5 showed a permanent physical change in its structure around 134°C. For all deposition experiments performed here with P5 no film growth was observed.

T_{decomp} for precursors have been suggested from TGA/DTA curves and deposition experiments. The thermal degradation was suggested from thermal stability test (TS). The results obtained from different analyses were in accordance with each other and no contradiction was seen during deposition tests. The combination of three tests did constrict the values further and showed the decomposition temperatures for P1, P2, P3, P4 and P5 are around 160°C, 100°C, 90°C, 80°C and 120°C, respectively.

The studied properties of grown films and in situ growth measurements did indicate towards thermal decomposition of precursors P1, P2, P3 and P5. However, precursor P1 had shown better results for deposition temperatures around 160°C and 180°C in comparison to P2, P3, P4 and P5 at all temperatures. The films grown from P1/H_2 process at temperatures below 180°C were smooth and thin. For films grown at 160°C the carbon and oxygen levels were around 17 atomic % with almost 40 atomic % of nickel. At 270°C of deposition temperature, the nickel as well as carbon content levels were increased to 80 atomic % and 20 atomic %, respectively. Second best results were found for the films grown from P3/H_2 at 180°C, which had shown 70 atomic % of nickel with considerably high amount of carbon ($\approx$ 25 atomic %). After all the measures that were adopted, it can be said that precursor P1, P2, P3, P4 and P5 cannot be deployed for achieving a self-limited growth characteristics by thALD.

Table 7.2 Comparing all nickel precursors used in this work. The $FDPC_{QCM}$ is a frequency drop per cycle found from in situ QCM measurements during deposition tests performed in this work. T_{decomp} for precursors has been suggested from techniques like: thermal analysis (TA) and ALD experiments. The thermal degradation (T_{degrad}) was found from thermal stability (TS) test.

Precursor	used co-reactants	growth mode	$FCPC_{QCM}$ (Hz)	T_{decomp} (°C)		T_{degrad} (°C)	$\vartheta_{deposition}$ (°C)	$\vartheta_{sublimator}$ (°C)	Remarks
				TA	ALD	TS			
Ni (amd)	air	ALD	6.9	> 270	> 270	> 200	180-270	95-100	self-limiting growth; no growth seen with NH_3 and H_2; smooth and dense films; non conductive NiOx films
P1	H_2; X	Decomposition; CVD	4-18	154	$\leq$ 160	170-200	160-270	144	thermal decomposition around 160°C; $\vartheta_{deposition}$> 180°C yielded in rough, thick, inhomogeneous films; high Ni and C content; conductive films
P2	H_2; NH_3; air;X	Decomposition; CVD	0.5	100	$\leq$ 170	100-150	170-250	140	thermal decomposition around 170°C; film was rough with islands, low density; high Ni and C content; less conductive films
P3	H_2	Decomposition; CVD	3-24	90	$\leq$ 180	90-130	180	90	thermal decomposition around 180°C; thick, rough, inhomogeneous, dense films; very high Ni and C content; conductive films
P4	-	-	-	80	-	80-100	-	-	P4m showed thermal degradation above 80°C
P5	H_2; air	no growth	-	190	-	120-134	140-270	50-168	P5 showed a permanent structure change above 134°C

8 CONCLUSIONS AND OUTLOOK

8.1 CONCLUSIONS

Despite a large number of practical applications of nickel in the microelectronic industry, only a few precursors are available for ALD of pure nickel [Knisley et al. 2013, p. 3226]. Moreover, these precursors had resulted in poor film qualities and the process properties were also limited [Knisley et al. 2013]. To overcome these issues, five novel nickel precursors (named as: P1, P2, P3, P4 and P5) were developed by the manufacturer and have been evaluated in this work. These precursors were specially designed to deposit pure nickel films from thermal based ALD technique with H_2 as a co-reactant.

The precursors under test were solid and obtained in small quantities ($\approx$ 2 g each, except 10 g for P1) and thus it was difficult to do extensive deposition tests for P2, P3, P4 and P5. In order to overcome this issue, a special methodology was adopted and successfully deployed to evaluate the suitability of new precursors for thermally enhanced ALD processes. The methodology includes utilization of various experimental techniques like: TGA/DTA curve analyses, thermal stability (TS) tests in which a tiny amount (< 0.1 g) of precursor was heated at elevated temperatures in sealed ampoules for several hours, deposition experiments and film characterizations. In addition, a short process development was done to verify the ALD behaviour of novel nickel precursors. Thereby, the growth was monitored with a help of in situ QCM and the deposited films were characterized in terms of chemical composition, physical phase, thickness, density, roughness and sheet resistance. The various metrological techniques used for investigating the properties of deposited films are XPS, XRR, XRD, SE, SEM and 4PP.

Before evaluating the novel nickel precursors, a benchmark ALD process was developed using Ni(amd) and air as a co-reactant. The goal of developing and optimizing such benchmark ALD process was to extract standard process parameters like second-reactant exposure time, Argon purge times, total process pressure, starting deposition temperature and gas flows. These standard process parameters were required to shorten the process development task as well as optimize the sublimation temperature for each novel nickel precursor (thus saving some precursor amount). The ALD behaviour was checked in terms of growth rate by varying the nickel precursor exposure time and precursor as well as deposition temperature, only. In addition, apart from H_2 various co-reactants like NH_3 and air were also tested.

From TGA/DTA, it is possible to suggest the sublimation and thermal decomposition temperatures of the novel precursors. The suggested sublimation temperature values for P1, P2, P3, P4 and P5 are around 150°C, 150°C, 110°C, 100°C and 105°C, respectively. From deposition experiments, the actual source temperature values at which precursors P1, P2 and P3 had sublimed were around 144°C, 140°C and 90°C, respectively. From TGA/DTA, the decomposition temperatures for P1, P2, P3, P4 and P5 can be suggested to be around 160°C, 100°C, 130°C, 80°C and 190°C, respectively. The thermal degradation temperatures from thermal stability tests for P1, P2, P3, P4 and P5 is between 170-200°C, 100-150°C, 90-130°C, 80-100°C and 120-134°C, respectively. The thermal

stability test results showed that the precursor P1 was more thermally stable than P2, P3, P4 and P5. However, P4 did not pass the thermal stability test (showed thermal degradation around 80°C) and hence it was rejected for thALD.

The self-limiting growth behaviour is one of the important characteristic of ALD and was verified from the growth rate over various nickel precursor exposure times. The optimized benchmark ALD process from Ni(amd) and air showed self-limiting growth behaviour with a saturated frequency drop per cycle (*FDPC*) around 7 Hz at 200°C and 200 Pa. However, unfortunately depositions from the novel nickel precursors did not lead towards ALD behaviour and the *FDPC* did not saturate to a paticular value. The *FDPC* and process conditions for all nickel precursors are given in tables 7.2 and 6.2.2. For all deposition experiments performed with P5, no film growth was observed.

The selected properties of nickel-based films grown in this work have been summarized in table 7.2 and relevant sections of chapter 7. Among all novel precursors used in this work, the P1 and P3 showed best results. The films grown from P1 and H_2 at 270°C had a nickel content of about 80 atomic % with possible nickel carbide or crystalline nickel phase with some carbon ($\approx$ 19 atomic %) as well as oxygen ($\approx$ 1 atomic %) contaminations. As the deposition temperature was reduced to 180°C, the corresponding nickel, carbon and oxygen content was decreased to approximately 58 atomic %, 25 atomic % and 17 atomic %, respectively. The films resulting from P1/H_2 processes at deposition temperatures above 200°C were more conductive (sheet resistance values in the range of 6-10$\Omega/\square$) than the films grown (sheet resistance values > 5 M$\Omega/\square$) at deposition temperatures between 160°C-180°C. The films produced from P3 and H_2 at 180°C had shown most probably nickel carbide composition and sheet resistance values in the range of 10-60$\Omega/\square$. The XPS results for the films deposited from P3 and H_2 revealed almost 70 atomic % of nickel, 25 atomic % of carbon and 5 atomic % of oxygen levels.

Finally, it can be concluded that the novel precursors P1 and P3 with H_2 as co-reactant can be utilized to grow nickel carbide films. However, none of the test precursors can be considered as a successful candidate for thALD (with H_2 as co-reactant) of pure metallic nickel films. On the other hand, they might be recommended to grow nickel-based films by using CVD or PEALD techniques. Undoubtedly, the methodology used here to evaluate novel nickel precursors (down to 2 g) has been successfully deployed. The results of this project can be incorporated and same methodology can be applied to study various other solid precursors.

8.2 OUTLOOK

In future, precursors with improved thermal stability (no thermal decomposition within their corresponding ALD process windows) are desirable. The availability of precursor vapour pressure curve can help to develope a deposition process and rule-out low vapour pressure precursors, in this way some evaluation time can be spared. In order to min-

imize the contaminations in the tool as well as deposited films, a liquid precursor is desirable (also suggested in [Dussarrat 2014]).

Moreover, an extensive precursor evaluation task can be made by obtaining higher amounts ($\geq$ 5 g) of the novel precursors. In this way a variation in the second reactant exposure time as well as both purge steps can also be tested. Moreover, different substrate pre-treatments and growth-inhibition phase can also be examined.

It is hard to distinguish precursor decomposition from the sublimation with a help of TGA curve alone. Therefore, in order to access the thermal stability of the precursor with a help of TGA/DTA analysis, it is important to test the sublimation under certain isothermal conditions (more details in [Arockiasamy et al. 2010]). This can significantly save the evaluation as well as maintenance time. Furthermore, TGA in combination with evolved gas analysis or mass spectroscopy can easily distinguish the sublimation from decomposition behaviour of the precursor.

REFERENCES

Abu-Lebdeh a. Davidson 2013
ABU-LEBDEH, Yaser ; DAVIDSON, Isobel: *Nanotechnology for lithium-ion batteries*. New York : Springer, 2013 (Nanostructure science and technology). – ISBN 9781461446057

Accurion 2013
ACCURION: *The next generation in imaging ellipsometry: product flyer*. http://www.accurion.com/imaging-ellipsometry/products/nanofilm_ep4/the_nanofilm_ep4.pdf. Version: 2013

Alchin 2014
ALCHIN, Linda: *Chemical properties of Nickel*. http://www.elementalmatter.info/nickel-properties.htm. Version: November 2014

Alexandrov a. Protopopova 2011
ALEXANDROV, S. E. ; PROTOPOPOVA, V. S.: Chemical Vapor Deposition of Ni–C Films from Bis-(Ethylcyclopentadienyl) Nickel. In: *Journal of Nanoscience and Nanotechnology* 11 (2011), Nr. 9, S. 8259–8263

Anders Stenman 2013
ANDERS STENMAN: *Electrochromic properties of nickel oxide in different electrolytes*, Uppsala Universiteit, Diss., 2013

Andrade 1985
ANDRADE, Joseph D.: *Surface and Interfacial Aspects of Biomedical Polymers: Volume 1 Surface Chemistry and Physics*. Boston and MA : Springer US, 1985. – ISBN 978–1–4684–8610–0

Arbuckle-Keil 2002
ARBUCKLE-KEIL, Georgia A.: *The Quartz Crystal Microbalance in Electrochemistry*. John Wiley & Sons, Inc., 2002. http://dx.doi.org/10.1002/0471266965.com054.pub2. http://dx.doi.org/10.1002/0471266965.com054.pub2. – ISBN 9780471266969

Arockiasamy et al. 2010
AROCKIASAMY, S. ; MANOJ, K. ; BHADBHADE, M.M ; MALLIKA, C. ; NAGARAJA, K.S: Syntheses, characterisation and vapour pressure of metallo-organic titanium precursor for MOCVD applications. In: *Inorganica Chimica Acta* 363 (2010), Nr. 10, S. 2243–2249

B. Johs et al. 1999
B. JOHS ; J. A. WOOLLAM ; C. HERZINGER ; J. HILFIKER ; R. SYNOWICKI ; C. BUNGAY: Overview of Variable Angle Spectroscopic Ellipsometry (VASE), Part II: Advanced Applications. (1999), S. 29–58

Bakovets et al. 2005
BAKOVETS, V. V. ; MITKIN, V. N. ; GELFOND, N. V.: Mechanism of Ni Film CVD with a Ni(ktfaa)2 Precursor on a Copper Substrate. In: *Chemical Vapor Deposition* 11 (2005), Nr. 2, S. 112–117

Becht et al. 1995
BECHT, M. ; GALLUS, J. ; HUNZIKER, M. ; ATAMNY, F. ; DAHMEN, K.-H: Nickel Thin Films Grown by MOCVD Using Ni(dmg) 2 as Precursor. In: *Le Journal de Physique IV* 05 (1995), Nr. C5, S. C5–465–C5–472

Bernd O. Kolbesen 2003
BERND O. KOLBESEN (Hrsg.): *Analytical and diagnostic techniques for semiconductor materials, devices, and processes: Joint proceedings of the symposia on*. Bd. *5133*. Pennington and N.J and Bellingham and Wash : Electrochemical Society and SPIE, 2003 (Proceedings of SPIE). – ISBN 9781566773485

Bhaskaran et al. 2009
BHASKARAN, M. ; SRIRAM, S. ; HOLLAND, A.S ; EVANS, P.J: Characterisation of nickel silicide thin films by spectroscopy and microscopy techniques. In: *Micron* 40 (2009), Nr. 1, S. 99–103

Birkholz et al. 2006
BIRKHOLZ, Mario ; FEWSTER, Paul F. ; GENZEL, Christoph: *Thin film analysis by X-ray scattering*. Weinheim and [Chichester : Wiley-VCH and John Wiley, distributor], 2006. – ISBN 9783527310524

Blasco a. Girard 2014
BLASCO, N. ; GIRARD, J.M.: Recent Development of Ligand Chemistries for Next Generation Conformal PEALD/ALD of Metal & Oxides. In: *ALD Workshop, Semicon Europa 2014, Grenoble, October 7th 2014 Air Liquide Electronics* (2014), S. 1–27

Borisenko 2000
BORISENKO, V. E.: *Springer series in materials science*. Bd. 39: *Semiconducting silicides*. Berlin and New York : Springer, 2000. – ISBN 3540661115

Bradley 2011
BRADLEY, K: Nickel Applications and Uses. In: *8th Annual China Nickel Conference, Shanghai, 18-19 May* (2011), 1–36. http://www.nickelinstitute.org/~/Media/Files/Presentations/NickelApplicationsandUsesShanghai0511.pdf

Bui et al. 2010
BUI, Q.V ; NAM, N.D ; CHOI, D.H ; LEE, J.B ; LEE, C.Y ; KAR, A. ; KIM, J.G ; JUNG, S.B: Corrosion protection of ENIG surface finishing using electrochemical methods. In: *Materials Research Bulletin* 45 (2010), Nr. 3, S. 305–308

Bullis 1977
BULLIS, W. M.: *Semiconductor measurement technology: progress report, January 1 to June 30, 1976*. U.S. Dept. of Commerce, National Bureau of Standards, 1977 (NBS special publication). http://books.google.de/books?id=J97vXqi1algC

Chamirian et al. 2003
CHAMIRIAN, O. ; KITTL, J.A ; LAUWERS, A. ; RICHARD, O. ; DAL, M. van ; MAEX, K.: Thickness scaling issues of Ni silicide. In: *Microelectronic Engineering* 70 (2003), Nr. 2-4, S. 201–208

Chen et al. 2005
CHEN, Hao-Long ; LU, Yang-Ming ; HWANG, Weng-Sing: Characterization of sputtered NiO thin films. In: *Surface and Coatings Technology* 198 (2005), Nr. 1-3, S. 138–142

Cheng et al. 2012
CHENG, Cathy I. ; CHANG, Yi-Pin ; CHU, Yen-Ho: Biomolecular interactions and tools for their recognition: focus on the quartz crystal microbalance and its diverse surface chemistries and applications. In: *Chemical Society Reviews* 41 (2012), Nr. 5, S. 1947

Chiaverina a. Lisensky 2014
CHIAVERINA, Chris ; LISENSKY, George: Nickel Curie point engine. In: *The Physics Teacher* 52 (2014), Nr. 4, S. 250–250. `http://dx.doi.org/http://dx.doi.org/10.1119/1.4868949`. – DOI http://dx.doi.org/10.1119/1.4868949

Chung et al. 2011
CHUNG, Taek-Mo ; LEE, Sun-Sook ; CHO, Won-Tae ; KIM, Min-Chan ; LEE, Young-Kuk ; HWANG, Jin-Ha ; AN, Ki-Seok ; KIM, Chang-Gyoun: Volatile Nickel Aminoalkoxide Complexes as Liquid Precursors for Non-volatile Memory Device of NiO Films by ALD. In: *Bulletin of the Korean Chemical Society* 32 (2011), Nr. 3, S. 783–784

Chunli et al. 2010
CHUNLI, Liu ; F, Kurnia ; HADIYAWARMAN ; C., U. J. ; S., B. L. ; S., M. Y. ; H., W. P. ; S., J. S. ; C., S. H.: Effect of NiO Growth Conditions on the Bipolar Resistance Memory Switching of Pt/NiO/SRO Structure. In: *Journal of the Korean Physical Society* 57 (2010), Nr. 61, S. 1856

Clendenning 2010
CLENDENNING, B. S. (Hrsg.): *Nitrogen-Mediated ALD of Metallic Nickel: Film Deposition and Mechanistic Insights*. 2010

Cloud et al. 2014
CLOUD, Andrew N. ; DAVIS, Luke M. ; GIROLAMI, Gregory S. ; ABELSON, John R.: Low-temperature CVD of iron, cobalt, and nickel nitride thin films from bis[di(tert-butyl)amido]metal(II) precursors and ammonia. In: *Journal of Vacuum Science & Technology A: Vacuum, Surfaces, and Films* 32 (2014), Nr. 2, S. 020606. `http://dx.doi.org/10.1116/1.4865903`. – DOI 10.1116/1.4865903

Colnatec 2014a
COLNATEC: *Quartz crystals*. `http://colnatec.com/colna_cms/wp-content/uploads/2014/01/crystalsDSp.pdf`. Version: 2014

Colnatec 2014b
COLNATEC, LLC.: *Crystal Buying Guide*. http://colnatec.com/colna_cms/wp-content/uploads/2014/04/crystalBuyingGuide.pdf. Version: 2014

Cordente et al. 2001
CORDENTE, Nadège ; RESPAUD, Marc ; SENOCQ, François ; CASANOVE, Marie-José ; AMIENS, Catherine ; CHAUDRET, Bruno: Synthesis and Magnetic Properties of Nickel Nanorods. In: *Nano Letters* 1 (2001), Nr. 10, S. 565–568

CoreTech 2014
CORETECH: *Theory of X-Ray Photoelectron Spectroscopy*. http://www.coretechint.com/technical_info-xps.php. Version: December 2014

Dale E. Morton et al. 2002
DALE E. MORTON ; BLAINE JOHS ; JEFF HALE: Optical Monitoring of Thin-films Using Spectroscopic Ellipsometry. In: *Society of Vacuum Coaters* (2002)

Davis 2000
DAVIS, J. R.: *Nickel, cobalt, and their alloys*. Materials Park and OH : ASM International, 2000 (ASM specialty handbook). – ISBN 9780871706850

Deduytsche et al. 2007
DEDUYTSCHE, D. ; DETAVERNIER, C. ; MEIRHAEGHE, R. L. ; JORDAN-SWEET, J. L. ; LAVOIE, C.: Formation and morphological stability of NiSi in the presence of W, Ti, and Ta alloying elements. In: *Journal of Applied Physics* 101 (2007), Nr. 4, S. 044508

Do et al. 2006
DO, Kwan-Woo ; YANG, Chung-Mo ; KANG, Ik-Su ; KIM, Kyung-Min ; BACK, Kyoung-Hum ; CHO, Hyun-Ick ; LEE, Heon-Bok ; KONG, Sung-Ho ; HAHM, Sung-Ho ; KWON, Dae-Hyuk ; LEE, Jong-Hyun ; LEE, Jung-Hee: Formation of Low-Resistivity Nickel Silicide with High Temperature Stability from Atomic-Layer-Deposited Nickel Thin Film. In: *Japanese Journal of Applied Physics* 45 (2006), Nr. 4S, 2975–2979. http://stacks.iop.org/1347-4065/45/i=4S/a=2975

Doering a. Nishi 2008
DOERING, Robert ; NISHI, Yoshio: *Handbook of semiconductor manufacturing technology*. 2. Boca Raton : CRC Press, 2008. – ISBN 9781574446753

Dussarrat 2014
DUSSARRAT, C.: Design, Synthesis and ALD Assessment of Organometallic Precursors for Semiconductor Applications. In: *ECS Transactions* 64 (2014), Nr. 9, S. 233–241

Egerton 2005
EGERTON, R. F.: Physical principles of electron microscopy: An introduction to TEM, SEM, and AEM. In: *Springer e-books* (©2005)

Emslie et al. 2013
EMSLIE, David J. ; CHADHA, Preeti ; PRICE, Jeffrey S.: Metal ALD and pulsed CVD: Fundamental reactions and links with solution chemistry. In: *Coordination Chemistry Reviews* 257 (2013), Nr. 23-24, S. 3282–3296. http://dx.doi.org/10.1016/j.ccr.2013.07.010. – DOI 10.1016/j.ccr.2013.07.010

Foggiato et al. 2004
FOGGIATO, John ; YOO, Woo S. ; OUAKNINE, Michel ; MURAKAMI, Tomomi ; FUKADA, Takahashi: Optimizing the formation of nickel silicide. In: *Materials Science and Engineering: B* 114-115 (2004), S. 56–60

Fouet et al. 2014
FOUET, J. ; TEXIER, M. ; RICHARD, M.-I ; PORTAVOCE, A. ; MANGELINCK, D. ; GUICHET, C. ; BOUDET, N. ; THOMAS, O.: Silicide formation during reaction between Ni ultra-thin films and Si(001) substrates. In: *Materials Letters* 116 (2014), S. 139–142

Fujiwara 2007
FUJIWARA, Hiroyuki: *Spectroscopic ellipsometry: Principles and applications*. Chichester and England and Hoboken and NJ : John Wiley & Sons, 2007. – ISBN 9780470060186

Gabbott 2008
GABBOTT, Paul: *Principles and applications of thermal analysis*. Oxford : Blackwell, 2008 http://www.loc.gov/catdir/enhancements/fy0802/2007029148-b.html. – ISBN 9781405131711

Gambino a. Colgan 1998
GAMBINO, J.P ; COLGAN, E.G: Silicides and ohmic contacts. In: *Materials Chemistry and Physics* 52 (1998), Nr. 2, S. 99–146

George 2010
GEORGE, Steven M.: Atomic Layer Deposition: An Overview. In: *Chemical Reviews* 110 (2010), Nr. 1, S. 111–131

Grimshaw 2013
GRIMSHAW, Scott: *High Temperature, High Accuracy Quartz Crystal (QCM) Measurement Technology for ALD*. http://tu-dresden.de/die_tu_dresden/fakultaeten/fakultaet_elektrotechnik_und_informationstechnik/ihm/news/semicon2013_talks/09_Grimshaw_Colnatec. Version: October 2013

Groner et al. 2004
GRONER, M. D. ; FABREGUETTE, F. H. ; ELAM, J. W. ; GEORGE, S. M.: Low-Temperature Al 2 O 3 Atomic Layer Deposition. In: *Chemistry of Materials* 16 (2004), Nr. 4, S. 639–645. http://dx.doi.org/10.1021/cm0304546. – DOI 10.1021/cm0304546. – ISSN 0897–4756

Gupta 2010
GUPTA, Tapan: *Copper Interconnect Technology*. Dordrecht and New York : Springer, ©2010 `http://books.google.de/books?id=UUFwuIYrSrQC`. – ISBN 9781441900760

Ha et al. 2010
HA, Jong-Bong ; YUN, Sang-Won ; LEE, Jung-Hee: Effect of poly silicon thickness on the formation of Ni-FUSI gate by using atomic layer deposited nickel film. In: *Current Applied Physics* 10 (2010), Nr. 1, S. 41–46

Hatakeyama a. Liu 1998
HATAKEYAMA, T. ; LIU, Zhenhai: *Handbook of thermal analysis*. Chichester and New York : Wiley, 1998. – ISBN 0471983632

Haugsrud 2003
HAUGSRUD, R.: On the high-temperature oxidation of nickel. In: *Corrosion Science* 45 (2003), Nr. 1, S. 211–235

Haynes et al. 2013
HAYNES, William M. ; LIDE, David R. ; BRUNO, Thomas J.: *CRC handbook of chemistry and physics: A ready-reference book of chemical and physical data : 2013-2014*. 94. Boca Raton (Fla.) and London and New York : CRC Press, 2013. – ISBN 9781466571143

Henke et al. 2014
HENKE, T. ; KNAUT, M. ; HOSSBACH, C. ; GEIDEL, M. ; REBOHLE, L. ; ALBERT, M. ; SKORUPA, W. ; BARTHA, J. W.: Flash-Lamp-Enhanced Atomic Layer Deposition of Thin Films. In: *ECS Transactions* 64 (2014), Nr. 9, S. 167–189

Herzinger et al. 1998
HERZINGER, C. M. ; JOHS, B. ; MCGAHAN, W. A. ; WOOLLAM, J. A. ; PAULSON, W.: Ellipsometric determination of optical constants for silicon and thermally grown silicon dioxide via a multi-sample, multi-wavelength, multi-angle investigation. In: *Journal of Applied Physics* 83 (1998), Nr. 6, S. 3323

Hilfiker et al. 2014
HILFIKER, J.N. ; SYNOWICKI, R.A. ; TOMPKINS, H.G.: *Spectroscopic Ellipsometry Methods for thin Absorbing Coatings*. `http://www.jawoollam.com/pdf/SE_Methods_for_Thin_Absorbing_Coatings.pdf`. Version: December 2014

Himcinschi et al. 2001
HIMCINSCHI, C. ; FRIEDRICH, M. ; MURRAY, C. ; STREITER, I. ; SCHULZ, S. E. ; GESSNER, T. ; ZAHN, D. R. T.: Characterization of silica xerogel films by variable-angle spectroscopic ellipsometry and infrared spectroscopy. In: *Semiconductor Science and Technology* 16 (2001), Nr. 9, S. 806–811

Hurle 1994
HURLE, D.T.J: *Handbook of crystal growth*. Bd. Bd. 3,Teil 2. North-Holland Elsevier, 1994 http://books.google.de/books?id=20NRAAAAMAAJ. – ISBN 9780444815569

Hyie et al. 2014
HYIE, Koay M. ; AHMAD, Athirah ; RESALI, Nor A. ; MUNIR, Mohd F. ; LI, Choong S. ; SAIDIN, Sheridan: Corrosion Study of Electrodeposited Co-Ni-Fe Protective Coating on Electroless Nickel Immersion Gold (ENIG) Flexible Printed Circuit. In: *Procedia Technology* 15 (2014), S. 793–798

Ishikawa et al. 2007
ISHIKAWA, M. ; MURAMOTO, I. ; MACHIDA, H. ; IMAI, S. ; OGURA, A. ; OHSHITA, Y.: Chemical vapor deposition of NiSi using Ni(PF3)4 and Si3H8. In: *Thin Solid Films* 515 (2007), Nr. 22, S. 8246–8249

Ismail et al. 2013
ISMAIL, Raid A. ; GHAFORI, Sa'ad ; KADHIM, Ghada A.: Preparation and characterization of nanostructured nickel oxide thin films by spray pyrolysis. In: *Applied Nanoscience* 3 (2013), Nr. 6, S. 509–514

Iwai et al. 2002
IWAI, Hiroshi ; OHGURO, Tatsuya ; OHMI, Shun-ichiro: NiSi salicide technology for scaled CMOS. In: *Microelectronic Engineering* 60 (2002), Nr. 1-2, S. 157–169

J.A. Woollam Co. 2011
J.A. WOOLLAM CO., Inc.: *Complete Ease: Data analysis Manual version (4.63)*. 645 M STREET, SUITE 102 LINCOLN, NE 68508-2243 USA : J.A. Woollam Co.,Inc., 2011

Jacques Curie a. Pierre Curie 1880
JACQUES CURIE ; PIERRE CURIE: Développement, par pression, de l'électricité polaire dans les cristaux hémièdres à faces inclinées. In: *Comptes rendus* 91 (1880), 294–295. http://gallica.bnf.fr/ark:/12148/bpt6k30485

Johannsmann 2014
JOHANNSMANN, Diethelm: *The quartz crystal microbalance in soft matter research: Fundamentals and modeling*. Springer, 2014 (Soft and Biological Matter). http://www.springer.com/materials/book/978-3-319-07835-9. – ISBN 9783319078366

Kada et al. 2005
KADA, T. ; ISHIKAWA, M. ; MACHIDA, H. ; OGURA, A. ; OHSHITA, Y. ; SOAI, K.: Volatile CVD precursor for Ni film: cyclopentadienylallylnickel. In: *Journal of Crystal Growth* 275 (2005), Nr. 1-2, S. e1115–e1119

Kang a. Rhee 2000
KANG, Jin-Kyu ; RHEE, Shi-Woo: Metalorganic Chemical Vapor Deposition of Nickel

Films from Ni(C5H5)2/H2. In: *Journal of Materials Research* 15 (2000), Nr. 08, S. 1828–1833

Kang a. Rhee 2001
KANG, Jin-Kyu ; RHEE, Shi-Woo: Chemical vapor deposition of nickel oxide films from Ni(C5H5)2/O2. In: *Thin Solid Films* 391 (2001), Nr. 1, S. 57–61

Kim et al. 2003
KIM, Jaebum ; CHAKRABARTI, Kuntal ; LEE, Jinho ; OH, Ki-Young ; LEE, Chongmu: Effects of ozone as an oxygen source on the properties of the Al2O3 thin films prepared by atomic layer deposition. In: *Materials Chemistry and Physics* 78 (2003), Nr. 3, S. 733–738. `http://dx.doi.org/10.1016/S0254-0584(02)00375-9`. – DOI 10.1016/S0254–0584(02)00375–9. – ISSN 02540584

Kim et al. 2013
KIM, T. ; CHAMBERLIN, R. V. ; BIRD, J. P.: Large Magnetoresistance of Nickel-Silicide Nanowires: Non-Equilibrium Heating of Magnetically-Coupled Dangling Bonds. In: *Nano Letters* 13 (2013), Nr. 3, S. 1106–1110

Kim et al. 2011
KIM, Woo-Hee ; LEE, Han-Bo-Ram ; HEO, Kwang ; LEE, Young K. ; CHUNG, Taek-Mo ; KIM, Chang G. ; HONG, Seunghun ; HEO, Jong ; KIM, Hyungjun: Atomic Layer Deposition of Ni Thin Films and Application to Area-Selective Deposition. In: *Journal of The Electrochemical Society* 158 (2011), Nr. 1, S. D1

Kittl et al. 2005
KITTL, Jorge A. ; LAUWERS, Anne ; PAWLAK, Malgorzata A. ; DAL, Mark J. ; VELOSO, Anabela ; ANIL, K.G ; POURTOIS, Geoffrey ; DEMEURISSE, Caroline ; SCHRAM, Tom ; BRIJS, Bert ; POTTER, Muriel d. ; VRANCKEN, Christa ; MAEX, Karen: Ni fully silicided gates for 45nm CMOS applications. In: *Microelectronic Engineering* 82 (2005), Nr. 3-4, S. 441–448

Knaut et al. 2013
KNAUT, Martin ; JUNIGE, Marcel ; NEUMANN, Volker ; WOJCIK, Henry ; HENKE, Thomas ; HOSSBACH, Christoph ; HIESS, AndrÃ© ; ALBERT, Matthias ; BARTHA, Johann W.: Atomic layer deposition for high aspect ratio through silicon vias. In: *Microelectronic Engineering* 107 (2013), Nr. 0, S. 80 – 83. `http://dx.doi.org/http://dx.doi.org/10.1016/j.mee.2013.01.031`. – DOI http://dx.doi.org/10.1016/j.mee.2013.01.031

Knisley 2012
KNISLEY, Thomas J.: *NEW PRECURSORS AND CHEMISTRY FOR THE GROWTH OF TRANSITION METAL FILMS BY ATOMIC LAYER DEPOSITION*. Detroit and Michigan, Wayne State University, Diss., 2012

Knisley et al. 2011
KNISLEY, Thomas J. ; ARIYASENA, Thiloka C. ; SAJAVAARA, Timo ; SALY, Mark J. ; WINTER, Charles H.: Low Temperature Growth of High Purity, Low Resistivity Copper Films by Atomic Layer Deposition. In: *Chemistry of Materials* 23 (2011), Nr. 20, S. 4417–4419

Knisley et al. 2013
KNISLEY, Thomas J. ; KALUTARAGE, Lakmal C. ; WINTER, Charles H.: Precursors and chemistry for the atomic layer deposition of metallic first row transition metal films. In: *Coordination Chemistry Reviews* 257 (2013), Nr. 23-24, S. 3222–3231

König et al. 2014
KÖNIG, Meike ; KASPUTIS, Tadas ; SCHMIDT, Daniel ; RODENHAUSEN, Keith B. ; EICHHORN, Klaus-Jochen ; PANNIER, Angela K. ; SCHUBERT, Mathias ; STAMM, Manfred ; UHLMANN, Petra: Combined QCM-D/GE as a tool to characterize stimuli-responsive swelling of and protein adsorption on polymer brushes grafted onto 3D-nanostructures. In: *Analytical and Bioanalytical Chemistry* 406 (2014), Nr. 28, S. 7233–7242

Kulkarni a. Canale 1991
KULKARNI, A.K ; CANALE, A.J: Electrical and structural characterization of Co and Ni silicide contacts to silicon. In: *Applied Surface Science* 48-49 (1991), S. 307–311

Lai et al. 2012
LAI, Willetta ; WONG, P. S. ; HSU, K. L. ; CHAN, C. M. ; CHAN, C. Y. ; BAYES, M. W. ; YEE, K. W.: Development of novel electroless nickel for Selective electroless nickel immersion gold applications. (2012), 80–85. `http://ieeexplore.ieee.org/xpl/articleDetails.jsp?arnumber=6420219`

Lansalot-Matras et al. 2014
LANSALOT-MATRAS, C. ; GATINEAU, J. ; JURCIK, B.J.: *Nickel bis diazabutadiene precursors, their synthesis, and their use for nickel containing films depositions*. `http://www.google.com/patents/US20140242298`. Version: August 28 2014. – US Patent App. 14/347,544

Lauwers et al. 2004
LAUWERS, Anne ; KITTL, Jorge A. ; DAL, Mark J. ; CHAMIRIAN, Oxana ; PAWLAK, Malgorzata A. ; POTTER, Muriel d. ; LINDSAY, Richard ; RAYMAKERS, Toon ; PAGES, Xavier ; MEBARKI, Bencherki ; MANDREKAR, Tushar ; MAEX, Karen: Ni based silicides for 45nm CMOS and beyond. In: *Materials Science and Engineering: B* 114-115 (2004), S. 29–41

Lee et al. 2010
LEE, Han-Bo-Ram ; BANG, Sung-Hwan ; KIM, Woo-Hee ; GU, Gil H. ; LEE, Young K. ; CHUNG, Taek-Mo ; KIM, Chang G. ; PARK, Chan G. ; KIM, Hyungjun: Plasma-Enhanced Atomic Layer Deposition of Ni. In: *Japanese Journal of Applied Physics* 49 (2010), Nr. 5, S. 05FA11

Lee et al. 2005
LEE, P. S. ; PEY, K. L. ; MANGELINCK, D. ; CHI, D. Z. ; OSIPOWICZ, T.: On the Morphological Changes of Ni- and Ni(Pt)-Silicides. In: *Journal of The Electrochemical Society* 152 (2005), Nr. 4, S. G305

Léonard a. Talin 2011
LÉONARD, François ; TALIN, A. A.: Electrical contacts to one- and two-dimensional nanomaterials. In: *Nature Nanotechnology* 6 (2011), Nr. 12, S. 773–783

Li et al. 2011
LI, Huazhi ; PERERA, Thiloma ; SHENAI, Deo V. ; LI, Zhefeng ; GORDON, Roy G.: New Ni Amidinate Source for ALD/CVD of NiNx, NiO and Ni. In: *The 11th International Conference on Atomic Layer Deposition* (2011). http://faculty.chemistry.harvard.edu/files/gordon/files/ccb_-_ald_ninx_nio_nisi_avs_ald2011.pdf

Li et al. 2010
LI, Zhefeng ; GORDON, Roy G. ; PALLEM, Venkateswara ; LI, Huazhi ; SHENAI, Deo V.: Direct-Liquid-Injection Chemical Vapor Deposition of Nickel Nitride Films and Their Reduction to Nickel Films. In: *Chemistry of Materials* 22 (2010), Nr. 10, S. 3060–3066

Lim et al. 2003a
LIM, Booyong S. ; RAHTU, Antti ; GORDON, Roy G.: Atomic layer deposition of transition metals. In: *Nature Materials* 2 (2003), Nr. 11, S. 749–754

Lim et al. 2003b
LIM, Booyong S. ; RAHTU, Antti ; PARK, Jin-Seong ; GORDON, Roy G.: Synthesis and Characterization of Volatile, Thermally Stable, Reactive Transition Metal Amidinates. In: *Inorganic Chemistry* 42 (2003), Nr. 24, S. 7951–7958

Lindahl et al. 2009a
LINDAHL, Erik ; OTTOSSON, Mikael ; CARLSSON, Jan-Otto: Atomic Layer Deposition of NiO by the Ni(thd) 2 /H 2 O Precursor Combination. In: *Chemical Vapor Deposition* 15 (2009), Nr. 7-9, S. 186–191

Lindahl et al. 2009b
LINDAHL, Erik ; OTTOSSON, Mikael ; CARLSSON, Jan-Otto: Chemical Vapour Deposition of Metastable Ni3N. In: *ECS Transactions* 25 (2009), Nr. 8, S. 365–372

Lindahl et al. 2010
LINDAHL, Erik ; OTTOSSON, Mikael ; CARLSSON, Jan-Otto: Growth and stability of CVD Ni3N and ALD NiO dual layers. In: *Surface and Coatings Technology* 205 (2010), Nr. 3, S. 710–716

Lu a. Czanderna 1984
LU, C. ; CZANDERNA, A. W.: *Applications of Piezoelectric Quartz Crystal Microbalances*. Oxford : Elsevier Science, 1984 (Methods and Phenomena). – ISBN 9780444596482

Lu et al. 2008
LU, H. L. ; SCAREL, G. ; WIEMER, C. ; PEREGO, M. ; SPIGA, S. ; FANCIULLI, M. ; PAVIA, G.: Atomic Layer Deposition of NiO Films on Si(100) Using Cyclopentadienyl-Type Compounds and Ozone as Precursors. In: *Journal of The Electrochemical Society* 155 (2008), Nr. 10, S. H807

Lund et al. 2014
LUND, Isaac N. ; LEE, Jae H. ; EFSTATHIADIS, Harry ; HALDAR, Pradeep ; GEER, Robert E.: Influence of catalyst layer thickness on the growth of nickel silicide nanowires and its application for Li-ion batteries. In: *Journal of Power Sources* 246 (2014), S. 117–123

Lüth 2010
LÜTH, H.: *Solid surfaces, interfaces and thin films*. 5. Heidelberg and New York : Springer-Verlag, 2010 (Graduate texts in physics). – ISBN 978–3–642–13592–7

MacKnight et al. 2004
MACKNIGHT, R.B ; TIMANS, P.J ; TAY, S.-P ; NENYEI, Z.: RTP application and technology options for the sub-45 nm nodes. In: *IEEE-International Conference on Advanced thermal processing of Semiconductors-RTP2004* (2004), S. 3–36. `http://dx.doi.org/10.1109/RTP.2004.1441707`. – DOI 10.1109/RTP.2004.1441707

Malandrino et al. 2007
MALANDRINO, Graziella ; PERDICARO, Laura M. S. ; FRAGALÀ, Ignazio L. ; LO NIGRO, Raffaella ; LOSURDO, Maria ; BRUNO, Giovanni: MOCVD Template Approach to the Fabrication of Free-Standing Nickel(II) Oxide Nanotube Arrays: Structural, Morphological, and Optical Properties Characterization. In: *The Journal of Physical Chemistry C* 111 (2007), Nr. 8, S. 3211–3215

Malygin 2013
MALYGIN, A.A.: FROM CHEMICAL REACTIONS ON A SOLID SURFACE TO MOLECULAR LAYERING NANOTECHNOLOGY (A REVIEW). In: *Bulletin of the Saint Petersburg State Institute of Technology (Technical University) No19(45)/2013* 11,25 (2013), Nr. 889-12, S. 61–67

Manbachi a. Cobbold 2011
MANBACHI, A. ; COBBOLD, R. S. C.: Development and application of piezoelectric materials for ultrasound generation and detection. In: *Ultrasound* 19 (2011), Nr. 4, S. 187–196

Mangelinck et al. 1999
MANGELINCK, D. ; DAI, J. Y. ; PAN, J. S. ; LAHIRI, S. K.: Enhancement of thermal stability of NiSi films on (100)Si and (111)Si by Pt addition. In: *Applied Physics Letters* 75 (1999), Nr. 12, S. 1736

Martinson et al. 2014
MARTINSON, A.B.F. ; LIBERA, J.A. ; ELAM, J.W. ; RIHA, S.C.: *Micro-balance sensor*

integrated with atomic layer deposition chamber. http://www.google.com/patents/US20140053779. Version: Februar 27 2014. – US Patent App. 13/591,498

Maruyama a. Tago 1993
MARUYAMA, T. ; TAGO, T.: Nickel thin films prepared by chemical vapour deposition from nickel acetylacetonate. In: *Journal of Materials Science* 28 (1993), Nr. 19, S. 5345–5348

Maruyama a. Arai 1993
MARUYAMA, Toshiro ; ARAI, Susumu: The electrochromic properties of nickel oxide thin films prepared by chemical vapor deposition. In: *Solar Energy Materials and Solar Cells* 30 (1993), Nr. 3, S. 257–262

Marx 2003
MARX, Kenneth A.: Quartz Crystal Microbalance: A Useful Tool for Studying Thin Polymer Films and Complex Biomolecular Systems at the Solution−Surface Interface. In: *Biomacromolecules* 4 (2003), Nr. 5, S. 1099–1120

Maydannik et al. 2014
MAYDANNIK, Philipp S. ; KÄÄRIÄINEN, Tommi O. ; LAHTINEN, Kimmo ; CAMERON, David C. ; SÖDERLUND, Mikko ; SOININEN, Pekka ; JOHANSSON, Petri ; KUUSIPALO, Jurkka ; MORO, Lorenza ; ZENG, Xianghui: Roll-to-roll atomic layer deposition process for flexible electronics encapsulation applications. In: *Journal of Vacuum Science & Technology A: Vacuum, Surfaces, and Films* 32 (2014), Nr. 5, S. 051603

Miikkulainen et al. 2013
MIIKKULAINEN, Ville ; LESKELÄ, Markku ; RITALA, Mikko ; PUURUNEN, Riikka L.: Crystallinity of inorganic films grown by atomic layer deposition: Overview and general trends. In: *Journal of Applied Physics* 113 (2013), Nr. 2, S. 021301

Min et al. 2007
MIN, K.-C ; KIM, M. ; YOU, Y.-H ; LEE, S.S ; LEE, Y.K ; CHUNG, T.-M ; KIM, C.G ; HWANG, J.-H ; AN, K.-S ; LEE, N.-S ; KIM, Y.: NiO thin films by MOCVD of Ni(dmamb)2 and their resistance switching phenomena. In: *Surface and Coatings Technology* 201 (2007), Nr. 22-23, S. 9252–9255

Murarka 1995
MURARKA, Shyam P.: Silicide thin films and their applications in microelectronics. In: *Intermetallics* 3 (1995), Nr. 3, S. 173–186

Nalwa 2002
NALWA, Hari S.: *Handbook of thin film materials*. San Diego : Academic Press, 2002. – ISBN 0125129092

NanoTech 2011
NANOTECH: *Cambridge NanoTech ALD tutorial*. http://www.cambridgenanotechald.com/atomic-layer-deposition-overview.html. Version: 2011

NASF 2014
NASF: *Nickel in computers @ONLINE*. http://www.nickelinstitute.org/~/media/Files/MediaCenter/NASF%20factsheets/201405-nasf-nickel-computer.ashx. Version: Oktober 2014

Nickel Institute 2014
NICKEL INSTITUTE, NASF: *Nickel in cell phones @ONLINE*. http://www.nickelinstitute.org/~/media/Files/NickelUseInSociety/AboutNickel/WhereWhyUsed/nasf_cell_phone.ashx. Version: Oktober 2014

Niinisto et al. 2014
NIINISTO, J. ; BLANQUART, T. ; SEPPALA, S. ; RITALA, M. ; LESKELA, M.: Heteroleptic Precursors for Atomic Layer Deposition. In: *ECS Transactions* 64 (2014), Nr. 9, S. 221–232

Parsons et al. 2013
PARSONS, Gregory N. ; ELAM, Jeffrey W. ; GEORGE, Steven M. ; HAUKKA, Suvi ; JEON, Hyeongtag ; KESSELS, W. M. M. ; LESKELÄ, Markku ; POODT, Paul ; RITALA, Mikko ; ROSSNAGEL, Steven M.: History of atomic layer deposition and its relationship with the American Vacuum Society. In: *Journal of Vacuum Science & Technology A: Vacuum, Surfaces, and Films* 31 (2013), Nr. 5, S. 050818/1–11

Puurunen 2005
PUURUNEN, Riikka L.: Surface chemistry of atomic layer deposition: A case study for the trimethylaluminum/water process. In: *Journal of Applied Physics* 97 (2005), Nr. 12, S. 121301. http://dx.doi.org/10.1063/1.1940727. – DOI 10.1063/1.1940727. – ISSN 00218979

Puurunen a. Vandervorst 2004
PUURUNEN, Riikka L. ; VANDERVORST, Wilfried: Island growth as a growth mode in atomic layer deposition: A phenomenological model. In: *Journal of Applied Physics* 96 (2004), Nr. 12, S. 7686

Puurunen 2003
PUURUNEN, R.L: Growth Per Cycle in Atomic Layer Deposition: Real Application Examplesof a Theoretical Model. In: *Chemical Vapor Deposition* 9 (2003), Nr. 6, S. 327–332

Qin et al. 2001
QIN, Ming ; POON, Vincent M. C. ; HO, Stephen C. H.: Investigation of Polycrystalline Nickel Silicide Films as a Gate Material. In: *Journal of The Electrochemical Society* 148 (2001), Nr. 5, S. G271

Ren et al. 2013
REN, R. ; WANG, J. ; ZHU, R.H ; GUO, Y.X: Fully passivated radial junction nanowire silicon solar cells with submerged nickel-silicide contact for efficiency enhancement. In: *Electronics Letters* 49 (2013), Nr. 12, S. 767–769

Rocklein a. George 2003
ROCKLEIN, M. N. ; GEORGE, S. M.: Temperature-Induced Apparent Mass Changes Observed during Quartz Crystal Microbalance Measurements of Atomic Layer Deposition. In: *Analytical Chemistry* 75 (2003), Nr. 19, S. 4975–4982. `http://dx.doi.org/10.1021/ac030141u`. – DOI 10.1021/ac030141u

Sauerbrey 1959
SAUERBREY, Günter: Verwendung von Schwingquarzen zur Wägung dünner Schichten und zur Mikrowägung. In: *Z. Physik (Zeitschrift für Physik)* 155 (1959), Nr. 2, S. 206–222

Schroder 2006
SCHRODER, Dieter K.: *Semiconductor material and device characterization*. 3. [Piscataway and NJ] and Hoboken and N.J : IEEE Press and Wiley, 2006. – ISBN 9780471749080

Sean Barry 2014a
SEAN BARRY (Hrsg.): *Thermogravimetric Methods for Assessing Precursors and the Effect of Ligand Design*. Koyoto, Japan : 14th International Conference on Atomic Layer Deposition, 2014

Sean Barry 2014b
SEAN BARRY ; SEAN BARRY (Hrsg.): *TGA analysis of ALD precursors*. 2014, October 17

Sharma 2014
SHARMA, Varun: *Spectroscopic ellipsometry for the in-situ investigation of atomic layer depositions*. Dresden, Germany, Institute of Semiconductors and Microsystems, Technische Universität Dresden, Diss., 2014. `http://nbn-resolving.de/urn:nbn:de:bsz:14-qucosa-146530`

Siah et al. 2013
SIAH, S.C ; HOEX, B. ; ABERLE, A.G: Accurate characterization of thin films on rough surfaces by spectroscopic ellipsometry. In: *Thin Solid Films* 545 (2013), S. 451–457

Smith a. Shirazi 2005
SMITH, Allan L. ; SHIRAZI, Hamid M.: Principles of quartz crystal microbalance/heat conduction calorimetry: Measurement of the sorption enthalpy of hydrogen in palladium. In: *Thermochimica Acta* 432 (2005), Nr. 2, S. 202–211. `http://dx.doi.org/10.1016/j.tca.2005.03.017`. – DOI 10.1016/j.tca.2005.03.017

So et al. 2007
SO, Byung-Soo ; YOU, Yil-Hwan ; KIM, Kyu-Hun ; HWANG, Jinha ; CHO, Wontae ; LEE, Sun S. ; CHUNG, Taek-Mo ; LEE, Young K. ; KIM, Chang G. ; AN, Ki-Seok ; KIM, Young-Cheol ; LEE, Young-Ho ; SEO, Won-Seon: Crystallization of Amorphous Silicon Thin Films Using Self-Limiting ALD of Nickel Oxide. In: *Electrochemical and Solid-State Letters* 10 (2007), Nr. 5, S. J61

Sparrow 2005
SPARROW, Giles: *Nickel*. New York : Benchmark Books/Marshall Cavendish, 2005 (Elements). – ISBN 9780761418115

Stimola 2007
STIMOLA, Aubrey: *Nickel*. 1. New York : Rosen Pub. Group, 2007 (Understanding the elements of the periodic table). – ISBN 9781404207042

Utriainen et al. 2000
UTRIAINEN, Mikko ; KRÖGER-LAUKKANEN, Minna ; JOHANSSON, Leena-Sisko ; NIINISTÖ, Lauri: Studies of metallic thin film growth in an atomic layer epitaxy reactor using M(acac)2 (M=Ni, Cu, Pt) precursors. In: *Applied Surface Science* 157 (2000), Nr. 3, S. 151–158

Van Bockstael 2010
VAN BOCKSTAEL, C: *In situ study of the formation and properties of Nickel silicides*, University of Ghent, Diss., 2010. http://www.cocoon.ugent.be/sites/default/files/phdtheses/PhDCVB.pdf

Van Bockstael et al. 2009
VAN BOCKSTAEL, C. ; DETAVERNIER, C. ; MEIRHAEGHE, R. L. ; JORDAN-SWEET, J. L. ; LAVOIE, C.: In situ study of the formation of silicide phases in amorphous Ni–Si mixed layers. In: *Journal of Applied Physics* 106 (2009), Nr. 6, S. 064515

Vashist a. Vashist 2011
VASHIST, Sandeep K. ; VASHIST, Priya: Recent Advances in Quartz Crystal Microbalance-Based Sensors. In: *Journal of Sensors* 2011 (2011), Nr. 6, S. 1–13

Venter a. Botha 2011
VENTER, Andre ; BOTHA, Johannes R.: Optical and electrical properties of NiO for possible dielectric applications. In: *South African Journal of Science* 107 (2011), Nr. 1/2

Wagner a. Muilenberg 1979
WAGNER, C. D. ; MUILENBERG, G. E.: *Handbook of x-ray photoelectron spectroscopy: a reference book of standard data for use in x-ray photoelectron spectroscopy*. Physical Electronics Division, Perkin-Elmer Corp, 1979 http://books.google.de/books?id=oY5TAAAAYAAJ

Wang et al. 2012
WANG, Xu ; HAN, Xuanding ; LIM, Mengfang ; SINGH, Nandan ; GAN, Chee L. ; JAN, Ma ; LEE, Pooi S.: Nickel Cobalt Oxide-Single Wall Carbon Nanotube Composite Material for Superior Cycling Stability and High-Performance Supercapacitor Application. In: *The Journal of Physical Chemistry C* 116 (2012), Nr. 23, S. 12448–12454

Wendlandt 1974
WENDLANDT, Wesley W.: *Chemical analysis*. Bd. 19: *Thermal methods of analysis*. 2. New York : Wiley, ©1974. – ISBN 0–471–93366–X

Windover et al. 2014
WINDOVER, D. ; GIL, D. L. ; AZUMA, Y. ; FUJIMOTO, T.: Determining sample alignment in x-ray reflectometry using thickness and density from GaAs/AlAs multilayer certified reference materials. In: *Measurement Science and Technology* 25 (2014), Nr. 10, S. 105007

Winter et al. 2014
WINTER, C.H. ; KNISLEY, T.J. ; ARIYASENA, T.: *Atomic layer deposition of transition metal thin films*. https://www.google.com/patents/US20140234550. Version: August 21 2014. – US Patent App. 14/130,987

Yang et al. 2007
YANG, Chung-Mo ; YUN, Sang-Won ; HA, Jong-Bong ; NA, Kyung-Il ; CHO, Hyun-Ick ; LEE, Heon-Bok ; JEONG, Jong-Hwa ; KONG, Sung-Ho ; HAHM, Sung-Ho ; LEE, Jung-Hee: Effectiveness of Self-Carbon and Titanium Capping Layers in NiSi formation with Ni Film Deposited by Atomic Layer Deposition. In: *Japanese Journal of Applied Physics* 46 (2007), Nr. 4B, S. 1981–1983

Yang et al. 2005
YANG, Taek S. ; CHO, Wontae ; KIM, Minchan ; AN, Ki-Seok ; CHUNG, Taek-Mo ; KIM, Chang G. ; KIM, Yunsoo: Atomic layer deposition of nickel oxide films using $Ni(dmamp)_2$ and water. In: *Journal of Vacuum Science & Technology A: Vacuum, Surfaces, and Films* 23 (2005), Nr. 4, S. 1238

Yang et al. 2014
YANG, Y. ; TAO, Q. ; SRINIVASAN, G. ; TAKOUDIS, C. G.: Cyclic Chemical Vapor Deposition of Nickel Ferrite Thin Films Using Organometallic Precursor Combination. In: *ECS Journal of Solid State Science and Technology* 3 (2014), Nr. 11, S. P345–P352

Yasaka 2010
YASAKA, Miho: X-ray thin-film measurement techniques. In: *The Rigaku Journal* 26 (2010), Nr. 2, 1-9. http://www.eng.uc.edu/~beaucag/Classes/Characterization/ReflectivityLab/X-ray%20thin-film%20measurement%20techniques_V_X-ray%20reflectivity%20measurement.pdf

Yeh a. Matsumura 1997
YEH, Wen-chang ; MATSUMURA, Masakiyo: Chemical Vapor Deposition of Nickel Oxide Films from Bis-π-Cyclopentadienyl-Nickel. In: *Japanese Journal of Applied Physics* 36 (1997), Nr. Part 1, No. 11, S. 6884–6887

Yokota et al. 2013
YOKOTA, Jiro ; LANSALOT, Clement ; KO, Changhee: *Proceedings of the 2013 IEEE International Interconnect Technology Conference: IITC ... June 13-15, 2013, Kyoto Research Park, Kyoto, Japan*. Piscataway and N.J : IEEE, 2013. – ISBN 978–1–4799–0438–9

Yoo et al. 2011
YOO, Seung H. ; CHOI, Hana ; KIM, Hyo-Suk ; PARK, Bo K. ; LEE, Sun S. ; AN, Ki-Seok ; LEE, Young K. ; CHUNG, Taek-Mo ; KIM, Chang G.: Synthesis and Characterization of Nickel(II) Aminoalkoxides: Application to Molecular Precursors for MOCVD of Ni Thin Films. In: *European Journal of Inorganic Chemistry* 2011 (2011), Nr. 11, S. 1833–1839

Yu et al. 2014
YU, Hui ; WANG, Feng ; XIE, Fangyan ; LI, Wenwu ; CHEN, Jian ; ZHAO, Ni: The Role of Chlorine in the Formation Process of "CH 3 NH 3 PbI 3-x Cl x " Perovskite. In: *Advanced Functional Materials* (2014)

Zhang a. Smith 2004
ZHANG, S.-L ; SMITH, U.: Self-aligned silicides for Ohmic contacts in complementary metal–oxide–semiconductor technology: $TiSi_2$, $CoSi_2$, and NiSi. In: *Journal of Vacuum Science & Technology A: Vacuum, Surfaces, and Films* 22 (2004), Nr. 4, S. 1361

Zhou a. Wang 2007
ZHOU, Weili ; WANG, Zhong L.: *Scanning microscopy for nanotechnology: Techniques and applications*. New York and London : Springer, 2007. – ISBN 9780387396200

ACKNOWLEDGMENTS

The research work reported in this Master thesis was carried out during the year 2013–2014 in the Institute of Semiconductors And Microsystems at University of Technology Dresden, Germany. The sample analysis was done at Fraunhofer Center Nanoelectronic Technologies (IPMS-CNT), Dresden. The novel precursors were developed and supplied by our industrial partner.

First, I owe my deepest gratitude to my supervisors, Dr.-Ing. Christoph Hoßbach and M.Sc. Sascha Bönhardt. Christoph, without your guidance this work would not have been done. You always had time for me and your rapid feedback concerning my ongoing project was just unbelievable. I had a great time during this complete year, working with you.

I would like to appreciate the contribution made by Dipl.-Ing. Stefan Riedel during the SEM, XRR/XRD measurements in very time-efficient way.

I am very thankful to Dipl.-Ing. Martin Knaut, Dipl.-Ing. Marion Geidel and Zulfija Ritter for their valuable suggestions and help in measuring the XPS data. Many thanks go to Dipl.-Ing. Marcel Junige for his help in building ellipsometry models.

I am very thankful to *Confidential data, any use is denied* for giving me opportunity to work on their new products and discussing results in the bi-weekly telecons.

I would also like to credit Dr. Jonas Sundqvist for his worthful ideas and fruitful discussions during this project.

I owe my warm thanks to Dipl.-Ing. Thomas Henke, Eckehard Kellner and Dipl.-Ing. Willi Haas for their kind help during this project.

My sincere thanks also goes to Dipl.-Chem. Sylva Waurenschk, Dr. rer. nat. Volker Neumann, Dr. rer. nat. Ulrich Künzelmann, for the permission to work in the chemistry lab.

My special thanks goes to my Professor Dr. rer. nat. Johann W. Bartha, for his valuable support and advice during this year inside and outside of the laboratory. I would also like to appreciate Dr.-Ing. Matthias Albert for his advice and timely evaluation of my presentations.

Finally, I am using this opportunity to express my gratitude to everyone who supported me while working in the lab.

III APPENDIX

A DEPOSITION TEMPERATURE CONTROL & ELLIPSOMETRY MODEL

A.1 TEMPERATURE AND VOLTAGE RELATION

The figure A.1.1 shows the actual deposition temperature obtained by a manual control of the voltage from the voltage source. The resitance of the heater from a tube-reactor was 530 Ω.

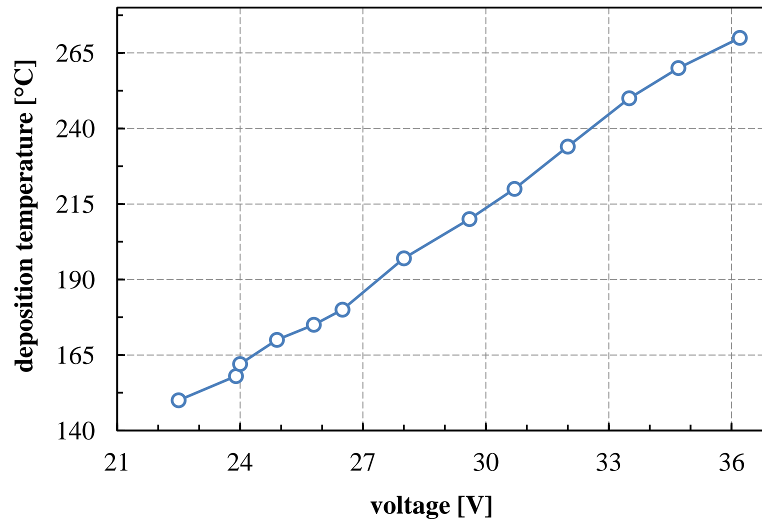

Figure A.1.1 Deposition temperature with respect to its corresponding voltage values

A.2 ELLIPSOMETRY MODEL

A.2.1 OLS model parameters

Figure A.2.1, shows the detailed information about the general oscillator parameters used for nickel-based film analysis. The figure also shows an amplitude and broadening values for both lorentz oscillators. According to the hardware settings, angle offset was always set to -0.1.

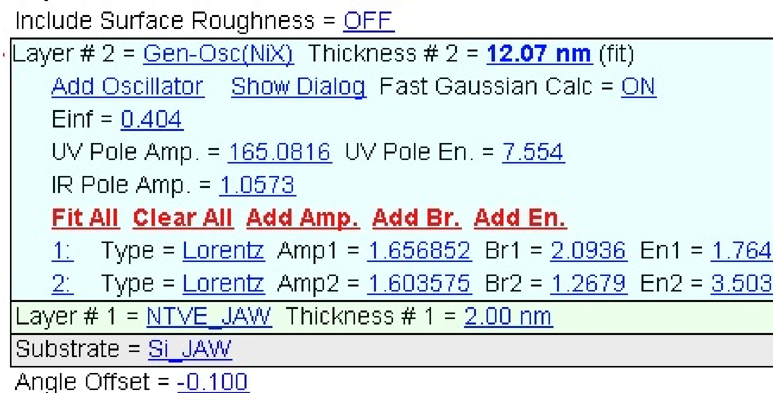

Figure A.2.1 General oscillator model parameters with thickness as a fit parameter. Two Lorentz oscillators were used with different amplitudes and broadenings.

A.2.2 Optical constant

A general oscillator material model shown in figure A.2.1 was parameterized with a set of optical constants shown in figure A.2.2. The values for 'n' and 'k' were parameterized for a nickel-based film grown at 160°C from precursor P1/H_2 and P1/air process. The nickel-based film grown was defined in the form of NiX, where X can be O or C.

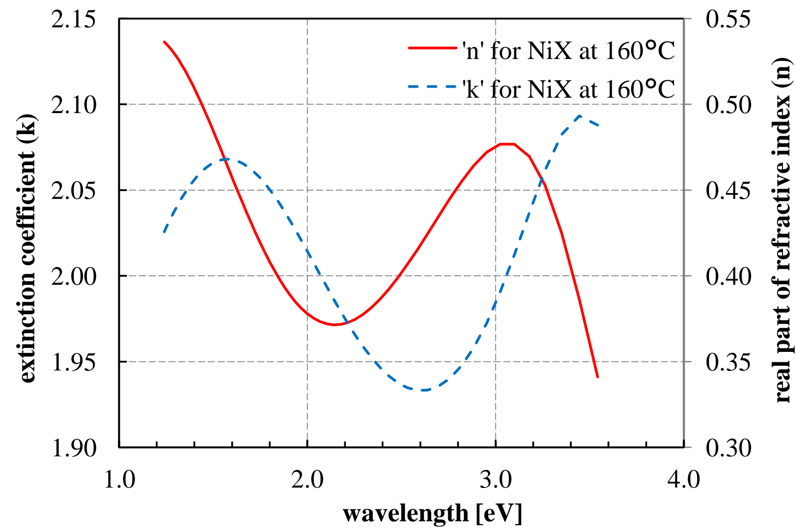

Figure A.2.2 Optical constants for the parameterized material layer. NiX denotes a layer that is predominantly based on nickel, oxygen and carbon.

B GAS FLOW PLAN

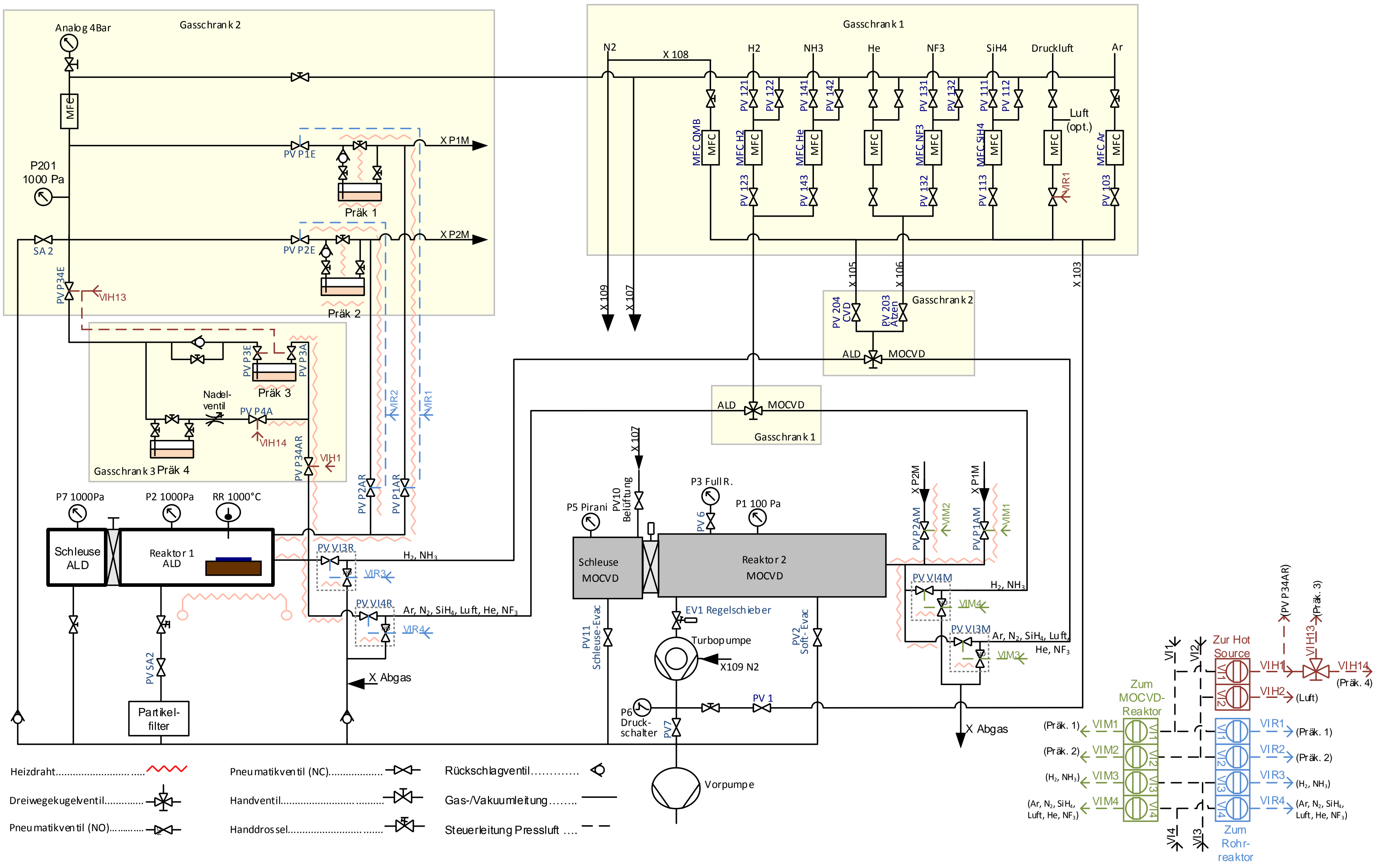
Gasschrank 2
Analog 4Bar
MFC
P201
1000 Pa
SA 2
PV P34E
VIH13
PV P1E
X P1M
Präk 1
PV P2E
X P2M
Präk 2
Gasschrank 1
N2
X 108
H2
NH3
He
NF3
SiH4
Druckluft
Ar
PV 121
PV 122
PV 141
PV 142
PV 131
PV 132
PV 111
PV 112
Luft
(opt.)
MFC QMB
MFC H2
MFC He
MFC NF3
MFC SiH4
MFC Ar
PV 123
PV 143
PV 132
PV 113
VIR1
PV 103
X 109
X 107
X 105
X 106
X 103
PV 204
CVD
PV 203
Ätzen
Gasschrank 2
ALD
MOCVD
ALD
MOCVD
Gasschrank 1
PV P3E
PV P3A
Präk 3
Nadel-
ventil
PV P4A
VIH14
Gasschrank 3 Präk 4
PV P34AR
VIH1
VIR2
VIR1
PV P2AR
PV P1AR
P7 1000Pa
P2 1000Pa
RR 1000°C
Schleuse
ALD
Reaktor 1
ALD
PV VI3R
VIR3
H_2, NH_3
PV VI4R
VIR4
Ar, N_2, SiH_4, Luft, He, NF_3
X Abgas
PV SA2
Partikel-
filter
X 107
PV10
Belüftung
P5 Pirani
P3 FullR.
PV 6
P1 100 Pa
Schleuse
MOCVD
Reaktor 2
MOCVD
EV1 Regelschieber
Turbopumpe
X109 N2
PV11
Schleuse-Evac
PV2
Soft-Evac
PV 1
P6
Druck-
schalter
PV7
Vorpumpe
X P2M
X P1M
PV P2AM
VIM2
PV P1AM
VIM1
PV VI4M
VIM4
H_2, NH_3
PV VI3M
VIM3
Ar, N_2, SiH_4, Luft,
He, NF_3
X Abgas
Heizdraht
Dreiwegekugelventil
Pneumatikventil (NO)
Pneumatikventil (NC)
Handventil
Handdrossel
Rückschlagventil
Gas-/Vakuumleitung
Steuerleitung Pressluft
Zum
MOCVD-
Reaktor
VI1
VI2
VI3
VI4
Zur Hot
Source
VIH1
VIH2
(Luft)
VIH13
VIH14
(PV P34AR)
(Präk. 3)
(Präk. 4)
(Präk. 1)
(Präk. 2)
(H_2, NH_3)
(Ar, N_2, SiH_4,
Luft, He, NF_3)
VIM1
VIM2
VIM3
VIM4
VIR1
VIR2
VIR3
VIR4
Zum
Rohr-
reaktor